Draft version July 3, 2014
Preprint typeset using LaTeX style emulateapj v. 5/2/11

arXiv:1405.4307v3 [astro-ph.GA] 2 Jul 2014

ABSORPTION-LINE DETECTIONS OF 10^{5-6} K GAS IN SPIRAL-RICH GROUPS OF GALAXIES

John T. Stocke, Brian A. Keeney, Charles W. Danforth, David Syphers, H. Yamamoto, J. Michael Shull, James C. Green & Cynthia Froning
Center for Astrophysics and Space Astronomy, Department of Astrophysical and Planetary Sciences, University of Colorado, 389 UCB, Boulder, CO 80309, USA; john.stocke@colorado.edu

Blair D. Savage, Bart Wakker & Tae-Sun Kim
Department of Astronomy, U of Wisconsin, Madison, WI 53706

Emma V. Ryan-Weber & Glenn G. Kacprzak
Centre for Astrophysics & Supercomputing, Swinburne University of Technology, VIC 3122, Australia
Draft version July 3, 2014

ABSTRACT

Using the Cosmic Origins Spectrograph (COS) on the *Hubble Space Telescope* (HST) the COS Science Team has conducted a high signal-to-noise survey of 14 bright QSOs. In a previous paper (Savage et al. 2014) these far-UV spectra were used to discover 14 "warm" ($T \geq 10^5$ K) absorbers using a combination of broad Lyα and broad O VI absorptions. A reanalysis of a few of this new class of absorbers using slightly relaxed fitting criteria finds as many as 20 warm absorbers *could be* present in this sample. A shallow, wide spectroscopic galaxy redshift survey has been conducted around these sightlines to investigate the warm absorber environment, which is found to be spiral-rich groups or cluster outskirts with radial velocity dispersions σ = 250-750 km s^{-1}. While 2σ evidence is presented favoring the hypothesis that these absorptions are associated with the galaxy groups and not with the individual, nearest galaxies, this evidence has considerable systematic uncertainties and is based on a small sample size so it is not entirely conclusive. If the associations are with galaxy groups, the observed frequency of warm absorbers ($d\mathcal{N}/dz$ = 3.5–5 per unit redshift) requires them to be very extended as an ensemble on the sky ($\sim$ 1 Mpc in radius at high covering factor). Most likely these warm absorbers are interface gas clouds whose presence implies the existence of a hotter ($T \sim 10^{6.5}$ K), diffuse and probably very massive ($> 10^{11}$ M$_\odot$) intra-group medium which has yet to be detected directly.

Subject headings: cosmological parameters—cosmology: observations—intergalactic medium—quasars: absorption lines—galaxies:halos—galaxies:spiral—galaxies:structure—ultraviolet: general

1. INTRODUCTION

On the basis of theoretical and observational considerations (e.g., Spitzer 1956; McGaugh et al. 2000; Pagel 2008) and numerical simulations (Klypin et al. 2001) a massive halo of gas is expected around every luminous late-type galaxy, otherwise these systems would be baryon deficient relative to dark matter (Klypin et al. 2001; Stocke et al. 2013). If present in spiral galaxy halos, these as yet undetected baryons could add considerably to the overall baryon inventory at $z \approx 0$, which has not yet been finalized (Fukugita, Hogan, & Peebles 1998; Bregman 2007; Shull et al. 2012). Additionally, while cosmological simulations find that the amount of gas accretion, both cold and hot, has declined by an order of magnitude since redshifts of 2–4 (Kereš & Hernquist 2009), there still needs to be sufficient infall in recent times to satisfy the constraints of the "G-dwarf problem" (Larson 1972; Pagel 2008) and to maintain the high star-formation-rates (SFR) in current day, massive spiral galaxies (Binney & Tremaine 1987; Chomiuk & Povich 2011).

On a larger scale, our Milky Way and virtually all large spirals are members of small groups of galaxies which may or may not be bound entities (Pisani, Ramella & Geller 2003; Berlind et al. 2006). Detailed studies of the Local Supercluster by Tully et al. (2009) concluded that there are virtually no isolated galaxies although more recently a few relatively isolated dwarfs have been located (Karachentseva, Karachentsev & Sharina 2010). Almost all galaxies in the Local Supercluster can be identified as members of bound groups and clusters or possibly unbound associations. Therefore, it is likely that the distinction between individual galaxy halos and a larger, intra-group medium in spiral-rich groups may be largely semantic; i.e., individual galaxy halos may merge to form a larger gas reservoir that could fill much or all of the volume of the group. Numerical simulations (Cen & Ostriker 1999; Davé et al. 1999) suggest that metal-enriched gas escaping from galaxies by supernova- and AGN-driven winds reaches distances of $\geq$ 1 Mpc and observations find that O VI absorbers (the most sensitive tracer of metal-enriched gas at low-z) extend $\sim$ 1 Mpc from the nearest L* galaxy (Tumlinson & Fang 2005; Stocke et al. 2006). However, the ultimate source, physical conditions and extent of this low-metallicity, halo/intra-group gas has not yet been identified and char-

acterized.

On the other hand, large reservoirs of low-metallicity ([Z] $\approx$ -0.5 solar) hot gas already are detected via thermal bremsstrahlung X-ray emission in groups and clusters of early-type galaxies (Sarazin 1988; Mulchaey 2000). The intra-cluster and intra-group gas contains a greater number of baryons than in the member galaxies and raises the baryon-to-dark matter ratio in groups and clusters to the cosmic mean (1:5; White et al. 1993). This suggests that these systems are "closed boxes" from an evolutionary perspective. However, only those clusters and groups sufficiently evolved dynamically to contain giant elliptical galaxies at or near their centers are detected in soft X-ray emission (Mulchaey 2000). Since no spiral-rich groups were detected in their large *ROSAT* survey of nearby groups of galaxies, Mulchaey et al. (1996) suggested that the intra-group gas in these systems is too cool to emit X-rays in sufficient numbers and energy to be detectable using current instruments. Using the observed scaling-relation between the X-ray determined gas temperature T_x and the group velocity dispersion σ_v, a factor of 5–30 cooler gas temperatures are predicted for spiral-rich groups based on their lower observed galaxy radial velocity dispersions of σ_v=100-300 km s^{-1} (Zabludoff & Mulchaey 1998; Mulchaey & Zabludoff 1998). Indeed, some of these groups may not even be fully gravitationally-bound much less virialized. Instead, Mulchaey et al. (1996) suggested that this $T \approx 10^6$ K gas would be most easily detected using absorption-line spectroscopy of background UV-bright sources. Given the expected temperature range for spiral group gas, the UV absorption doublet of O VI 1032, 1038 Å would be the most sensitive indicator. However, the fraction of oxygen which is in the quintuply-ionized state is small ($\leq$10%) in T $\geq 10^6$ K gas with most of the oxygen being in more highly-ionized states (O VII and O VIII), which are detectable in soft X-ray absorption lines. If imaging such sources of diffuse, very soft X-ray emitting gas were possible, then their physical extents, covering factors, densities, metallicities and temperatures could be measured. But this is not currently possible. Following Savage et al. (2014, Paper 1 hereafter) we will term this potential reservoir "warm gas" (T$\sim 10^{5-6}$ K), in contrast to cool (T$\sim 10^4$ K), photo-ionized gas and hot (T$\geq 10^6$ K) intra-group and cluster gas.

Since the original proposal of Bahcall & Spitzer (1969), it has been suspected that many of the multitude of absorption lines seen in the spectra of high-z QSOs are due to galaxy halos. The discovery of the low-z Lyα "forest" (Morris et al. 1991; Bahcall et al. 1991) with the *Hubble Space Telescope* (HST) offers us an opportunity to test these theoretical predictions for spiral galaxies and their environments. An FUV QSO absorption-line method for detecting this warm gas is feasible: Broad Lyα Absorbers (BLAs) with b-values $\geq$ 40 km s^{-1} corresponding to $T \geq 10^{5.0}$ K (Richter et al. 2004; Lehner et al. 2007; Danforth, Stocke & Shull 2010; Narayanan, Wakker & Savage 2009; Savage et al. 2010, and Paper 1) and the O VI 1032,1038 Å absorption doublet associated with these BLAs. But BLAs are very difficult to detect in low or even modest signal-to-noise (S/N) spectra (e.g., S/N $\leq$ 15) obtained with the Goddard High Resolution Spectrograph (GHRS) or the Space Telescope Imaging Spectrograph; (STIS; Lehner et al. 2007; Danforth, Stocke & Shull 2010; Tilton et al. 2012). Currently, HST's Cosmic Origins Spectrograph (COS; Green et al. 2012; Osterman et al. 2011) is routinely returning S/N $\geq$ 20 $R \approx$ 18,000 far-ultraviolet (FUV) spectra in the 1150-1750 Å band.

The COS Science Team has obtained S/N$\geq$ 20 FUV spectra of 14 bright QSOs for the purpose of conducting a sensitive spectroscopic survey, including searching for O VI absorption and BLAs (Paper 1 and Savage et al. 2010, 2011a; Savage, Lehner, & Narayanan 2011b) that could be associated with warm gas. Starting with 54 detected O VI absorption systems containing 85 individual O VI components, Paper 1 identified 54 possibly aligned O VI and Lyα components, out of which temperature measurements were possible for 45 of the 54. Of these forty-five, 31 (69%) show association with cool, photo-ionized gas; the remaining 14 aligned components have observed b-values which are indicative of T>10^5 K gas and are most likely collisionally-ionized. The O VI in the misaligned O VI components could be produced in warm collisionally-ionized or in cool photoionized-ionized gas. HST/COS is our first opportunity to study these unusual absorbers in some detail; for the most part the warm absorbers studied here are detected at too low a contrast to have been discovered and studied previously (but see Narayanan et al. 2010; Savage et al. 2010, 2011a; Savage, Lehner, & Narayanan 2011b, for early reports from this survey). Despite very high S/N ground-based optical spectra, similar BLA detections have not been made at $z \geq$2 owing to the density of the photo-ionized Lyα forest absorptions at those redshifts.

HST/STIS and COS already have provided the first detailed look at the cooler, metal-enriched clouds in galaxy halos at low redshift using H I absorption with log $N_{HI} \geq$ 14.0 cm^{-2} (all column densities herein will be quoted in cm^{-2}) and b-values of 20-30 km s^{-1} (all b-values will be quoted in km s^{-1}) and metal ion absorption in species such as C II, Si II, Si III, C III, Si IV, C IV, N V and O VI. Targeting specific galaxy halos at $z \sim 0.2$ with COS, Tumlinson et al. (2011) discovered log $N_{O\ VI} \geq$ 14.3 O VI absorption out to 150 kpc radius around late-type galaxies at high covering factor. While ion states lower than O VI are well-modeled as being in photo-ionization equilibrium (e.g., Werk et al. 2014), the ionization source for the O VI absorption associated with these cool clouds remains controversial (Tripp et al. 2008; Danforth & Shull 2008; Davé & Oppenheimer 2007). Stocke et al. (2006), Wakker & Savage (2009) and Prochaska et al. (2011a,b) used STIS archival spectra to make galaxy halo detections serendipitously. These studies showed that O VI absorption extends much further away from galaxies than the lower ions, as much as $\sim$ 1 Mpc away from $L \geq L^*$ galaxies, much farther than the virial radius of an L* galaxy (see Stocke et al. 2013 for the luminosity-determined virial radius values used herein). These stronger O VI systems are more readily detected in lower S/N COS spectra (e.g., Tumlinson et al. 2011) than the broad, shallow O VI associated with BLAs in the warm absorbers studied here and in Paper 1 in higher-S/N spectra. Often the much stronger, photo-ionized ab-

sorbers are present in the same absorber complex with BLAs and aligned O VI. It is the presence of the cooler clouds which ultimately sets the detectability of the warm absorbers in many cases rather than the raw S/N of the spectra.

Werk et al. (2013, 2014); Stocke et al. (2013); Keeney et al. (2013, 2014) and others have studied these cooler clouds using simple photo-ionization modeling to determine approximate physical conditions in cool halo clouds: $T \sim 10^4$ K; log n_{HI} = -3 to -4 cm^{-3} and metallicities ranging from $< 1\%$ solar to slightly super solar. These cloud conditions are inferred by assuming single phase, uniform density clouds in photo-ionization equilibrium with the extragalactic ionizing radiation field. Given the very high covering factors observed for the H I and metal-line absorption ($\sim 100\%$ inside the virial radius of late-type, $L \geq 0.1L^*$ galaxies; Prochaska et al. 2011a; Stocke et al. 2013), these clouds must be quite numerous with a very large total mass. Stocke et al. estimate a total mass in these clouds approaching 10^{10} $M_\odot$ for L^* galaxies, comparable to the mass in the parent galaxy disk. Werk et al. (2014) suggest an even larger mass in the photo-ionized clouds.

The O VI absorption lines usually are not included as constraints in this modeling because the O VI may not be photo-ionized in all cases (Davé & Oppenheimer 2007; Tripp et al. 2008; Danforth & Shull 2008; Smith et al. 2011; Shull et al. 2012). If the ubiquitous O VI absorption discovered by Tumlinson et al. (2011) is a shock-heated interface between these cool clouds and a hotter medium, then what is the nature of the hotter medium, its physical conditions, extent, total mass, metallicity and source? Based on the few, early warm absorber detections and the properties of the cool clouds, Stocke et al. (2013) hypothesized that this warm reservoir of halo gas could contain $\geq 10^{11}$ $M_\odot$ of gas. If this is correct, then, as with more virialized groups and clusters of galaxies, this warm halo gas could contain most of the baryons in the system.

Following the lead of Paper 1 (see also Savage et al. 2010, 2011a,b) we use BLA plus O VI absorption to investigate this warm halo gas in the light of the group gas hypothesis. In Section 2 and Appendix A we reanalyze a small fraction of the O VI plus H I absorbers presented in Paper 1 to determine a plausible *maximum* number of warm absorbers. The detailed component model fits for these few warm absorber candidates are shown in the Appendix A, for which a summary of results is provided at the end of Section 2.

In Section 3 the galaxy environment of the low-z warm absorbers is presented. Since the data in-hand comes from wide-field multi-object spectroscopy (MOS) on 4m-class telescopes, it is not exceptionally deep, limiting discussions of warm absorber environments to $z < 0.15$. A comparison between warm absorber environments and those in which cooler, photo-ionized absorbers are found also is presented. Sections 3.4 and 3.5 provide a summary of the inferences from the galaxy group analysis. Section 4 describes the major pieces of evidence that favor the hypothesis that these warm absorbers are the detection of a massive reservoir of gas in spiral galaxy groups. Section 5 summarizes the main results of this study. Throughout this paper we use the WMAP-9 cosmology with H_0= 70 km s^{-1} Mpc^{-1} (Hinshaw et al. 2013).

2. BROAD LYMAN ALPHA IN WARM GAS AT $T \geq 10^5$ K

Paper 1 presented an investigation of all 14 high-S/N COS FUV spectra obtained by the COS Science Team's Guaranteed Time Observations (GTO). These 14 sightlines were chosen to provide the highest quality FUV spectra in the shortest observing time. In these spectra Paper 1 identified 14 potential warm absorbers defined as having inferred temperatures T $\geq 10^5$ K based on their Lyα and O VI thermal line widths in systems for which the H I and O VI absorptions are aligned in velocity. The thermal (T) and non-thermal (NT) widths of these absorption lines were determined from the observed H I and O VI line widths by assuming that the NT width is independent of species while the T width is inversely proportional to the square root of atomic weight. Also these different species must arise in the same parcel of gas, an assumption allowed for but not demanded by their alignment in velocity. For this type of analysis to be robust, several species, not just H I and O VI, are required, but are generally not available.

One physical source of line-broadening not specifically addressed in Paper 1 is Hubble flow broadening. Because later in this paper we will propose that these warm absorbers might be associated with groups of galaxies requiring their physical extents to be ~ 1 Mpc, significant Hubble flow broadening could be present if the associated galaxy groups are not gravitationally-bound. As with other NT broadening mechanisms, if Hubble flow were important it would require near equality of H I and O VI b-values (as well as for other species detected) and so would be taken into account in the analysis of Paper 1. A few of the identified "warm absorber" systems do have significant b_{NT} values, which could be Hubble broadening but this does not alter the temperature determinations found herein.

Paper 1 also identifies two broad O VI absorbers without associated Lyα absorption, PKS 0405-123/0.16716 (Savage et al. 2010) and PHL 1811/0.13280 (Paper 1; Figure 10d) which are likely warm absorbers (throughout this paper we identify a particular absorber by its sightline/redshift). Although they do not meet the selection criteria adopted in Paper 1 because a BLA is not detected, their inferred T $\geq 10^5$ K makes these probable warm absorbers. Except for the few potential warm absorbers described here and reanalyzed in Appendix A, we adopt the classification of the other ~ 30 H I + O VI absorbers from Paper 1 as "cool" photo-ionized absorbers and "misaligned" H I Lyα/O VI absorbers.

Here we adopt a complementary tactic in reanalyzing a *few* of the Paper 1 potential warm absorbers by starting with the O VI line profile and width, which is often less confused by lower temperature (i.e., cool, photo-ionized) absorption than the BLA. If the O VI data comes from COS, then the S/N is usually sufficient to determine if the profile is symmetrical enough to be well-fit with a single Gaussian profile. In some cases where H I Lyα is detected by COS at low-redshift ($z < 0.12$), the O VI lines are in the spectroscopic band covered by the *Far Ultra-violet Spectroscopic Explorer* (FUSE) satellite; for these 14 very bright targets FUSE spectra often possess the quality to permit such an assessment as well. We do **not** reanalyze those absorbers with complex O VI line

Table 1
O VI Absorbers Reanalyzed Here

Sight Line	$z_{\rm abs}$	aligned?	new fit	Comments
PKS 2155−304	0.05722	NO	NO	Lyα complex; possible O VIII absorption
3C 273	0.09010	NO	Fig. 12	probable red wing to Lyα
PG 1116+215	0.13850	YES	Fig. 13	$b_{NT} \gg b_{thermal}$ suggested by Paper 1
PHL 1811	0.17651	NO	NO	
H 1821+643	0.17036	NO	NO, Fig. 15	O VI absorption very weak
Ton 236	0.19457	YES	Fig. 16	broad absorber location uncertain
HE 0153−4520	0.40052	YES	NO	
PKS 0405−123	0.09657	YES	NO	O VI association with broad or narrow H I ?
PKS 0405−123	0.29770	YES	Fig. 17	
3C 263	0.11389	NO	NO	BLAs without associated O VI

profiles, arguing that in these cases there is ample evidence for considerable turbulent or component motion. However, for those O VI absorbers well-fit with a single, smooth Gaussian component, we assume that the observed O VI width is almost entirely thermal. While this is not guaranteed, it would be quite unlikely (but not impossible) for turbulent or component motion to mimic a single Gaussian profile. We then determine whether the Lyα profile is consistent with a broader, thermal Gaussian profile at a velocity consistent with the O VI thermal width. An alignment between the BLA and the O VI absorption and log T(K) $\geq$ 5.0 are required for an absorber identification as "warm". In some cases the S/N is insufficient to make this determination while in others a symmetric Gaussian is not a good fit to the O VI profile or the O VI does not align with the BLA. In these cases we do not attempt a reanalysis and we adopt the spectral fits presented in Paper 1 as final. In fact, all line-fits derived in Paper 1 are fully acceptable but, owing to blends of broad, shallow components and saturated cool components, the Lyα line widths and velocity centroids are uncertain in some cases.

We emphasize that the Lyα line fits, whether in Paper 1 or herein, are inherently uncertain due to the complex superposition of "warm" and "cool" components to the absorption. And in some cases the uncertainties in the temperature estimates are large, although almost all absorbers classified as "warm" are unambiguously at log T(K) $\geq$ 5.0.

Scrutiny of the O VI absorbers in Paper 1 finds only seven cases where a reanalysis is suggested by the O VI line profile (see Table 1). In these cases the O VI absorption profile is symmetric but Paper 1 identified a large proportion of the line width as NT or did not find a corresponding Lyα component aligned with the O VI. Table 1 contains the identification of these seven absorbers by sightline and redshift, listing b-values, whether the Lyα and O VI components are aligned in velocity as determined in Paper 1, whether a new fit is presented herein and whether a new warm absorber is proposed. The intent of these reanalyses is to determine if more warm absorbers *could* be present in this sample if a different approach to the line-fitting is performed. These reanalyses were performed by an independent set of co-authors (JTS, CWD) from the analysis in Paper 1.

To this list we have added three absorbers which were not classified as broad, symmetric and aligned by Paper 1, PKS 2155-304/0.05722, PG 1116+215/0.13850 and 3C 263/0.11389. The former absorber has a tentative O VIII absorption detection in a *Chandra ACIS/LETG* grating spectrum (Fang, Canizares, & Yao 2007) indicative of warm gas if the O VIII absorption is real. The second absorber possesses a very symmetric O VI line profile and weak broad wings to Lyα, which were ascribed to non-thermal motion in Paper 1. The third absorber has a BLA that appears to be consistent in its large b-value between Lyα and Lyβ but has no associated O VI. The detailed reanalysis of each of these absorbers can be found in Appendix A, from which we now summarize the results.

Our reanalysis found that in six cases there was no reasonable alternative to the model solutions found by Paper 1, so that for these six absorbers and all others not reanalyzed, we adopt the model solutions presented in Paper 1 (see Table 2 and Paper 1, Table 5 for a list of the warm absorbers in order of their quality). An updated solution is suggested only for four absorbers, which are presented in Table 3 and summarized below.
(1) In the case of 3C 273/0.09010 a fourth Lyα component aligned with the O VI was added but with poorly constrained b-values. For our best-fit result, the b-values derived suggest that a warm absorber probably is present.
(2) For PG 1116+215/0.13850 our reanalysis finds that a much broader fit to Lyα is plausible, which is a better match to the broad, symmetric O VI profile. This new solution obviates the need for an absorber model which is dominated by NT motions despite having O VI 1032, 1038 Åline profiles which are demonstrably smooth and symmetric to the limits of the COS signal-to-noise. In this new model the broad absorber has line profiles which are dominated by thermal broadening and a high value of log T(K)=5.6.
(3) For Ton 236/0.19457 a viable, alternative fit is suggested which does not differ significantly from the results of Paper 1 and the presence of a single "warm absorber" is confirmed but with a hotter temperature (log T(K)=5.8) than the Paper 1 solution.
(4) For PKS 0405-123/0.29770 we have found that a very broad Lyα absorber aligned with the broad O VI absorption can be fit to the data. Thus, we consider the existence of this warm absorber at log T(K)=5.7 as probable.

In addition, for the 3C 263/0.11389 absorber we confirm the detailed fits in Paper 1 but also find that a warm absorber is possibly present based on a smooth, symmetric BLA detected consistently in Lyβ (i.e., both line-fits yield consistent column densities and b-values). There is no detection of O VI absorption coincident with this

Table 2
Properties of Collisionally-Ionized "Warm Absorbers"

Sight Line	$z_{\rm abs}$	$\log N_{\rm HI}$ ($\rm cm^{-2}$)	$b_{\rm HI}$ ($\rm km\ s^{-1}$)	$\log N_{\rm OVI}$ ($\rm cm^{-2}$)	$b_{\rm OVI}$ ($\rm km\ s^{-1}$)	$\log T$ (K)
HE 0153−4520	0.22600	13.58 ± 0.05	151 ± 15	14.23 ± 0.01	37 ± 1	$6.14^{+0.08}_{-0.10}$
Mrk 290	0.01027	14.38 ± 0.01	53 ± 2	13.65 ± 0.10	31 ± 10	$5.07^{+0.13}_{-0.19}$
H1821+643	0.26656	13.64 ± 0.02	46 ± 2	13.61 ± 0.03	24 ± 2	$4.99^{+0.05}_{-0.06}$
3C 263	0.14072	13.47 ± 0.10	87 ± 15	13.60 ± 0.09	33 ± 12	$5.62^{+0.15}_{-0.24}$
PKS 0405−123	0.49507	14.14 ± 0.03	51 ± 5	14.31 ± 0.02	32 ± 2	$5.00^{+0.12}_{-0.18}$
Mrk 876	0.00315	14.00 ± 0.02	58 ± 2	13.38 :	35 :	$5.14^{+0.16}_{-0.25}$
3C 273	0.00336	13.54 ± 0.10	64 ± 7	13.39 ± 0.08	43 ± 10	$5.16^{+0.20}_{-0.38}$
PHL 1811	0.15785	13.25 ± 0.04	97 ± 10	13.68 ± 0.03	31 ± 3	$5.73^{+0.09}_{-0.11}$
HE 0226−4110	0.20701	13.45 ± 0.16	100 ± 25	14.37 ± 0.01	36 ± 1	$5.75^{+0.20}_{-0.37}$
H 1821+643	0.22497	13.94 ± 0.17	95 ± 11	14.25 ± 0.01	45 ± 1	$5.65^{+0.11}_{-0.15}$
H 1821+643	0.12141	13.80 ± 0.05	82 ± 7	13.69 ± 0.04	58 ± 7	$5.33^{+0.15}_{-0.24}$
PHL 1811	0.07773	13.60 ± 0.07	82 ± 10	13.53 ± 0.08	43 ± 7	$5.49^{+0.13}_{-0.19}$
HE 0238−1904	0.47204	13.83 ± 0.03	47 ± 4	14.16 ± 0.01	20 ± 1	$5.06^{+0.08}_{-0.10}$
H 1821+643	0.17035	13.65 ± 0.01	54 ± 2	13.20 ± 0.22	31 ± 2	$5.10^{+0.14}_{-0.22}$
PKS 0405−123	0.16716	... [a]	...	13.85 ± 0.01	56 ± 2	> 6.1
PHL 1811	0.13280	... [b]	...	13.57 ± 0.03	25 ± 2	~ 5.7

[a] HI non-detection
[b] Marginally detected

Table 3
Properties of Probable Collisionally-Ionized "Warm Absorbers"

Sight Line	$z_{\rm abs}$	$\log N_{\rm HI}$ ($\rm cm^{-2}$)	$b_{\rm HI}$ ($\rm km\ s^{-1}$)	$\log N_{\rm OVI}$ ($\rm cm^{-2}$)	$b_{\rm OVI}$ ($\rm km\ s^{-1}$)	$\log T$ (K)
3C 273	0.09010	13.23 ± 0.02	49 ± 3	13.0 ± 0.3	20 :	≈ 5.1
PG 1116+215	0.13850	13.6 ± 0.1	86 ± 11	13.8 ± 0.1	35 ± 5	$5.6^{+0.1}_{-0.2}$
Ton 236	0.19457	13.7 ± 0.1	90 ± 9	13.6 ± 0.2	40 ± 17	$5.8^{+0.2}_{-0.3}$
PKS 0405−123	0.29770	13.15 ± 0.10	100 ± 10	13.55 ± 0.10	57 ± 4	$5.7^{+0.1}_{-0.2}$

Table 4
Properties of Photo-Ionized "Cool Absorbers"

Sight Line	$z_{\rm abs}$	$\log N_{\rm HI}$ ($\rm cm^{-2}$)	$b_{\rm HI}$ ($\rm km\ s^{-1}$)	$\log N_{\rm OVI}$ ($\rm cm^{-2}$)	$b_{\rm OVI}$ ($\rm km\ s^{-1}$)	$\log T$ (K)
PG 0953+414	0.00212	13.15 ± 0.03	38 ± 3	13.60 ± 0.06	43 ± 8	< 4.5
HE 0226-4110	0.01750	13.20 ± 0.04	27 ± 4	13.91 ± 0.16	10 ± 6	$4.61^{+0.14}_{-0.22}$
H 1821+643	0.02443	14.24 ± 0.01	29 ± 1	13.42 ± 0.09	23 ± 7	$4.30^{+0.31}_{-0.30}$
PG 1259+593	0.04625	15.30 ± 0.20	30 ± 1	13.90 ± 0.10	40 ± 13	< 4.80
PG 1259+593	0.04625	14.70 ± 0.20	25 ± 10	13.70 ± 0.15	17 ± 8	$4.50^{+0.50}_{-0.30}$
PG 1116+215	0.05897	13.57 ± 0.01	33 ± 2	13.49 ± 0.05	27 ± 16	$4.36^{+0.54}_{-0.36}$
PG 0953+414	0.06808	14.34 ± 0.05	19 ± 1	14.29 ± 0.03	12 ± 1	$4.14^{+0.11}_{-0.14}$
3C 273	0.12007	13.50 ± 0.01	23 ± 1	13.38 ± 0.02	10 ± 2	$4.44^{+0.06}_{-0.07}$
PG 0953+414	0.14231	13.57 ± 0.01	26 ± 1	14.09 ± 0.01	19 ± 1	$4.21^{+0.08}_{-0.10}$
PG 0953+414	0.14213	13.47 ± 0.01	29 ± 1	13.60 ± 0.03	29 ± 4	< 4.25
HE 0153-4520	0.14887	13.26 ± 0.03	34 ± 4	14.02 ± 0.01	25 ± 1	$4.53^{+0.18}_{-0.32}$

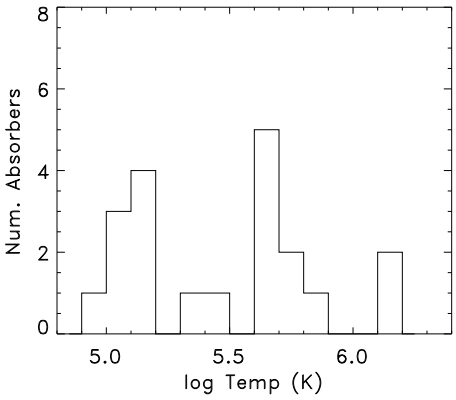

Figure 1. The Inferred Temperatures for the 20 Warm Absorbers in the COS High-S/N Survey. The errors bars on the log T values are typically 0.1-0.3 dex (see Tables 2 and 3).

BLA.

With these revisions there is a net gain of three warm absorbers to the BLA + broad O VI list. By including the two O VI-only absorbers from Paper 1 (PHL 1811/0.13280 and PKS 0405-123/0.16716) as also being probably warm, a total of as many as 20 warm absorbers can be present in this sample. (The possible warm absorber, 3C 263/0.11389, is not included in this tally). The distribution of temperature values for the 20 members of the COS/GTO warm absorber sample is shown in Figure 1. Unlike the initial discovery of the O VI-only system PKS 0405-123/0.16716 (Savage et al. 2010), most of the derived temperatures are below T$\sim 10^6$ K. Tables 2 and 3 provide the basic observational data for all of the warm absorbers in this sample. Table 2 compiles the spectral data from Paper 1 for the warm absorbers for which we have adopted the Paper 1 line-fits. Table 3 lists the same information for the warm absorbers for which this paper supplies revised line-fits (see Appendix A). Table 4 provides the same observational data for the sample of low-z "cool", photo-ionized absorbers which are used for statistical purposes herein (11 from Paper 1 and two, PG 1259+593/0.04625a and b, added from another high-S/N COS spectrum and which is described in Danforth et al. (2014)).

Due largely to the presence of narrow Lyα and O VI components that are plausibly cool halo clouds and their shocked interfaces (Tumlinson et al. 2011; Stocke et al. 2013) and due somewhat to the limited S/N of the COS spectra, we cannot dismiss the possibility that very low contrast, very broad ($b > 100$ km s^{-1}) Lyα lines are present in some of these absorber complexes. We can state that their presence is neither required by the constraints of the O VI and Lyα line fits of Paper 1 nor by the reanalysis in the Appendix. But as the very high S/N COS spectra of 3C 273, PKS 2155-304 and PKS 0405-123 show, it is the presence of the cooler component absorption, not the S/N, which is the major hindrance in discovering more warm absorber systems. These limitations are difficult to quantify, so we make no attempt to do so. Rather we determine the total pathlength for discovering warm absorbers using a simplified calculation set by the S/N of the COS spectra alone.

The pathlength (δz) for warm absorber discovery is estimated using the entire redshift path of the 14 QSOs observed in this program minus the obscuration created by the Galactic damped Ly α line plus the high and low ionization metal lines that arise in the Galactic disk or halo. In this case we obtain a $\delta z = 4.0$ (see Danforth et al. 2014) and the number of warm absorbers per unit redshift, $d\mathcal{N}/dz$ = 3.5–5 based on the range in the number of warm absorbers in these 14 sightlines: 14 proposed by Paper 1; 20 by this paper. This is approximately 4 times the $d\mathcal{N}/dz$ for Mg II/Lyman limit system absorbers, which are thought to be optically-thick clouds in extended galaxy halos of radius ~ 100 kpc with high covering factors (Steidel 1995; Churchill et al. 2000; Kacprzak et al. 2010, 2011). If the warm absorbers also are associated only with luminous galaxies similar to the Mg II absorbers, their numbers suggest an absorber size of ~ 200 kpc, comparable to the virial radius of an L* galaxy. As with the class of Mg II absorbers this inference needs to be confirmed by detecting galaxies associated with these warm absorbers. Luckily the combination of HST/COS and *FUSE* UV spectroscopy provides some detections at very low redshift by historical absorption line standards (i.e., $z \leq 0.15$) whose fields can be searched for associated galaxies.

3. GALAXY GROUPS ASSOCIATED WITH O VI ABSORBERS

In order to determine the galaxy environment of the warm and cool absorbers (see Tables 2, 3 & 4 for a summary of observed properties of the warm and cool absorbers considered here), we have used a combination of large-area redshift surveys like the Sloan Digital Sky Survey (SDSS) and the 2dF survey done at the Anglo-Australian Telescope (AAT) and our own multi-object spectroscopy (MOS) program centered on the sightlines observed by the COS Science Team. Stocke et al. (2006, 2013) contains a description of our use of the large-area sky survey redshift catalog, which includes targeted observations made by others of specific sightlines in this survey (e.g., Morris et al. 1993; Tripp et al. 1998; Chen & Mulchaey 2009; Prochaska et al. 2011b; Johnson, Chen & Mulchaey 2013). Our new observations include all but one of the 14 sightlines in Paper 1 and extend $\sim$ 2–3 magnitudes deeper than the SDSS (Keeney et al. 2014); the H 1821+643 field has not yet been observed by our survey because the target was observed with COS only recently (the only galaxy redshift observations in this region were reported by Tripp et al. (1998) and have a somewhat uncertain depth and breadth reported). For these 14 sightlines spectra and redshifts were obtained mostly at the Wisconsin-Indiana-Yale-NOAO (WIYN) 3.5-m telescope using the HYDRA MOS. Additional observations of southern targets were obtained at the Cerro-Tololo Inter-American Observatory's (CTIO) 4m Blanco Telescope using the version of HYDRA available there. A few additional southern targets were observed at the AAT using the AAOmega MOS system. Occasional long-slit spectra of galaxies nearest to absorbers were obtained at the Apache Point Observatory (APO) 3.5m telescope using the Dual-Imaging Spectrograph (DIS). Individual galaxy redshifts from this survey have typical velocity errors of $\pm$ 30 km s^{-1}.

The MOS grating setup was selected to obtain good

Table 5
Galaxy Groups Associated with Warm O VI Absorbers

Sight Line	$z_{\rm abs}$	$L_{\rm ng}$ (L^*)	$\rho_{\rm ng}$ (kpc)	$\rho_{\rm ng}/R_{\rm vir}$	$\Delta v_{\rm ng}$ (km s^{-1})	$L_{\rm grp}$ (L^*)	$N_{\rm grp}$	$\rho_{\rm grp}$ (kpc)	$\rho_{\rm grp}/R_{\rm vir}$	$\Delta v_{\rm grp}$ (km s^{-1})	$\sigma_{\rm grp}$ (km s^{-1})	$\sigma_{\rm vir}$ (km s^{-1})	$L_{\rm comp}$ (L^*)
Mrk 876	0.00315	0.25	188	1.65	−34	0.30	4	279	0.93	−4	90	104	0.019
3C 273	0.00336[a]	0.021	77	1.20	−108	32	161	525	0.37	537	500^{+40}_{-50}	491	< 0.001
Mrk 290	0.01027	1.7	434	2.00	−69	6.0	24	814	1.00	302	270^{+80}_{-110}	282	0.011
PHL 1811	0.07773[b]	0.94	310	1.75	−22	55	126	410	0.24	333	630^{+110}_{-120}	591	0.060
H 1821+643	0.12141	2.3	158	0.65	34	···	···	···	···	···	···	···	0.19 (659) / 1.2
PHL 1811	0.13280	3.0	227	0.87	−48	26	30	1114	0.85	568	440^{+190}_{-200}	458	0.19
PG 1116+215	0.13850	1.5	138	0.67	−55	3.8	4	568	0.81	−9	50	242	0.33
3C 263	0.14072	1.7	620	2.88	39	···	···	···	···	···	···	···	0.34

[a] The closest group galaxy to the QSO sight line is a $0.005\,L^*$ galaxy at $\rho = 46$ kpc ($0.89\,R_{\rm vir}$), but it has a large velocity separation of $\Delta v = 610$ km s^{-1} with respect to $z_{\rm abs}$ (Stocke et al. 2004).

[b] The closest group galaxy to the QSO sight line is a $0.70\,L^*$ galaxy at $\rho = 35$ kpc ($0.22\,R_{\rm vir}$), but it has a large velocity separation of $\Delta v = 904$ km s^{-1} with respect to $z_{\rm abs}$ (Jenkins et al. 2003).

Table 6
Galaxy Groups Associated with Cool O VI Absorbers

Sight Line	$z_{\rm abs}$	$L_{\rm ng}$ (L^*)	$\rho_{\rm ng}$ (kpc)	$\rho_{\rm ng}/R_{\rm vir}$	$\Delta v_{\rm ng}$ (km s^{-1})	$L_{\rm grp}$ (L^*)	$N_{\rm grp}$	$\rho_{\rm grp}$ (kpc)	$\rho_{\rm grp}/R_{\rm vir}$	$\Delta v_{\rm grp}$ (km s^{-1})	$\sigma_{\rm grp}$ (km s^{-1})	$\sigma_{\rm vir}$ (km s^{-1})	$L_{\rm comp}$ (L^*)
PG 0953+414	0.00212	0.025	227	3.44	−31	1.5	13	722	1.40	−14	130 ± 80	179	< 0.001
HE 0226–4110	0.01750	2.8	596	2.32	98	25	21	911	0.69	−101	480^{+120}_{-160}	456	0.003 (643) / 0.15
H 1821+643	0.02443	1.7	1255	5.75	40	3.7	4	1260	1.82	72	240	241	0.008 (148) / 0.048 (891) / 1.2
PG 1259+593	0.04625	0.50	138	0.96	−3	9.6	23	352	0.37	34	350^{+100}_{-170}	329	0.032 (1095) / 0.24
PG 1116+215	0.05897	0.13	131	1.40	297	9.3	16	334	0.36	340	230^{+50}_{-80}	326	0.053 (1376) / 0.49
PG 0953+414	0.06808	0.88	607	3.50	306	8.4	14	913	1.01	318	290^{+70}_{-120}	316	0.072 (1572) / 0.63
3C 273	0.12007	6.2	2119	6.36	−99	11	4	2009	2.10	19	80	346	0.42 (1306) / 2.0
PG 0953+414	0.14231	4.7	438	1.43	128	9.5	6	331	0.35	123	270	329	0.35
HE 0153–4520	0.14887	2.5	1081	4.37	227	3.5	3	1084	1.60	210	145	235	0.24

Table 7
Galaxy Groups Associated with Misaligned O VI Absorbers

Sight Line	$z_{\rm abs}$	$L_{\rm ng}$ (L^*)	$\rho_{\rm ng}$ (kpc)	$\rho_{\rm ng}/R_{\rm vir}$	$\Delta v_{\rm ng}$ (km s^{-1})	$L_{\rm grp}$ (L^*)	$N_{\rm grp}$	$\rho_{\rm grp}$ (kpc)	$\rho_{\rm grp}/R_{\rm vir}$	$\Delta v_{\rm grp}$ (km s^{-1})	$\sigma_{\rm grp}$ (km s^{-1})	$\sigma_{\rm vir}$ (km s^{-1})	$L_{\rm comp}$ (L^*)
Mrk 876	0.01169	0.10	266	3.03	11	···	···	···	···	···	···	···	0.26
PKS 2155–304	0.05422[a]	3.7	544	1.95	−91	17	8	380	0.33	648	340^{+70}_{-210}	403	0.087 (636) / 0.13
PKS 2155–304	0.05722	3.0	429	1.65	−176	17	8	380	0.33	−205	340^{+70}_{-210}	403	0.097 (669) / 0.14
3C 263	0.06342	0.21	63	0.58	−56	···	···	···	···	···	···	···	0.062 (1472) / 0.30
3C 273	0.09010	1.9	478	2.14	−110	24	13	1833	1.43	89	560^{+60}_{-190}	445	0.24 (1014) / 1.1
PKS 0405–123	0.09192	0.020	72	1.14	104	0.41	5	115	0.35	−155	210	115	0.004 (500) / 0.14
3C 263	0.11389	1.2	982	5.08	318	4.8	7	958	1.27	245	270	262	0.21

[a] This absorber and the absorber at $z = 0.05722$ in the PKS 2155–304 sight line are associated with the same group of galaxies. The closest galaxy to the higher redshift absorber is the galaxy with the smallest impact parameter from this absorber, but it has a large velocity difference of $\Delta v = 677$ km s^{-1}.

throughput just long-ward of 4000 Å so that Ca II H & K might be detectable even for faint and diffuse targets at low redshift. At WIYN the 60′ field-of-view (FoV) corresponds to 6.7 Mpc at $z = 0.1$ and so is excellent for determining the large-scale environment of low-z absorbers. The FoVs at the CTIO 4m (40′ = 4.5 Mpc at $z = 0.1$) and at the AAT (120′ = 13.4 Mpc at $z = 0.1$) are also good matches to this goal. The > 90% completeness magnitude for our observations at WIYN/HYDRA (in approximately two-hour exposure times) is $g = 20$. The 90% completeness limit at AAT/AAOmega is $g = 20.5$, but CTIO's HYDRA system is less efficient than its counterpart at WIYN, with the CTIO observations being 90% complete to $g = 19$. A $g = 20$ mag limit corresponds to $0.16\,L^*$ at $z = 0.1$ and $1.2\,L^*$ at $z = 0.25$. Since it is necessary to find other associated galaxies at least 2 magnitudes fainter than L^* in order to determine with some confidence if a small galaxy group is present or not, this 4m MOS survey is excellent for determining details of the galaxy environments only at $z \leq 0.10$. And it will provide some preliminary information for $0.10 \leq z \leq 0.15$, but little detail in most cases at $z > 0.15$. Details of the wide-angle 4-m galaxy survey work can be found in Keeney et al. (2014).

3.1. *Procedure for Defining Groups of Galaxies Associated with Absorbers*

In this discussion and throughout this paper we use the term "galaxy group" to describe the large-scale (2-5 Mpc) galaxy environment of the absorbers studied here. We have defined these groups entirely by the observational properties provided by individual galaxy redshifts and sky locations using a "friends-of-friends" (FoF) approach similar to that employed by Berlind et al. (2006, 2008) using the SDSS data; i.e., we do not require detections of soft X-ray bremsstrahlung, which occurs only in elliptical-dominated groups (Mulchaey 2000), nor a theoretically-inferred dark matter halo mass threshold. Indeed, most of the groups we have found do not contain early-type galaxies nor are they known sources of diffuse, soft X-ray emission but rather these groups are similar in galaxy content to spiral-rich groups found in the Local Supercluster (e.g., the M101/M51 group or the M96 group; see Section 3.2). Our use of the term "galaxy group" does not necessarily imply that these physical entities are either bound or virialized. Using standard crossing time arguments (Pisani, Ramella & Geller 2003; Berlind et al. 2006), the velocity dispersions measured for these groups are sufficient for only one or two crossing times in a Hubble time. Further, many of these groups do not have Gaussian-distributed velocity distributions and physical locations required for such arguments to be robust (see the velocity distributions and galaxy locations for these groups in Figures 2, 3 & 4). Therefore, by using the term "galaxy group", we imply only that these absorbers are surrounded by large and small galaxies in their vicinity, for which we have measured velocity distributions whose dispersions provide characteristic kinetic energies to which the gas kinetic energies can be compared using the COS-observed line-widths. Deeper spectroscopic observations for many of these groups are underway to further characterize the group memberships and velocity distributions; present observations limit a detailed discussion of group properties to all absorbers at $z \leq 0.10$ and a few others out to $z \leq 0.15$, based on the depth to which galaxy surveys have been completed in those regions.

Tables 5, 6 & 7 list the basic characteristics of nearest galaxies and galaxy groups found around the QSO sightlines at the redshifts of the absorbers. For each absorber in these tables the galaxy group was identified and its membership defined using an FoF analysis (e.g., Berlind et al. 2006). Table 5 lists the galaxy environment data for the warm absorbers at $z \leq 0.15$. Similar data are shown in Table 6 for absorbers judged to be in photo-ionization equilibrium (i.e., "cool" absorbers at $\log T(K) < 5.0$) and Table 7 for absorbers whose Lyα and O VI absorption lines are "misaligned" so that no unambiguous model can be constructed for these absorbers (see Paper 1 for details). Information in these Tables includes (in columns 1 & 2) the sightline and absorber redshift; (3) the nearest galaxy luminosity (L_{ng}) in L* units; (4) the impact parameter (ρ) to the nearest galaxy in kpc; (5) the impact parameter as a fraction of the virial radius of the nearest galaxy (R_{vir}). The virial radii for the nearest galaxies are calculated using the "halo matching" scaling between luminosity and virial radius due to Moster et al. (2013) as shown in Figure 1 of Stocke et al. (2013); (6) the velocity difference between the absorber and the nearest galaxy (Δv_{ng}) in km s^{-1} ($\pm$ 30 km s^{-1}); (7) the integrated group luminosity using all group galaxies observed (L_{grp}) in L* units; (8) the number of galaxies in the group (N_{grp}); (9) the impact parameter (ρ_{grp}) to the group centroid in kpc; (10) the group impact parameter in units of the virial radius (R_{vir}). The virial radii for the galaxy groups were calculated using $M_{\rm grp}/L_{\rm grp} = 500\,(M/L)_{500}$ in solar units, which is close to the mean value for groups of the richness found (see discussion below); (11) the velocity difference between the absorber and the group mean velocity (Δv_{grp}) in km s^{-1} ($\pm$ 30 km s^{-1}); (12) the group velocity dispersion (σ_{grp} and its associated error; see detailed discussion below) in km s^{-1}. Values and errors are listed for all groups with $N_{grp} \geq 8$. Single valued estimates are made for groups with $N_{grp} \geq 3$ (see detailed discussion below); (13) a second estimate of the group velocity dispersion assuming that the observed group is virialized using the procedure of Bryan & Norman (1998, see detailed discussion below); and (14) the galaxy survey >90% completeness limit (L_{comp}) in L* units at the absorber redshift out to 2 Mpc radius from the sightline.

The velocity differences between absorbers and galaxies (column 6) or groups (column 11) are computed as follows: $\Delta v = c(z - z_{abs})/(1 + z_{abs})$. Due to the range in redshifts and the variation in galaxy survey work along these sightlines, the completeness limits (column 14) can vary substantially. In some cases the completeness luminosity is a function of impact parameter; e.g., the H 1821+643/0.12141 field has deeper MMT/MOS close to the sightline as reported by Tripp et al. (1998). In these cases the completeness luminosity is listed with its associated impact parameter (in kpc) in parentheses and the narrow/deep survey limit separated from the broad/shallow survey limit by a "/" in column (14).

Our group finding algorithm has several steps. In each case we start with a catalog of all galaxies within $\pm$1000 km s^{-1} of the absorber redshift with impact pa-

rameters ≤ 2 Mpc from the QSO sight line. Then we use an FoF algorithm to search for galaxies associated with the closest galaxy to the QSO sight line. In our FoF algorithm each galaxy has individualized linking lengths equal to $5R_{\rm vir}$ on the sky and five times larger than that in velocity space to match the relative scalings between the plane-of-the-sky linking length and the redshift linking length ($l_{\rm sky}$ and l_z) from Berlind et al. (2006). In order to make sure that we have investigated a large enough volume around the absorber to locate all group members, we proceed as follows. We assume that all of our potential groups have $M_{\rm grp}/L_{\rm grp} = 500\,(M/L)_{500}$ in solar units, which provides a scaling relation between a group's luminosity and its radius and velocity dispersion (this mass-to-light ratio is close to the median value for the groups we have found (see analysis associated with Figure 1 in Stocke et al. 2013)). Using the preliminary group luminosity, L_{grp}, we then estimate the "virialized" group radius and velocity dispersion using:

$$R_{\rm grp} = \left(\frac{3M_{\rm grp}}{4\pi\Omega_{\rm m}\Delta^0_{\rm vir}\rho_{\rm crit}}\right)^{1/3} = 446\left(\frac{M}{L}\right)^{1/3}_{500}\left(\frac{L_{\rm grp}}{L^*}\right)^{1/3}\ {\rm kpc} \quad (1)$$

$$\sigma_{\rm vir} = \sqrt{\frac{GM_{\rm grp}}{2R_{\rm grp}}} = 155\left(\frac{M}{L}\right)^{1/3}_{500}\left(\frac{L_{\rm grp}}{L^*}\right)^{1/3}\ {\rm km\,s^{-1}}, \quad (2)$$

where we have assumed $\Omega_m = 0.282$ (Hinshaw et al. 2013), $\Delta^0_{\rm vir} \equiv \Delta_{\rm vir}(z = 0) = 350$ (Bryan & Norman 1998), and $\rho_{\rm crit} = 9.205 \times 10^{-30}\,h^2_{70}$ g cm^{-3} (Shull et al. 2012). Since all of our groups have $z_{\rm grp} < 0.15$, we ignore any evolution of $\Omega_{\rm m}$ or $\Delta_{\rm vir}$ with redshift. While we make no correction in this calculation to account for galaxies with luminosities below our completeness limit, such a correction is small in all cases for which there are sufficient group galaxies identified to quote reliable velocity disperisons ($N_{grp} \geq 8$). Values calculated using equation (2) above are listed in column (13) of Tables 5, 6 and 7. After the values of $R_{\rm grp}$ and $\sigma_{\rm vir}$ are calculated, we check to ensure that our search volume is large enough to include $\pm 5\sigma_{\rm vir}$ from the group redshift and $2.5R_{\rm grp}$ from the group center. If it is not, then we expand the search volume, determine a new FoF group with updated values of $R_{\rm grp}$ and $\sigma_{\rm vir}$, and iterate until our search volume satisfies these criteria.

Once this process is complete we use the FoF group as the first step in an iterative procedure within the final search volume to define the final group membership. At each step we determine the group's center on the sky and in redshift space and identify all galaxies (i.e., not just those identified as members in the previous step) within $\pm 3\sigma_{\rm vir}$ of the group redshift and $1.5R_{\rm grp}$ of the group center as being group members. We then repeat this process until the group membership does not change from one iteration to the next. Usually the group membership converges in ≤ 3 iterations.

We have utilized the robust statistics described in Beers, Flynn & Gebhardt (1990) to minimize the effect of potentially spurious group members on the physical quantities of interest for our groups. The geometric center of the group on the sky and the group redshift are determined using the bi-weight location estimator, and the group's velocity dispersion ($\sigma_{\rm grp}$) is calculated using the "gapper" scale estimator (Beers, Flynn & Gebhardt 1990), which involves ordering the recession velocities $v_i = cz_i/(1 + z_{\rm grp})$ from smallest to largest and defining weights, w_i, and gaps, g_i, such that:

$$w_i = i\,(N_{\rm grp} - i) \qquad (3)$$
$$g_i = v_{i+1} - v_i, \qquad i = 1, 2, ..., N_{\rm grp} - 1.$$

The rest-frame velocity dispersion of the group is then:

$$\sigma_{\rm grp} = \frac{\sqrt{\pi}}{N_{\rm grp}(N_{\rm grp} - 1)} \sum_{i=1}^{N_{\rm grp}-1} w_i g_i. \qquad (4)$$

These values are listed in column (12) in Tables 5, 6 and 7.

Our group finding procedure must indicate that a putative group has more than two members for us to quote any group properties. For groups with 3–7 members we list tentative group properties with approximate velocity dispersions (see column 12 for listings without formal error estimates). When a group has $N_{\rm grp} \geq 8$ members we estimate the 90% confidence interval of the velocity dispersion with an "m out of n" bootstrap method using 10,000 resamplings of size $8 \leq m \leq N_{\rm grp}$, where m is chosen using the prescription of Bickel & Sakov (2008). When a group has $N_{\rm grp} < 8$ members we quote the dispersion returned by the gapper estimator without error bars because we have too few samples of the parent distribution to generate reliable confidence intervals. These 90% confidence errors are much greater than the typical uncertainty of our galaxy redshifts (~ 30 km s^{-1}). The measured velocity dispersion, $\sigma_{\rm grp}$, usually agrees remarkably well with that predicted solely from the group's luminosity, $\sigma_{\rm vir}$ (see Equation 2), and for groups with $N_{\rm grp} \geq 8$ members $\sigma_{\rm vir}$ is within the 90% confidence interval of $\sigma_{\rm grp}$ for all but one case, PG 1116+215/0.05897, whose σ values differ by an amount just greater than the estimated 90% confidence interval. We take the general agreement between these two values as an indication that our group identifications are relatively secure and that most of these systems are close to being virialized.

Associated groups with $N_{\rm grp} < 8$ members may have significantly larger dispersions than we have calculated (Beers, Flynn & Gebhardt 1990; Zabludoff & Mulchaey 1998; Osmond & Ponman 2004; Helsdon, Ponman & Mulchaey 2005); for this reason we have not quoted errors on these values. Deeper observations are required to characterize these groups adequately since both their group boundaries and memberships and also their velocity dispersions can change appreciably with the discovery of a few new group members. Basic galaxy identifiers, sky positions and redshifts for all group members shown in Figures 2, 3 and 4 ($N_{grp} \geq 8$) can be found in Appendix B. Full galaxy redshift results from our on-going survey along these and other COS sightlines can be found in Keeney et al. (2014).

Figures 2 (warm absorbers), 3 (cool absorbers) and 4 (misaligned absorbers) show all groups in this study for which ≥ 8 group members were identified by the group finding analysis described above. These figures

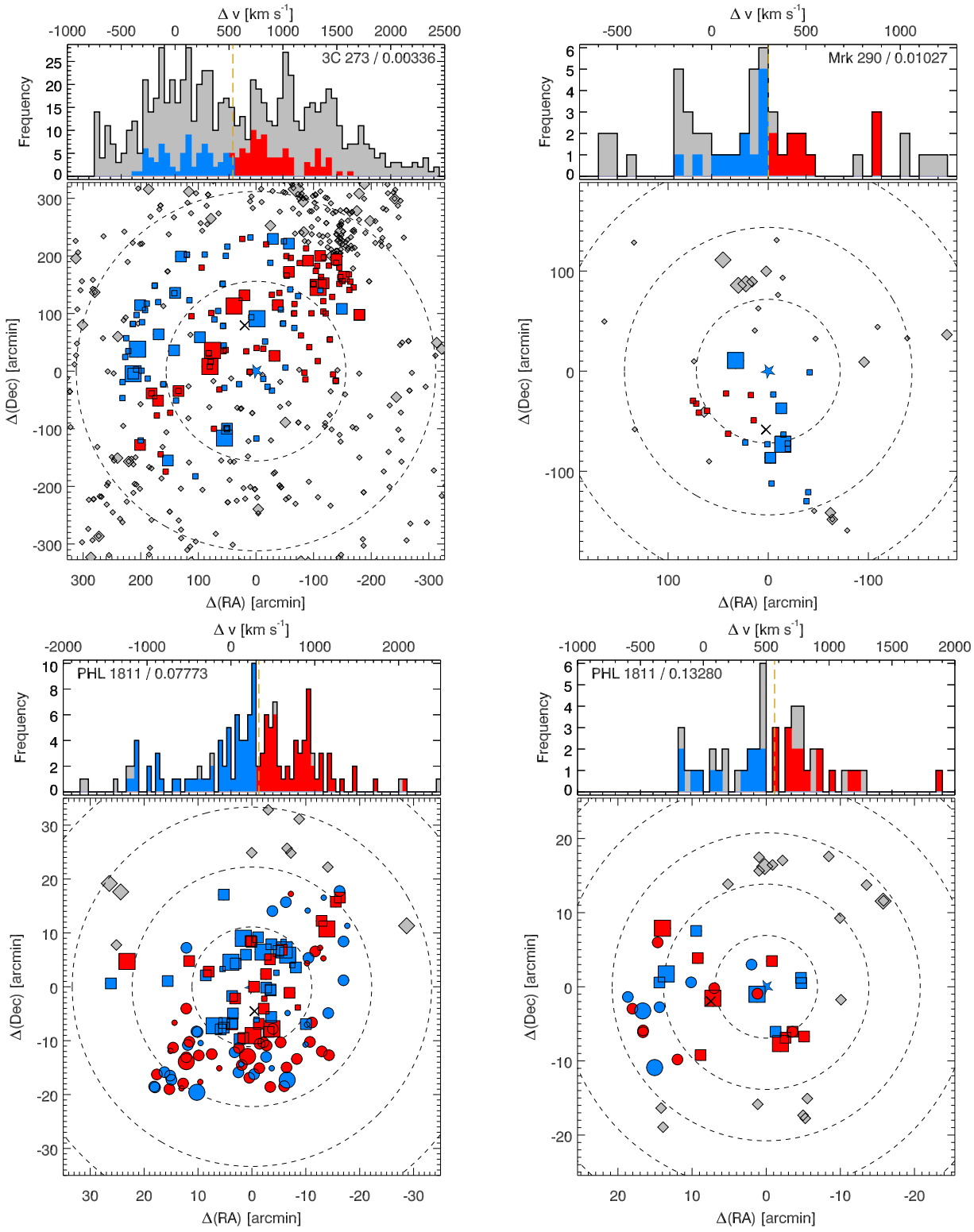

Figure 2. A montage of four galaxy groups associated with warm absorbers (see Table 5). At the top of each absorber plot is a histogram of galaxy radial velocities in Δv relative to the absorber. The colored bins are the group members, blue and red bins are blueshifted and redshifted relative to the group centroid; the grey bins are the galaxies excluded by the group finding algorithm. The dashed yellow vertical line is the group velocity centroid. At bottom is the spatial distribution of galaxies around the absorber on the sky. The coordinates are in arcminutes relative to the QSO sightline which is indicated by the large star at the origin. The dashed circles show impact parameters in 1 Mpc units increasing outwards. The positions of group galaxies are marked with squares for redshift data from SDSS or our nearby galaxy catalog (see Stocke et al. 2006, and Appendix B) or circles for redshift data from our own 4m MOS survey (see Keeney et al. 2014, and Appendix B); the grey diamonds are non-group members (see Keeney et al. 2014). The symbol size indicates the galaxy luminosity: large = super-L*, medium = sub-L*, and small = dwarfs. Blue symbols mark group galaxies with $z < z_{grp}$; red symbols are group galaxies with $z > z_{grp}$. The large "X" is the group centroid on the plane of the sky.

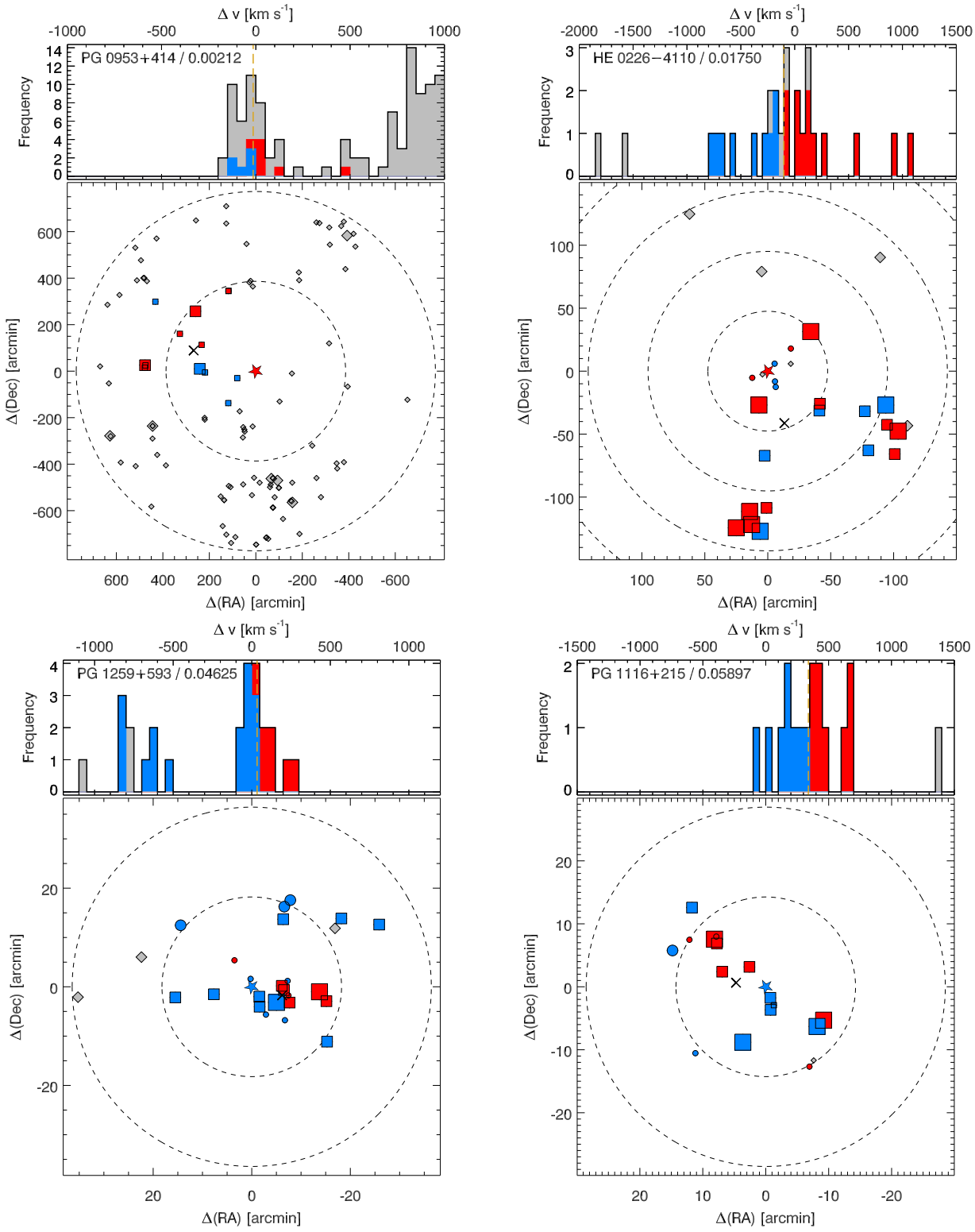

Figure 3. A montage of five galaxy groups associated with cool absorbers (see Table 6). Coordinates and symbology are described in the caption to Figure 2. See the text for a detailed discussion of the absorber groups shown in this Figure.

show group members as colored circles or squares with non-group members in the same regions as grey triangles. The presence of grey triangle galaxies within the search region for virtually all these groups indicates that the group memberships are limited by the linking length criteria not the imposed boundaries of the search. However, two of these "groups" may extend beyond the initial search regions; these two groups are also much richer than the others in this study and contain luminous elliptical galaxies:

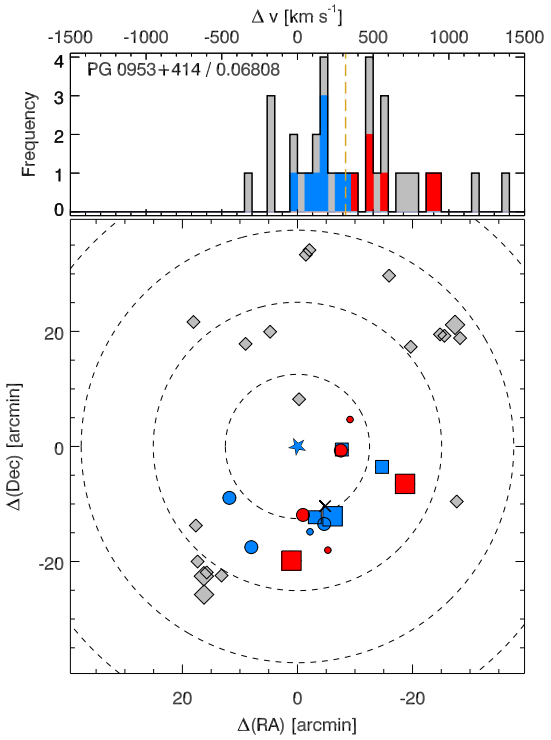

Figure 3. (continued)

1. 3C273/0.00336 (Tripp et al. 2002; Rosenberg et al. 2003; Stocke et al. 2004; Yoon et al. 2012) is in the southern outskirts of the Virgo Cluster (see Figure 2). When left unrestricted the FoF technique includes nearly 1000 galaxies in this group, including luminous ellipticals near the Virgo Cluster center > 5 Mpc away. However, in an effort to better characterize the more local environment of this absorber, we have decreased the linking lengths by a factor of two and restricted the search region to ≤ 1 Mpc from the absorber. The resulting values are still unusually large among warm absorber associations both in galaxy numbers ($\sim$ 150) and also in total group luminosity ($\sim$ 32 L*). While the FoF algorithm identifies only a fraction of the galaxies in this restricted region as group members (colored vs. grey symbols in the 3C 273/0.00336 panel in Figure 2), inclusion of all of the grey-symboled galaxies (mostly dwarfs) as group members does not change the calculated velocity dispersion by an amount more than the quoted 90% confidence error range. The agreement between $\sigma_{\rm grp}$ and $\sigma_{\rm vir}$ in this case (see Table 5) are suggestive that our restrictive approach has defined a warm absorber group within a larger supercluster region.

2. The other very rich group found around warm absorber locations (PHL 1811/0.07773) is between two rich clusters, Abell 2402 and SDSS-C4 2012. However, the algorithm does identify a group confined within the search region with a few non-group members present within the region (see Figure 2). We conclude that this is a well-defined group with a well-defined velocity dispersion (see the approximately Gaussian velocity distribution in Figure 2) within a larger supercluster region.

Three other fields deserve some brief comments with regard to the FoF group membership algorithm. In the case of the cool absorber group PG 0953+414/0.00212 (see Figure 3) the FoF analysis finds a fairly isolated group even though a higher redshift group ($\Delta v \geq 400$ km s^{-1}) is also present between 1 and 2 Mpc to the south (concentration of grey points to the south of the absorber and at higher radial velocities in the Δv histogram). However, many small galaxies which might be included in the cool absorber group are excluded by the FoF analysis (grey symbols in the spatial plot and histogram mixed in with the identified group members). If those excluded galaxies are instead included, this group increases from 1.5L* to 3.0L* in total luminosity but the velocity dispersion remains nearly identical to the value reported in Table 6. Therefore, despite potential differences in group membership accounting, the characteristics of this group are fairly robust.

The warm absorber group Mrk 290/0.01027 shown in Figure 2 has been pointed out previously by Narayanan et al. (2010), who describe this group as being in a "filament" of galaxies. Indeed, the FoF analysis links to galaxies out to $\sim$ 3 Mpc from the absorber but we truncate our analysis at $\pm$ 1.5R_{grp} and 3σ_{vir}. While either the group or filament descriptions seem valid, we retain the values shown in Table 2 for this warm absorber group for this analysis.

There are two anomalies created by the procedure of group identification above (see table notes to Table 5). For the PHL 1811/ 0.07773 absorber, a > 100 member group is identified which is well-centered around the absorber on the plane of the sky but offset in velocity (Δv$_{grp}$ = 330 km s^{-1}) and with a very large velocity dispersion (σ = 630 km s^{-1}). In this case there is an 0.7 L* group member which is closer on the sky to the absorber (0.22 R$_{vir}$ away) than a similarly bright galaxy, which is 1.75 R$_{vir}$ away (as listed in Table 5). However, this proximate galaxy has a Δv = 904 km s^{-1} relative to the absorber, which greatly exceeds our adopted maximum velocity difference of 400 km s^{-1} to be associated with the absorber. This same galaxy has been identified as the one associated with a slightly higher redshift LLS absorber in the PHL 1811 FUV spectrum (Jenkins et al. 2003). Similarly, in the 3C 273/0.00336 absorber region there is an extreme dwarf (< 1% L*) quite close to the sightline (ρ = 46 kpc) but at substantial Δv = 610 km s^{-1}; this dwarf is associated with a slightly higher redshift absorber in this same sightline (Stocke et al. 2004).

3.2. *Spiral-Rich Galaxy Groups Associated with Warm Absorbers at $z \leq 0.15$*

For the four warm absorbers at $z \leq 0.10$ our 4m survey is more than adequate to supply a good description of their associated galaxy groups; all but one (Mrk 876/0.00315) have > 10 group members for galaxy survey completeness levels deeper than 0.1 L*. A fifth absorber, PHL 1811/0.13280, has also been surveyed deeply enough to establish the presence of a rich group. These four have velocity dispersions $\sigma_{\rm grp} \approx 250$–$650$ km s^{-1} and total group luminosities of $\sim$ 5–50 L*. These numbers correspond to significant (4–100$^+$) overdensities in galaxies.

While the richness, total luminosity and velocity dispersion of the Mrk876/0.00315 group would be much larger if many of the dwarfs in its region were included in this group by the FoF analysis, its listed (Table 5)

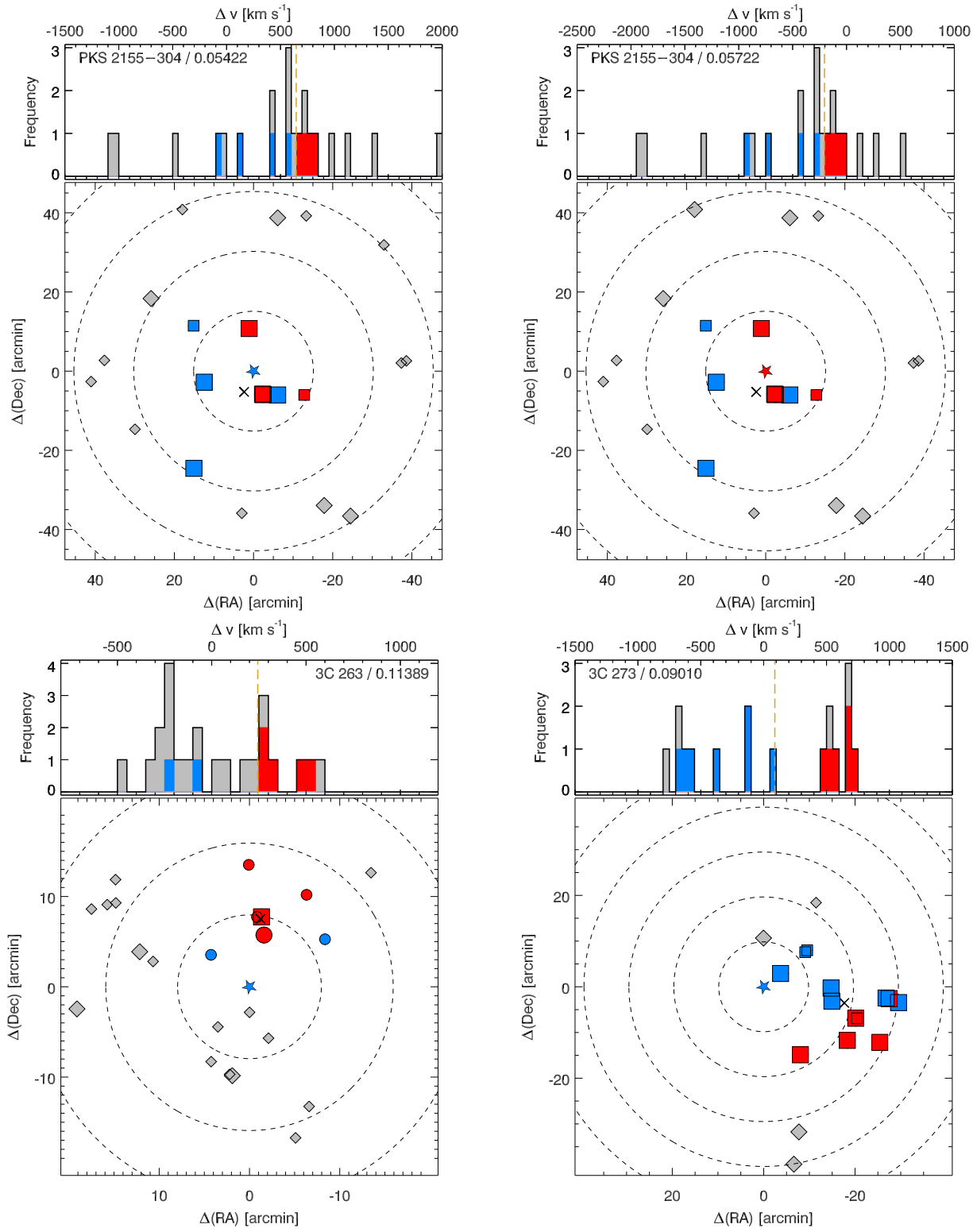

Figure 4. A montage of four galaxy groups which are associated with "misaligned" absorbers (Table 7). Coordinates and symbology are described in the caption to Figure 2. The two PKS 2155-304 O VI + H I absorber groups at top are the same physical group since these absorbers bracket the redshifts of this group (Shull et al. 1998).

values are less than the Local Group, dominated by a single 0.25L* galaxy. If we were to include all the 22 galaxies in the original search volume as group members, this "group" would have a total group luminosity of $\sim$ 2L* and a velocity dispersion $\sigma \sim 250$ km s^{-1}, which would make it comparable to the Local Group and only slightly poorer but with a velocity dispersion comparable to the Mrk 290/0.01027 group. The lack of sufficient

group members to provide a robust velocity dispersion leads us to discard this group from the statistical analysis despite having a warm absorber at log T(K) = 5.14 (Paper 1).

The two richest absorber environments have velocity dispersions comparable to many elliptical-dominated groups of galaxies (see Table 2 and Zabludoff & Mulchaey 1998; Mulchaey 2000). The richest "group", associated with 3C 273/0.00336, is in the southern outskirts of the Virgo Cluster with a couple of luminous early-type galaxies (NGC 4636, a 2L* E0 and NGC 4643, a 1.6L* SB0) $\sim$ 0.8 Mpc away from the sightline. The 5L* Sbc spiral M61 is the most luminous galaxy in the region. Similarly the PHL 1811/0.07773 group is also in the vicinity of richer galaxy regions and has a total group luminosity (55 L*) and velocity dispersion of $\sim$ 600 km s^{-1}, very large for an isolated spiral-rich group (see Table 5, Figure 2 and Zabludoff & Mulchaey 1998; Mulchaey 2000). This group also contains several early-type galaxies including 2MASX J21551727-0917517 (see also Jenkins et al. 2003), a 2L* elliptical 0.6 Mpc from the sightline. Given its large velocity dispersion and approximately Gaussian-distributed positions and velocities (comparable to many poor clusters of galaxies), this group should be searched for diffuse soft X-ray emission. Evidently, warm absorbers can be found either in small spiral-rich groups, in richer galaxy groups within filaments or in regions on the outskirts of clusters of galaxies.

A fifth nearby group is associated with the *possible* warm absorber, 3C 263/0.11389 (listed as a "misaligned absorber" by Paper 1 but see Appendix A for a reanalysis of this possible warm absorber). This absorber region has been surveyed for galaxies to 0.2 L^*, has 7 identified group members and a velocity dispersion of $\geq$270 km s^{-1}. The three other low-z warm absorbers in Table 5 have regions surveyed to 0.2–0.3L* and only 4 group members identified. While an extrapolation from these few galaxy identifications using a standard luminosity function (Montero-Dorta & Prada 2009) suggests the presence of groups comparable in richness to Mrk 290/0.01027, deeper MOS is required to characterize them more precisely. Therefore, based on the eight absorbers in Table 5 and a ninth, possible warm absorber in Table 7 (3C 263/0.11389), the warm absorber environment is usually spiral-rich galaxy groups with total luminosities of 2–20L* (assuming the larger value for the Mrk 876/0.00315 group) and velocity dispersions of 250–450 km s^{-1}. A couple of absorbers are found within richer groups and in cluster outskirts with larger total luminosities and velocity dispersions. These conclusions are all based on a small size sample and need to be confirmed by discovering many more warm absorbers at very low redshifts, where galaxy groups can be characterized in detail. It will be particularly important to target groups with well-defined properties, selected consistently from large galaxy databases (e.g., SDSS Berlind et al. 2008) to verify the diversity of groups associated with these "warm absorbers".

3.3. *Galaxy Groups Associated with Cool and Misaligned Absorbers*

Table 6 lists all the lower temperature O VI + Lyα absorbers at z $\leq$ 0.15 from Paper 1. Generally the cool absorbers are in groups of galaxies with slightly lower total luminosities ($L_{\rm grp}$ = 1.5–25 L*) and velocity dispersions ($\sim$ 130–500 km s^{-1}) than the warm absorber groups. These small differences between warm and cool absorber environments are not due to these fields having a brighter completeness luminosity as all but three absorbers (3C 273/0.12007; PG 0953+414/0.14231 and HE 0153-4520/0.14887; i.e., the three highest redshift absorbers in Table 6) have been surveyed well below 0.1 L^*. Due to the dearth of cool absorbers with good galaxy data we have added PG 1259+593/0.04625 to Table 6. This QSO has a high-S/N (36:1) COS spectrum and has been well-surveyed for galaxies using the same galaxy redshift database and WIYN/HYDRA MOS described in Section 3.1 despite not being a sightline included in Paper 1. A detailed analysis of this absorber complex is presented in Appendix A. See Figure 3 for the galaxy distributions around cool absorbers with $\geq$ 8 group members identified.

Interestingly, despite having similarly faint completeness limits, galaxy redshift surveys fail to find many galaxies around the misaligned absorbers (see Table 7). Only three misaligned absorber groups have sufficient numbers of identified group galaxies to quote a firm velocity dispersion (i.e., $N_{grp} \geq 8$). The three well-sampled groups associated with misaligned absorbers are shown in Figure 4 along with the $N_{grp} = 7$ group associated with 3C 263/0.11389, which may contain a "warm absorber" (see Appendix A).

3.4. *Statistical Properties of Galaxy Groups Associated with Warm Absorbers*

In this Sub-section we explore the possible differences between the nearest galaxies and the galaxy groups surrounding warm and cool absorbers. Since the COS spectroscopy provides only single probes through this gas, it is not obvious whether these absorbers are small ($\leq$ 20 kpc) and more closely related to an individual galaxy or are large ($\geq$ 100 kpc) and are associated with an entire group of galaxies. We perform three observational tests to determine which of these two possibilities is more likely: (1). Do nearest galaxy properties or galaxy group properties differ between warm and cool absorbers? (2). Do the observed absorber line-widths and inferred gas temperature values correlate with the kinetic energy in the group as measured by the group velocity dispersion? and (3). Which potential association, nearest galaxy or galaxy group, provides an absorber size which better matches the observed impact parameters shown in columns (4) and (9) of Table 5? This third test will be presented in the next sub-Section.

Each of these tests is limited both by the small sample size and by the statistical and systematic errors in the absorber and group measurements. While the O VI line widths offer the most unambiguous measurement of the temperature of the warm or cool gas, the O VI line profiles also may include some contribution from unresolved components, turbulence or Hubble flow motions (see Paper 1 and Appendix A). For example, the PG 0953+414/0.14231 absorber includes two O VI components with b=19$\pm$7 and 29$\pm$4 km s^{-1}, but from which

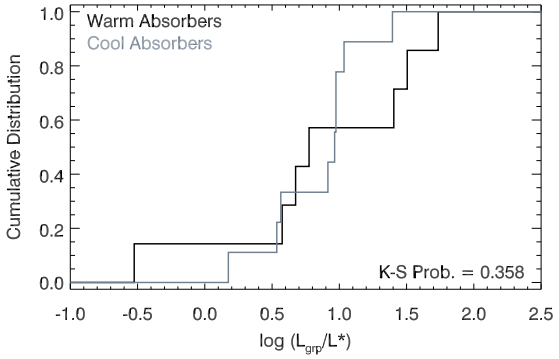

Figure 5. Cumulative distribution functions of total group luminosity, $L_{\rm grp}$.

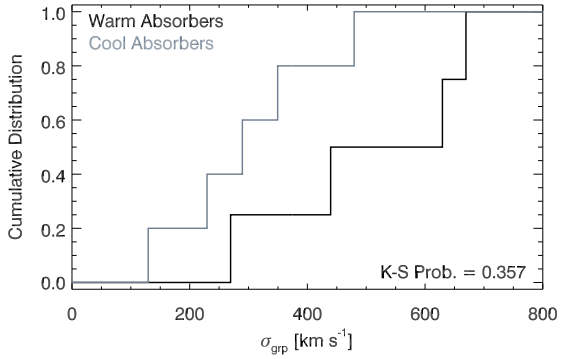

Figure 6. Cumulative distribution functions of group velocity dispersion, $\sigma_{\rm grp}$, for groups with $N_{\rm grp} > 8$ members.

similar gas temperatures (log T(K)< 4.25 and log T(K) = 4.21) are derived when the O VI and H I b-values are used together. Secondly, the Lyα line-widths are derived from best-fits to multiple components within a complicated line profile (see Appendix A and Paper 1). This makes the Lyα b-values less reliable than $b_{O\ VI}$ due to the presence of strong, photo-ionized absorption in Lyα, which creates both statistical and systematic errors. Finally, gas temperatures are derived from a combination of the measured O VI and Lyα b-values and so have the greatest statistical uncertainties. But this procedure does allow for the removal of other contributors to the line widths that otherwise would create large systematic errors in log T. This makes the temperatures the most reliable of these three measures since the systematical uncertainties are minimized, so that the statistical errors are a good measurement of the total uncertainties in log T. Further, the number of group members defined by the FoF algorithm is modest in most cases analyzed, making both the statistical and the systematic errors in the velocity dispersion values potentially quite large. Of particular concern are the non-Gaussian distributed velocities and sky locations of the group galaxies (see Figures 2, 3 and 4). At issue is not only the detailed methodology for computing velocity dispersions for small numbers of galaxies (Beers, Flynn & Gebhardt 1990) but also the robustness of the group membership algorithms (Berlind et al. 2006), including our choice of "linking lengths". However, our tests in Section 3.1 show that the velocity dispersions computed from group membership agree to within the errors with the group velocity dispersion computed from total group galaxy luminosities under the assumption that the group is virialized. This agreement provides some confirmation for the group definition process we have used, but it may be that a combination of systematic and statistical errors in measuring absorber and group properties (T_{abs}, σ_{grp}, etc) may actually obscure any real correlations that are present.

With these caveats in mind, the very slight systematic differences in galaxy group environments between the warm and cool absorbers in this sample are shown not to be significant in Figures 5 and 6. The warm absorbers are found in galaxy groups which are both slightly richer (marginally greater total luminosity; K-S test probability of chance occurrence $\sim$ 36%) and which possess systematically larger velocity dispersions (K-S test probability of chance occurrence $\sim$ 36%). For Figure 5 we have used

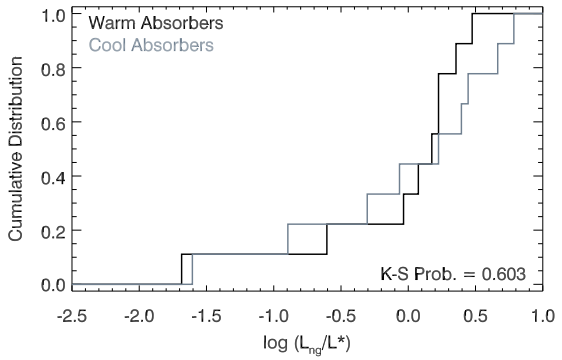

Figure 7. Cumulative distribution functions of nearest galaxy luminosity, $L_{\rm ng}$.

all warm absorbers in Table 5 (plus the possible warm absorber 3C 263/0.11389 from Table 7) and cool absorbers in Table 6, judging that all of these fields have been surveyed deeply enough to find most of the total luminosity of the groups. For Figure 6 we have used only those groups in Tables 5 and 6 which have $\geq$ 8 members surveyed, so that a velocity dispersion with estimated errors is quoted. Including all groups with N$\geq$ 3 (i.e., all values in Tables 5, 6 & 7 where a σ_{grp} value is quoted) decreases the K-S test probability for chance occurrence to $\sim$ 10%, but this comparison simply requires more groups before it can be judged to show a significant difference or not. Thus, using the most secure velocity dispersion data, we find only a very slight difference ($<1\sigma$ level) that the warm absorber groups have a larger velocity dispersion and higher total luminosities.

Figure 7 shows that there is no dichotomy at all between the warm and cool absorbers if the luminosity of the nearest associated galaxy is plotted. In this case we have used all the absorbers in Tables 5 and 6 because the two samples have a comparable range of completeness luminosities close to their sightlines. A K-S Test yields a probability of $\sim$60% that these two distributions have been drawn from the same parent population. These comparisons offer no strong support for or against an association between these absorbers and either their nearest galaxy neighbors or the groups in which they are imbedded.

Dividing the full galaxy groups sample by absorber temperature may actually obscure a more conclusive result for test (1) above because the statistical uncertainties in the measured temperature for some absorbers are

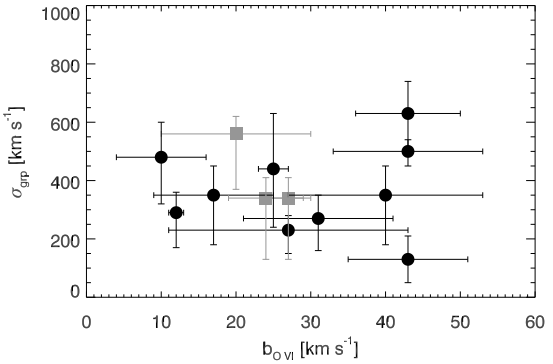

Figure 8. The relationship between the line widths of the O VI absorption (b_{OVI}) and the group velocity dispersion (σ_{grp}). The black circles are from Tables 5 and 6 (warm and cool absorbers); the grey squares are from Table 7 (misaligned absorbers). There is no correlation present either using the misaligned absorbers or not.

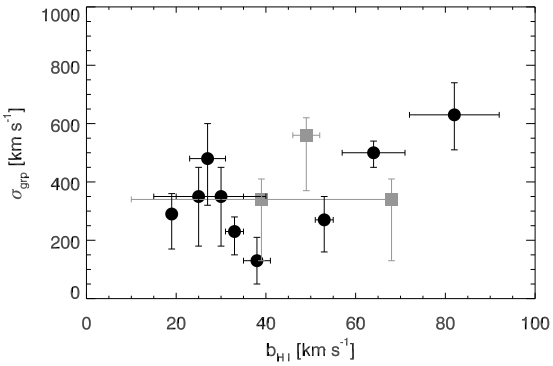

Figure 9. The relationship between the line widths of the H I Lyα absorption ($b_{H\ I}$) and the group velocity dispersion (σ_{grp}). The black circles are from Tables 5 and 6 (warm and cool absorbers); the grey squares are from Table 7 (misaligned absorbers). There is a very slight (50% probability) correlation present either using the misaligned absorbers or not. However, if one point, PHL 1811/0.07773, was removed no correlation is present.

so large. Therefore, in test (2) we use the raw line-width data as well as the derived temperature values, but taking the uncertainties explicitly into account. In Figure 8 we show a plot of O VI b-values versus $\sigma_{\rm grp}$. No correlation between these quantities is present. A weak correlation ($\sim$ 50% probability of chance occurrence) may be present between the Lyα line width and $\sigma_{\rm grp}$ (Figure 9) but its existence depends entirely on the one point associated with PHL 1811/0.07773. While any real correlation between these quantities could be masked by the potentially large systematic errors in the line-fitting, these plots offer no substantial support for or against a group origin for this gas.

However, some support for a group origin for the warm and cool O VI gas detected spectroscopically by COS is shown in Figures 10 & 11 (n.b., these plots are not fully independent since group luminosities and velocity dispersions correlate). These plots use the inferred absorber gas temperatures (Tables 2, 3 & 4) and the group velocity dispersions and luminosities (Tables 5, 6 & 7) to determine whether there is a relationship between the energy in the gas and in the galaxies as would be expected if they trace the same gravitational potential. All absorbers with reasonably robust velocity dispersions ($N_{grp} \geq 8$ members) have been included in Figures 10 & 11 as filled black symbols. These data result in a correlation between these two variables at the 95% level ($\sim 2\sigma$) using various statistical tests (e.g., Kendall and Spearman rank correlation coefficients). These possible correlations are far from compelling due to the small sample size and requires new observations to be confirmed (e.g., two groups, H 1821+643/0.12141 and 3C 263/0.14072, which do not appear in Figures 10 & 11 and which have log T (K) > 5.5 are in regions not yet surveyed deeply for galaxies). However, the derived temperatures may provide a better indication of the specific energy in the gas compared to the raw line widths due to the removal of non-thermal contributions to $b_{O\ VI}$ and $b_{H\ I}$.

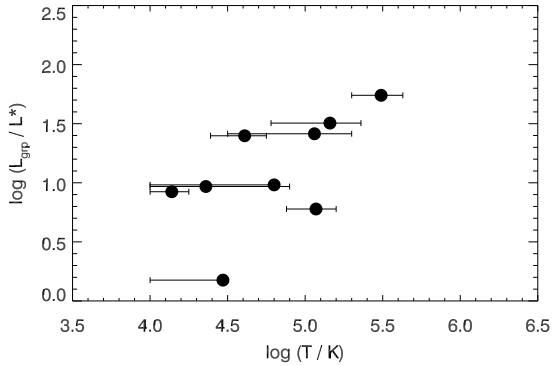

Figure 10. Plot of $\log T$ versus $L_{\rm grp}$. The black symbols are those groups with $N_{\rm grp} \geq 8$ members. These data result in a 95% confidence (2σ) level correlation.

Also, as a follow-up to the possible correlation between group luminosity and absorber temperature, it will be important to conduct a quantitative comparison between the galaxy morphologies in warm and cool groups. While such an analysis is beyond the scope of this paper, it may provide important insights into the dynamical evolution of these groups and will be presented at a later time (Keeney et al. 2014).

3.5. *Inferred Sizes of Warm Absorbers*

The third test for discriminating between nearest galaxy or galaxy group associations with warm absorbers uses the number density $d\mathcal{N}/dz$= 3.5–5 per unit redshift as a discriminator (see Section 2). The bounds on the $d\mathcal{N}/dz$ value above refer to the number of warm absorbers found in Paper 1 (14 plus 2 O VI-only absorbers) and herein (20 in total, including those same two O VI-only absorbers). We use $d\mathcal{N}/dz$= 4$\pm$1 per unit redshift for this analysis as a compromise value between the results of Paper 1 and the results in Section 2 and Appendix A herein. Note that this value is several times less than the $d\mathcal{N}/dz$ for all O VI absorbers (Danforth & Shull 2008). Here, by using a mean space density of associated objects (galaxies of varying luminosities and galaxy groups) we can use the observed $d\mathcal{N}/dz$ value to compute a characteristic size for the absorber assuming an 100% covering fraction. These characteristic sizes can then be compared with the observed impact parameters to determine if an association with each object class is viable.

Previously this type of analysis had been conducted for photo-ionized absorbers, which have been found to be associated with individual galaxy halos at $\rho \leq R_{vir}$ at high covering factors (Tumlinson et al. 2011; Prochaska et al.

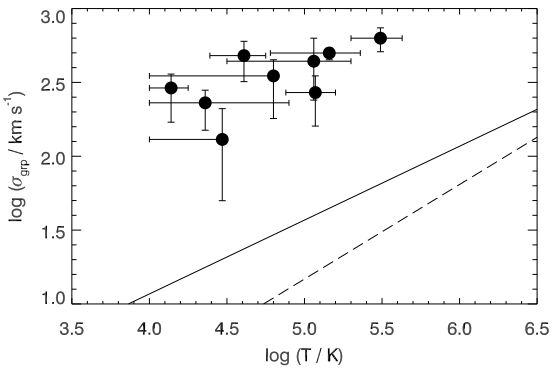

Figure 11. Plot of $\log T_{gas}$ versus $\sigma_{\rm grp}$ for the "cool"' and "warm" groups listed in Tables 5 & 6. This plot includes only those absorber groups with robust velocity dispersions; i.e., ≥ 8 members with measured redshifts. For a few of the photo-ionized absorbers, we have truncated the error bars on temperature from Paper 1 at log T (K)= 4.0 to be consistent with standard photo-ionization models. These data result in a 95% confidence (2σ) level correlation between these two variables. The solid line is the extrapolation of $\beta_{spec} = 1$ (energy equipartition between galaxies and gas) from the clusters and groups data found in Osmond & Ponman (2004); see their Figure 16. The dashed line is an extrapolation of the best-fit power-law for clusters and groups from Wu, Xue & Fang (1999). See Section 4 for a discussion of the spiral-group data in comparison to the extrapolations of Osmond & Ponman (2004) and Wu, Xue & Fang (1999).

2011a; Stocke et al. 2013). These studies find near unity covering fractions around $L \geq 0.1\,L^*$ galaxies at $\rho \leq R_{vir}$. Stocke et al. (2013) also finds substantial covering fractions around dwarfs at $\rho \leq R_{vir}$. Among the warm absorption complexes studied in detail here (i.e., those in Table 5), only two absorbers (PHL 1811/0.07773 and PG 1116+215/0.13850) have low metal ions (e.g., Si II, Si III, etc) present, which are associated with the narrow Lyα component in the absorption complex. These are photo-ionized clouds that may or may not be associated physically with the warm absorber. As has been found by the three studies referenced above, these two are at low impact parameter (0.22 and 0.67 R_{vir}) from the nearest galaxy in the group. The remainder in Table 5 have only H I + O VI present and are found at larger impact parameters (typically at $\rho > R_{vir}$) from the nearest galaxy in the groups.

Here we use the SDSS luminosity function of Montero-Dorta & Prada (2009) to determine the space density of galaxies using our assumed $H_0 = 70$ km s^{-1} Mpc^{-1} value (see Table 8). Recently Berlind et al. (2006, 2008) have undertaken a census of nearby galaxy groups using the SDSS. Using their median catalog of groups converted to $H_0 = 70$ km s^{-1} Mpc^{-1} yields $\phi = 3 \times 10^{-4}$ Mpc^{-3}. Pisani, Ramella & Geller (2003) used a different approach which nets approximately the same space density for a group velocity dispersion of $\sigma \geq 200$ km s^{-1}, which appears to be a reasonable lower limit to use in this estimate based on the warm absorber group values in Table 5. An earlier study by Girardi & Giuricin (2000) found a slightly larger value for the space density of groups, 4.5 to 6.5 $\times$ 10^{-4} Mpc^{-3}, but included lower mass groups that are not as good a match to the current sample of warm absorbers groups.

The Berlind et al. value ($\phi = 3 \times 10^{-4}$ Mpc^{-3}), which will be used here for the space density of galaxy groups (see Table 8), is ten times less than the space density of L^* galaxies, $\phi(L \geq L^*) = 2.8 \times 10^{-3}$ Mpc^{-3}. The Berlind et al. catalog of galaxy groups are dominated by small (3–5 L> L*, members), spiral-rich groups, $\geq 80\%$ of which are found to be virialized on the basis of crossing times < 0.3 Hubble times. Almost all of these groups are significantly richer and with higher velocity dispersions than the Local Group and so are similar to the warm absorber groups found here.

Using the observed $d\mathcal{N}/dz = 4\pm1$ (Poisson error) of warm absorbers and assuming a unity covering factor, the required absorber sizes listed in Table 8 (column 3) were computed using the Montero-Dorta & Prada (2009) luminosity function integrated from the lower bound (L_{low}) in column (1) to infinity. The quoted errors in column (3) are the quadrature addition of the $d\mathcal{N}/dz$ Poisson error and the errors in ϕ in column (2). The inferred sizes obtained by this calculation are half-again larger than the virial radii of L_{low} galaxies but much less than the maximum impact parameter observed between the warm absorbers and the nearest galaxies at L $\geq L_{low}$. If the covering factor of these absorbers is < 1 then the required absorbers sizes are larger still and so must be much larger than the virial radii of the nearest galaxies to provide a plausible association. For the 8 warm absorbers in our small sample (9 including the possible warm absorber 3C 263/0.11389 in Table 7), we find a maximum impact parameter to the nearest $L \geq L^*$ galaxy of > 2 Mpc and a range of nearest L> L^* galaxy neighbors of 140 kpc to > 2 Mpc. Lower luminosity bins have similar discrepancies. The last column in Table 8 shows that for all galaxy luminosities the percentage of cases where the observed impact parameter (ρ) is less than the required maximum absorber size (R_{abs}) is small. Unless the covering factors of these absorbers are $\ll 1$ and their gaseous extents are $\gg R_{vir}$, an association between warm absorbers and individual galaxies appears unlikely. However, caution involving this conclusion is required with respect to a possible association between warm absorbers and dwarf galaxies due to the very small numbers of absorbers (3 or 2) which have been surveyed to 0.03 or 0.01L* completeness levels. Deeper observations of many of these groups are required.

On the other hand, the largest observed impact parameter between the warm absorbers and their associated galaxy group's centroid is 1.11 Mpc (PHL 1811/0.13280), with a spread in ρ/R_{vir} values of 0.24–1.27 (see column 10 in Table 5 and the last row of values in Table 7). Unlike for the individual galaxies, these values fit closely with the 1 Mpc required absorber radius in Table 8. Additionally, these numbers suggest that the warm absorbers are found approximately within the virial radius of the galaxy group. If only a fraction of spiral-galaxy groups contain warm absorbers and/or if the covering factor of these absorbers is significantly less than unity, an even larger size than 1 Mpc is required for the gas in these groups to account for the observed $d\mathcal{N}/dz$ value. Note well, that this size is a statistically-determined extent of the ensemble of these absorbers at high covering factor, not the physical size of any one absorbing cloud.

In summary, small galaxy groups or groups in cluster outskirts with velocity dispersions of $\sigma \sim$ 250-650 km s^{-1} are typical warm absorber environments. While simple

Table 8
Collisionally-Ionized "Warm Absorber" Size Estimates

Galaxy Luminosity Range (L_{low}/L^*)	$\phi(L_{low})$ ($\times 10^{-3}$ Mpc^{-3})	Required Absorber Radius R_{abs} (Mpc)	Max Observed Impact Parameter ρ (Mpc)	Sample Size	Percent with $\rho < R_{abs}$
≥ 1.0	2.8 ± 0.2	0.33 ± 0.18	> 2.0	9	45%
≥ 0.1	4.9 ± 0.6	0.25 ± 0.15	0.62	4	50%
≥ 0.03	7.7 ± 1.4	0.20 ± 0.10	0.43	3	33%
≥ 0.01	12.1 ± 2.8	0.16 ± 0.08	0.43	2	50%
Galaxy Groups	0.30	1.0 ± 0.55	1.11	10	90%

[a] calculations assume $d\mathcal{N}/dz = 4\pm1$ and unity covering factor

comparisons between warm absorber groups and groups associated with cooler, photo-ionized O VI absorbers find little difference between these two samples, the sample sizes are small and systematics in the observables can be large. However, using the absorber temperature rather than the O VI and H I line widths results in modest (95% confidence, 2σ) correlations between log T and group luminosity and log T and group velocity dispersion. These marginal differences are suggestive, but not conclusive, that the warm absorbers found in high-S/N COS spectra are detections of diffuse gas in small, spiral-rich galaxy groups. But, using the observed absorber $d\mathcal{N}/dz$ and the impact parameters found for these absorbers relative to the galaxy group centroid finds support for a group association. The rather substantial $d\mathcal{N}/dz \approx 4$ per unit redshift requires these absorbers to be extended over $\sim$ 1 Mpc in radius at high covering factor. This large extent is consistent with the observed impact parameters between the QSO sightlines and the foreground group centroids.

4. DISCUSSION

The existence of a massive circum-galactic medium (CGM) or gaseous halo around individual late-type galaxies is now well-established. Several recent studies (Prochaska et al. 2011a; Tumlinson et al. 2011; Stocke et al. 2013; Tumlinson et al. 2013; Werk et al. 2014) have discovered and investigated cool, photo-ionized galaxy halo clouds found within the virial radii of large and small galaxies. These studies used STIS and COS spectroscopy to detect photo-ionized Lyα and metal lines at very high covering factor out to at least the virial radius from the nearest, usually star-forming galaxy. The presence of similar clouds around early-type galaxies has been proposed but is still controversial (Thom et al. 2012). Where sufficient ions were available to provide good constraints on photo-ionization modeling, single-phase, homogeneous models were used to calculate cloud temperatures and densities from which sizes and masses were inferred (Stocke et al. 2013; Werk et al. 2014; Keeney et al. 2014). The resulting sizes (diameters of 0.1 - 30 kpc) and masses (10^{1-8} M$_\odot$) of these halo clouds are consistent with estimates for high-velocity-clouds (HVCs) in the Milky Way (e.g., Wakker et al. 2007, 2008). Estimates of the ensemble mass of the cool, photo-ionized clouds around a super-L* galaxy exceeds 10^{11} M$_\odot$ (Stocke et al. 2013; Werk et al. 2014). Computing internal pressures for these clouds based on the derived temperatures and densities from the photo-ionization modeling finds $\langle P/k \rangle \approx 10$ cm^{-3} K ($\pm$ 0.5 dex) (Stocke et al. 2013).

Surprisingly, Stocke et al. (2013) found no evidence for a declining pressure while Werk et al. (2014) finds 2.3σ evidence for a shallow decrease in density $n \sim (\rho/\mathrm{R}_{vir})^{-0.8}$. In either case the density decline in the halo is unexpectedly slight. It is important to be cautious in this interpretation since it rests on data from single sightline probes past many galaxies as indicative of the CGM around any single galaxy in the sample. This conclusion also assumes that the gaseous halo is centered on the nearest galaxy, which would not necessarily be the case if the confining medium were related to an entire group of galaxies. If this result is interpreted in the context of pressure equilibrium between these clouds and a hotter, more diffuse medium, the absence of a rapid decrease in cool cloud pressure with increasing impact parameter is unexpected if these clouds (and any surrounding intra-cloud medium) are related exclusively to an individual galaxy (Anderson & Bregman 2010, 2011).

The discovery of the 20 warm absorbers studied here may be related to the existence of the hotter gas whose presence is suggested by the cool, photoionized cloud pressures. It is important to recall that the absorbers found by Paper 1 and studied herein are too shallow and broad to have been detected in the lower S/N COS and STIS spectra published earlier. The strong O VI absorbers previously studied by Tumlinson et al. (2011); Prochaska et al. (2011a); Werk et al. (2013); Stocke et al. (2013); Werk et al. (2014) are found well within R_{vir} of the nearest galaxy's halo and appears associated in some way with the cool, photoionized clouds. As found in the previous section, these "warm absorbers" are located on average much farther from their nearest galaxy neighbor (i.e., typically at $\rho > R_{vir}$) but within the confines of a galaxy group containing that nearest galaxy. Most of these warm absorbers do not contain lower ions within the absorption complex which differs from the higher column density O VI systems found by Tumlinson et al. (2011).

While simple correlation studies fail to show strong evidence for this proposed absorber/group association, modest ($\sim 2\sigma$) correlations between absorber temperature and group luminosity and velocity dispersion were found (n.b., these are not independent correlations). Also, the observed impact parameters to the nearest galaxy appear much too large (i.e., $\rho \gg R_{vir}$ in most cases) to explain an individual galaxy association with these absorbers unless the gas is extremely patchy. An association with group gas is more likely based on a match between the observed absorber impact parameters from group centroids and the required cloud sizes. While suggestive, the current data are too sparse to war-

rant a claim that the warm absorbers are the first solid detections of an intra-group medium in spiral-rich galaxy groups. While this is a possibility, the 10^{5-6} K temperatures of these absorbers are an order of magnitude too low to be the intra-group medium **if** these groups are virialized. Most likely these absorbers mark the transition regions between the hot, intra-group gas and cooler, photo-ionized absorbers (Smith et al. 2011; Shull et al. 2012; Cen 2013).

Figure 11 in the previous Section showed the T-σ absorber/group data with extrapolations from hotter temperature groups and clusters shown as solid and dashed lines. The dashed line indicates the extrapolation of the best-fit power-law from Wu, Xue & Fang (1999, as shown in Mulchaey 2000, Figure 4) for clusters and groups into the T-σ domain of the spiral groups studied here. It is on the basis of an extrapolation like this that M96 predicted that a typical spiral-rich group with σ=100 km s^{-1} would possess an intra-group gas with log T(K)=6.3. When Savage et al. (2010) discovered a broad O VI-only absorber in the COS spectrum of PKS 0405-123 whose b-value and absence of associated H I Lyα strongly suggested log T(K)=6.1, it was natural to associate this absorption line detection of warm gas with the prediction of M96. However, as shown in Figures 1 & 11 the observed (absorption-line determined) temperatures in spiral-rich groups presented herein are at least an order of magnitude lower than as predicted by the velocity dispersions of spiral-rich groups *if* an extrapolation of the Wu, Xue & Fang (1999) rich cluster and group data is appropriate.

More recently Osmond & Ponman (2004) constructed a large group catalog using the *ROSAT* all-sky X-ray survey and a number of nearby group catalogs. The resulting log T vs log σ correlation found for these groups compared to a sample of rich clusters is shown in Osmond & Ponman (2004, see their Figure 16). What is most apparent is that the groups have a much larger spread in velocity dispersion at a given log T$_x$ than the rich clusters. It is controversial whether a single power-law fits both the cluster and group data or whether the slope steepens in the group regime (e.g., Mulchaey 2000; Osmond & Ponman 2004; Helsdon, Ponman & Mulchaey 2005). But neither the cluster plus group best-fit slope (0.71), nor the group-only best-fit slope (1.15), predicts the gas temperatures that we observe for the spiral-rich groups. An extrapolation of a single power-law which fits both the clusters and the most X-ray luminous, hottest groups (but not the lower L$_x$ E-dominated groups) and is theoretically motivated by equipartition of energy between gas and galaxies; i.e., $\beta_{spec} = 1$ (Osmond & Ponman 2004) is shown in Figure 11 as a solid line.

While the solid-line extrapolation comes closer to predicting the temperatures for the warm absorbers, even the $\beta_{spec} = 1$ extrapolation falls well below the spiral data points from this study, indicating that there is proportionately more energy in the galaxies than in the warm absorber gas. If a group is still in the process of virializing, it is *possible* that the galaxy motions have not had the time required to heat the gas to a virial equilibrium temperature in the case that the gas has been ejected from the galaxies only recently. But it is also possible that the O VI + H I warm absorbers are sensitive only to that portion of the intra-group gas closest to the temperature where the fraction of oxygen in the O VI ion maximizes (log T(K) $\approx$ 5.5) and that these warm absorbers indirectly trace the presence of even hotter gas, to which the HST/COS spectra are not sensitive. At T $> 10^6$ K the neutral fraction of hydrogen is $f_{HI} \sim 10^{-7}$ (Danforth et al. 2010) and the fraction of oxygen which is in the O VI ion is $< 10\%$ (Bregman 2007). If the bulk of the intra-group gas is at temperatures much hotter than 10^6 K, the warm absorbers could be interfaces with or cooler portions of this hotter gas and the bulk of the intra-group gas has not been detected directly as yet.

It is also reasonable to consider the possibility that the warm absorbers are a diffuse, high filling-factor gas in these groups as a limiting case; i.e., while not yet in equilibrium with the energy in the galaxies, these warm absorbers are nevertheless the bulk of the intra-group medium. To illustrate the consequences of this possibility, we assume pressure balance between the cool, photo-ionized clouds ($\langle P/k \rangle \approx 10$ cm^{-3} K) and a "warm" diffuse medium with T$\sim 10^{5.5}$ K based on our warm absorber detections (see Figure 1). This constrains the density of this diffuse gas to be $\sim 10^{-4.5}$ cm^{-3} over a region with a minimum radius of $\geq$ 300 kpc. These density and minimum size estimates yield a *minimum* warm mass reservoir of $\geq 10^{11}$ M$_\odot$. An even larger gas extent at high covering factor is required by the $d\mathcal{N}/dz$ of the warm absorbers ($\sim$ 1 Mpc in radius; see Section 3.5). Assuming a standard β-model (Mulchaey & Zabludoff 1998) with $\beta = 0.67$ for the warm gas density profile with a 300 kpc core radius, a maximum gas radius of 1 Mpc and a central gas density of 3×10^{-5} cm^{-3} yields a total warm gas mass of $\sim 10^{12}$ $M_\odot$. However, the large extent of this diffuse gas would create unacceptably large line widths for the O VI and Lyα absorption. We estimate that the required velocity dispersions in such large structures would create line widths at least 2–3 times larger than what we find for these absorbers (see Table 2) either from Hubble flow broadening (unbound case) or from the substantial velocity dispersions of these groups (bound case). Also gas at the temperatures of these warm absorbers has a very short cooling time and so is unlikely to be the dominant gas reservoir around late-type galaxies and in their groups (Shull et al. 2012; Cen 2013). Smith et al. (2011) find that in the present epoch, most of the gas at log T(K) = 5.0-6.0 has recently cooled from hotter gas that is the dominant WHIM reservoir at $z \sim$0.

In order to satisfy the observations of nearly constant pressure over a minimum impact parameter of $\sim$ 300 kpc as well as the likely, but not firm, association of the warm absorbers with galaxy groups rather than individual galaxies, a diffuse hot medium is still required. Using Figure 11 as a guide, a reasonable temperature for the intra-group medium in groups with σ_{grp} = 250-450 km s^{-1} is T$\sim 10^{6.5}$ K. Pressure balance then requires a central gas density of 3×10^{-6} cm^{-3} and a total hot gas mass of $\sim 10^{11}$ $M_\odot$ (see previous paragraph). The core radius (300 kpc) and full extent (1 Mpc) we assume are similar to what is found in elliptical-dominated groups (Mulchaey 2000) but the total mass is significantly less. While we have assumed a value of β comparable to that found for clusters of galaxies, Osmond & Ponman (2004) find evidence for a somewhat smaller value of β in groups

which leads to a shallower density profile and a greater mass. Truncating the mass distribution at 1 Mpc may also be artificial and a substantial gas reservoir could be present farther away than 1 Mpc ($> R_{vir}$) as in the rich clusters (Simionescu et al. 2011). Therefore, the bulk of the evidence presented herein suggests that the warm absorbers are an *indirect, not a direct* detection of a massive baryon reservoir of hot gas in small, spiral-rich groups of galaxies at T$\sim 10^{6.5}$ K.

5. SUMMARY OF CONCLUSIONS

The Cosmic Origin Spectrograph (COS) Science Team has conducted a high-S/N ($\geq$20:1), high resolution (R $\approx$ 18,000) far-UV spectroscopic survey of 14 bright QSOs. Paper 1 reported some of the results from this survey concentrating on the absorbers detected in O VI. Specifically, Paper 1 identified a new class of broad, shallow O VI and Lyα absorbers which are demonstrably hot enough to be fully in the collisionally-ionized regime; we term these "warm absorbers" in Paper 1 and herein (see Figure 1). As a class these warm absorbers have not been detected or studied heretofore in any detail due to the absence of sufficiently high-S/N FUV spectra, which the COS GTO observations have now provided.

Additional absorption systems with and without metals from these spectra are presented in Danforth et al. (2014). Most of the O VI absorbers were also detected in H I Lyα with COS but two O VI absorbers were not detected in H I at all and a few with broad Lyα (BLA) detections had O VI detections in the *FUSE* band. One *possible* warm absorber contains a BLA in Lyα, which is confirmed to be warm using the observed Lyβ width but has no corresponding O VI. Fourteen broad O VI + BLA detections in the Science Team's survey have absorption in these two species aligned in velocity with b-values requiring collisionally-ionized gas at T $\geq 10^5$ K, so called, "warm gas". Two other absorbers found in the spectra analyzed in Paper 1 possess broad O VI absorption with no corresponding H I Lyα absorption, also requiring the presence of warm gas. In this paper the galaxy environments of these warm absorbers are investigated in order to determine the most likely type of galaxy or galaxy group with which they are physically associated. Given an association with either individual galaxies or with the entire galaxy group, the spatial extent and gas mass of these warm absorbers is also estimated. We find the following results:

1. We have reviewed the results of Paper 1 concentrating on those few broad, symmetric O VI absorbers suggestive of warm gas which were not identified as such by Paper 1 (see Section 2). While almost all of the model fits made by Paper 1 were confirmed, we suggest alternative fits for 4 absorbers only (see Appendix A). These reevaluations, plus two O VI-only absorbers that lack associated Lyα, suggest that as many as 20 warm absorbers may be present in this sample compared to 14 (plus 2 O VI-only) warm absorbers identified in Paper 1. Using the pathlength probed by these 14 high-S/N spectra of $\delta z = 4.0$, we find a $d\mathcal{N}/dz$ for warm absorbers of 3.5-5 per unit redshift, several times the number density of Mg II/LLS absorbers and about one-quarter of the $d\mathcal{N}/dz$ value for all previously-detected O VI absorbers (Danforth & Shull 2008).

2. Spiral-rich galaxy groups are found around the location of most of these warm absorbers with total luminosities of $\sim$2–26L* and velocity dispersions, σ = 250–450 km s^{-1}. These groups have 2–5 bright (L$\geq$L*) group members that are usually luminous early-type spirals. However, two warm absorbers have galaxy environments more appropriately described as cluster outskirts or as a galaxy group within a filament between clusters. These two warm absorber groups have velocity dispersions of $\geq$ 500 km s^{-1}, total luminosities of $\sim$30-60 L* and brightest galaxies that are 2-4 L* early-types.

3. Evidence is presented in Section 3 that the warm absorbers are more likely associated with the galaxy group than the nearest galaxy, although this evidence is not entirely conclusive due to the small sample size. Group properties associated with either warm or cool absorbers do not show significant differences. Modest (95% probability) 2σ correlations are found between both the total group luminosity and also the gas temperature in comparison with the group velocity dispersion (Figures 10 and 11). On the other hand we find no evidence favoring an association with the nearest galaxy neighbors to these absorbers.

4. The large $d\mathcal{N}/dz\approx$ 4 per unit redshift favors an association with galaxy groups rather than individual galaxies (see Table 8 in Section 3.5). Regardless of their luminosity, most of the nearest galaxies are systematically too far away from the warm absorbers to be viably associated. On the other hand, if the associations are with galaxy groups, then the impact parameters match the absorber sizes of $\sim$ 1 Mpc radius required in the case of high covering factors. One Mpc is also the approximate size of the virial radius of these groups, if they are in fact gravitationally bound. But in this case the rather narrow O VI and Lyα line widths observed are explicable only if these absorbers are individually small with respect to the galaxy group but which in ensemble cover the entire group at very high covering factor.

5. While the T-σ relation for spiral groups in this sample (Figure 11) lies well above an extrapolation of the relation seen for clusters and elliptical dominated groups, the data for spiral-rich groups lie much closer to an extrapolation of the cluster + group X-ray data if equipartition of energy between gas and galaxies (β_{spec} = 1) is assumed. However, the temperatures of the warm gas (see Figure 11) are approximately one order of magnitude too cool to be diffuse group gas if $\beta_{spec} = 1$ and if the group is virialized. The origin of this discrepancy is not known. It could be that the O VI absorption is **not** tracing the bulk of the intra-group gas but rather the gas at the temperature to which the O VI is most sensitive, T $\approx 10^{5.5}$ K. In this case hotter gas likely is present in these groups but is not easily detected in the COS FUV absorption-line spectra.

6. The observed, nearly-constant, cool cloud internal pressures ($\langle P/k \rangle \approx 10$ cm^{-3} K; Stocke et al. 2013; Werk et al. 2014) as a function of impact parameter require a very large, diffuse intra-cloud gas to confine these clouds. While the warm absorbers could be detections of this massive, diffuse gas reservoir, it is more plausible that these warm clouds are a tracer of even hotter, diffuse gas which confines the cool, photoionized clouds. Three observables favor this interpretation: (a) the warm absorber O VI and H I line widths are too narrow to be gas distributed over a large region of a bound or unbound

galaxy group; (b) the warm absorber temperatures are in a regime where diffuse gas is quite unstable to rapid cooling so that a large diffuse gas reservoir would be difficult to maintain at that temperature; and (c) the warm absorber temperatures are an order of magnitude too cool to be virialized gas in the groups we have found (σ=250-450 km s^{-1}; see Figure 11). In the context of a standard β-model with a core radius of $\sim$ 300 kpc and a full extent of $\sim$ 1 Mpc (based on the results described in the previous Section) we find a total mass of $\sim 10^{11}$ M$_\odot$ for this hotter gas based on pressure equilibrium with the cool, photoionized clouds. These values for the spiral intra-group medium suggests a similar extent to the gas in elliptical-dominated groups (Mulchaey 2000), but less mass. This amount of gas also is quite similar to the amount of "missing" baryons required to bring spiral galaxy groups up to the cosmic mean ratio of baryons to dark matter. **If** the conclusions summarized in this paragraph are correct, spiral galaxy groups could be "closed boxes" for cosmic evolution like their more massive counterparts which contain dominant ellipticals.

Regardless of their detailed interpretation, these warm absorbers are detections of local baryons not inventoried before. As such these absorbers will add to the baryon census, but with an amount that can only be determined by making an independent measurement of their size and filling factor. New HST/COS FUV spectroscopy of QSO sightlines passing through pre-defined low-redshift galaxy groups will be important in confirming or denying the presence of warm gas in spiral-rich galaxy groups. These suggested observations could establish the cosmic importance of this warm gas and the hotter gas which it probably traces.

This work was supported by NASA grants NNX08AC146 and NAS5-98043 to the University of Colorado at Boulder and the University of Wisconsin at Madison for the *HST*/COS project. JTS, BAK and HY are partially supported on NSF grant AST-1109117 for the galaxy redshift survey work. TSK acknowledges current support from a European Research Council Starting Grant in cosmology and the IGM under Grant Agreement (GA) 257670. ERW acknowledges support of Australian Research Council Grant DP1095600. Dr. Steven Penton is thanked for help with the galaxy redshift survey database. The authors thank an anonymous referee for her/his persistence in pointing out to us the line-width problems created by models in which these absorber detections are a diffuse gas reservoir.

Facilities: HST (COS), FUSE, WIYN (HYDRA), APO 3.5 m, CTIO/Blanco (Hydra), AAT (AAOmega)

REFERENCES

Anderson, M. E. & Bregman, J. N. 2010, ApJ, 714, 320
Anderson, M. E. & Bregman, J. N. 2011, ApJ, 737, 22
Bahcall, J.N. & Spitzer, L., 1969, ApJ, 156, L63
Bahcall, J. N., Jannuzi, B. T., Schneider, D. P., et al. 1991, ApJ, 377, L5
Beers, T. C., Flynn, K. & Gebhardt, K. 1990, AJ, 100, 32
Berlind, A.A. et al. 2006, ApJS, 167, 1
Berlind, A.A. et al. 2008, yCat, 21670001
Bickel, P.J. & Sakov, A. 2008, Statistica Sinica, 18, 967
Binney, J. & Tremaine, S. 1987, Galactic Dynamics (Princeton: Princeton Univ. Press), pp. 567-575
Bregman, J. N. 2007, ARA&A, 45, 221
Bryan, G. & Norman, M. 1998, ApJ, 495, 80
Cen, R. & Ostriker, J. P. 1999, ApJ, 514, 1
Cen, R. 2013, ApJ, 770, 139
Chen, H.-W. & Mulchaey, J. S. 2009, ApJ, 701, 1219
Chomiuk, L. & Povich, M. S. 2011, AJ, 142, 197
Churchill, C. W., Mellon, R. R., Charlton, J. C., et al. 2000, ApJ, 543, 577
Danforth, C. W. & Shull, J. M. 2008, ApJ, 679, 194
Danforth, C. W., Stocke, J. T. & Shull, J. M. 2010, ApJ, 710, 613
Danforth, C. W., Shull, J. M., Stocke et al. 2014, in preparation
Davé, R., Hernquist, L., Katz, N., & Weinberg, D. H. 1999, ApJ, 511, 521
Davé, R. & Oppenheimer, B. D. 2007, MNRAS, 374, 427
Fang, T., Canizares, C. R., & Yao, Y. 2007, ApJ, 670, 992
Fang, T., Bullock J. S., & Boylan-Kolchin, M. 2013, ApJ, 762, 20
Fukugita, M., Hogan, C. J., & Peebles, P. J. E. 1998, ApJ, 503, 518
Girardi, M. & Giuricin, G. 2000, ApJ, 540, 45
Green, J. C., Froning, C. S., Osterman, S., et al. 2012, ApJ, 744, 60
Gupta, A., Mathur, S., Krongold, Y., Nicastro, F., & Galeazzi, M. 2012, ApJ, 756, L8
Helsdon, S.F., Ponman, T.J. & Mulchaey, J.S. 2005, ApJ, 618, 679
Hinshaw, G., Larson, D., Komatsu, E., et al. 2013, ApJS, 208, 19
Jenkins, E. B., Bowen, D. V., Tripp, T. M., et al. 2003, AJ, 125, 2824
Johnson, S.D., Chen, H-W. & Mulchaey, J.S. 2013, MNRAS, 434, 1765
Kacprzak, G. G., Churchill, C. W., Ceverino, D., et al. 2010, ApJ, 711, 533
Kacprzak, G. G., Churchill, C. W., Barton, E. J., & Cooke, J. 2011, ApJ, 733, 105
Karachentseva, V.E., Karachentsev, I.D. & Sharina, M.E. 2010, Astrophysics, 53, 462
Keeney, B. A., et al. 2013, ApJ, 765, 27
Keeney, B. A., et al. 2014, in preparation
Kereš, D. & Hernquist, L. 2009a, ApJ, 700, L1
Klypin, A., Kravtsov, A. V., Bullock, J. S. & Primack, J. R. 2001, ApJ, 554, 903
Larson, R. B. 1972, MNRAS, 157, 121
Lehner, N., Savage, B. D., Richter, P., et al. 2007, ApJ, 658, 680
Lehner, N. & Howk, J. C. 2011, Science, 334, 955
Lehner, N., Howk, J. C., Tripp, T. M., et al. 2013, ApJ, 770, 138
McGaugh, S. S., Schombert, J. M., Bothun, G. D., & de Blok, W. J. G. 2000, ApJ, 533, L99
Miles, T.A. et al. 2004, MNRAS, 355, 785
Montero-Dorta, A. D. & Prada, F. 2009, MNRAS, 399, 1106
Morris, S. L., Weymann, R. J., Savage, B. D., & Gilliland, R. L. 1991, ApJ, 377, L21
Morris, S. L., Weymann, R. J., Dressler, A., et al. 1993, ApJ, 419, 524
Moster, B. P., Naab, T., & White, S. D. M., 2013, MNRAS, 428, 1321
Mulchaey, J. S., Mushotzky, R. F., Burstein, D., & Davis, D. S. 1996, ApJ, 456, L5 (M96)
Mulchaey, J.S. & Zabludoff, A. I. 1998, ApJ, 496, 73
Mulchaey, J. S. 2000, ARA&A, 38, 289
Narayanan, A.P., Wakker, B.P & Savage, B.D. 2009, ApJ, 703, 74
Narayanan, A.P., Wakker, B.P, Savage, B.D., et al. 2010, ApJ, 721, 960
Osmond, J. P. F & Ponman, T.J. 2004, MNRAS, 350, 1511
Osterman, S., Green, J., Froning, C., et al. 2011, Ap&SS, 335, 257
Pagel, B.E.J. 2008, in "Pathways through an Eclectic Universe", ed. J. H. Knapen, T. J. Mahoney, and A. Vazdekis (San Francisco: Astronomical Society of the Pacific), ASP Conference #390, 483
Pisani, A., Ramella, M & Geller, M.J. 2003, AJ, 126, 1677
Prochaska, J. S., Weiner, B., Chan, H.-W., Cooksey, K., & Mulchaey, J. 2011, ApJS, 193, 28
Prochaska, J. X., Weiner, B., Chen, H.-W., Mulchaey, J., & Cooksey, K. 2011a, ApJ, 740, 91
Richter, P., Savage, B. D., Tripp, T. M. & Sembach, K. R. 2004, ApJS, 153, 165
Rosenberg, J. L., Ganguly, R., Giroux, M. L., & Stocke, J. T. 2003, ApJ, 597, 677

Sarazin, C. L. 1988, X-ray Emission from Clusters of Galaxies (Cambridge: Cambridge University Press)
Savage, B. D., Narayanan, A., Wakker, B. P., et al. 2010, ApJ, 721, 960
Savage, B. D., Narayanan, A., Lehner, N., & Wakker, B. P. 2011, ApJ, 731, 14
Savage, B. D., Lehner, N., & Narayanan, A. 2011, ApJ, 743, 180
Savage, B.D. et al. 2014, ApJS, in press; arXiv:1403.7542 (Paper 1)
Shull, J. M., Penton, S. V., Stocke, J.T. et al. 1998, AJ, 116, 2094
Shull, J. M., Tumlinson, J.T. & Giroux, M.L. 2003, ApJ, 594, L107
Shull, J. M., Smith, B. D., & Danforth, C. W. 2012, ApJ, 759, 23
Simionescu. A. et al. 2011, Science, 331, 1576
Smith, B.D., Hallman, E.J., Shull, J.M. & O'Shea, B.W. 2011, ApJ, 731, 6
Spitzer, L. 1956, ApJ, 124, 20
Steidel, C. C. 1995, in QSO Absorption Lines, ed. G. Meylan (Garching: Springer), 139
Stocke, J. T., Keeney, B. A., McLin, K. M., et al. 2004, ApJ, 609, 94
Stocke, J. T., Penton, S. V., Danforth, C. W., et al. 2006, ApJ, 641, 217
Stocke, J. T., Keeney, B. A., & Danforth, C.W. et al. 2013, ApJ, 763, 148
Thom, C., Tumlinson, J., Werk, J. K., et al. 2012, ApJ, 758, L41
Tilton, E. M., Danforth, C. W., Shull, J. M., & Ross, T. L. 2012, ApJ, 759, 112
Tripp, T. M., Lu, L., & Savage, B. D. 1998, ApJ, 508, 200
Tripp, T. M., Jenkins, E. B., Williger, G. M., et al. 2002, ApJ, 575, 697
Tripp, T. M., Wakker, B. P., Jenkins, E. B., et al. 2003, AJ, 125, 3122
Tripp, T. M., Sembach, K. R., Bowen, D. V., et al. 2008, ApJS, 177, 39
Tully, B. R., Rizzi, L., Shaya, E. J., et al. 2009, AJ, 138, 323
Tumlinson, J. & Fang, T. 2005, ApJ, 623, L97
Tumlinson, J., Thom, C., Werk, J. K., et al. 2011, Science, 334, 948
Tumlinson, J., Thom, C., Werk, J. K., et al. 2013, ApJ, 777, 59
Voit, G.M & Bryan, G.L. 2001, Nature, 414, 425
Wakker, B. P. 2001, ApJS, 136, 463
Wakker, B. P., York, D. G., Howk, J. C., et al. 2007, ApJ, 670, L113
Wakker, B. P., York, D. G., Wilhelm, R., et al. 2008, ApJ, 672, 298
Wakker, B. P. & Savage, B. D. 2009, ApJS, 182, 378
Werk, J., Prochaska, J. X., Thom, C., et al. 2013, ApJS, 204, 17
Werk, J., Prochaska, J.X., Tumlinson, J.T., et al. 2014, ApJ, in press (arXiv: 1403.0947).
White, S. D. M., Navarro, J. F., Evrard, A. E., & Frenk, C. S. 1993, Nature, 366, 429
White, D.A. 2000, MNRAS, 312, 663
Wu X-P, Xue Y-J, Fang L-Z. 1999, ApJ, 524, 22
Yao, Y., Shull, J. M., Wang, Q. D., & Cash, W. 2012, ApJ, 746, 166
Yoon, J. H. Putman, M. E., Thom, C. Chen, H-W and Bryan, G. L. 201, 2ApJ, 754, 84
Zabludoff, A.I. & Mulchaey, J.S. 1998, ApJ, 496, 39

APPENDIX

A. DETAILED REANALYSIS OF A FEW "WARM ABSORBER" CANDIDATES

In this Appendix we present detailed line fits to a few BLA plus broad O VI absorbers which may contain T $> 10^5$ K gas, but were not included as warm absorbers in Paper 1. These fits *do not* replace the line fitting done in Paper 1 which was accomplished with no prior conditions and executed in a conservative manner; e.g., minimum number of components, no requirement to have Lyα align with O VI necessarily, etc. (see Appendix in Paper 1). Here we take a different tactic by adopting an aim to determine the maximum number of plausible warm absorbers which might be present in this sample. We do this by first analyzing the O VI absorption which is less contaminated by lower temperature, photo-ionized gas than Lyα. If the O VI absorption is smooth and symmetrical to the limits of the S/N, then we fit this absorption with a single component and assume that the observed b-value is mostly due to thermal motions. With the O VI fit in-mind we then fit the complex, multi-component Lyα line, constraining the fit to include a component aligned with the broad O VI absorption. If this analysis shows that a BLA can be present with a velocity consistent with the O VI and an observed b-value consistent with T $> 10^5$ K gas, then this absorber is added to the list of plausible warm absorbers in this sample.

See the Appendix and Table 5 of Paper 1 for the Lyα and O VI line fits of these 10 absorbers, which we now discuss one-by-one. For each absorber we first describe the results of Paper 1 and then the new analysis is presented in the second paragraph. We emphasize that these re-analyses represent alternative absorption-line component deconvolutions, not necessarily superior ones, to those found in Paper 1.

A.1. *PKS2155-304/0.05722*

Because the Lyα and O VI absorptions do not align in velocity, Paper 1 did not analyze this system in detail. However, the O VI absorption visible in a high-S/N *FUSE* spectrum is quite symmetrical and has a velocity within the span of the Lyα profile. This system has been studied in detail by Shull et al. (1998, 2003) including a reconciliation of the O VI detection and possible *Chandra* O VIII detections. Shull et al. (1998) also identified a small foreground group of galaxies at the absorber redshift and provides accurate H I emission velocities for each group member detected. Therefore, it is worthwhile to consider this absorber in the context of warm gas.

Despite attempts to constrain a BLA absorption component to be coincident in velocity with the broad O VI, the closest offset finds the O VI centroid 46 km s^{-1} higher in velocity than the nearest Lyα component. Because the Lyα absorption is found in both a COS and a STIS spectrum and the O VI was detected by *FUSE*, a velocity offset is possible. However, the *FUSE* LiF2a spectrum and the COS spectrum detect the same Galactic Fe II 1144.8Å line with a velocity offset of only -10 km s^{-1}. Therefore, the O VI absorption remains inconsistent (Δv $\geq$ 36 km s^{-1}) with any Lyα component and no warm absorber is present in agreement with the conclusion of Paper 1.

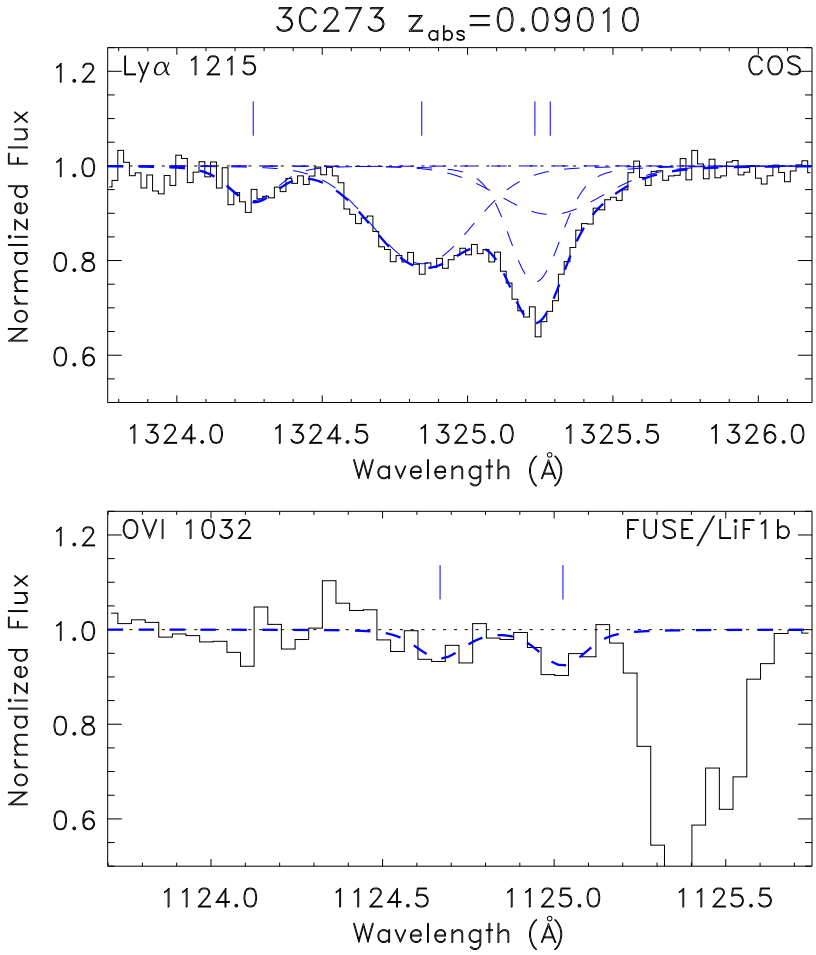

Figure 12. The Lyα and O VI 1032 Å absorption lines for the 3C 273 $z_{\rm abs} = 0.09010$ absorber with our revised models (see Table 9) in blue. The redward (longest wavelength) BLA was constrained to match the redward of two O VI absorbers to Δv of $\pm$10 km s^{-1}

Table 9
Profile Fit Results: 3C 273 $z_{\rm abs} = 0.09010$

Species	λ_0 (Å)	v (km s^{-1})	b (km s^{-1})	log N (cm^{-2})
Lyα	1216	-226 ± 3	22 ± 4	12.47 ± 0.05
		-83 ± 2	49 ± 3	13.23 ± 0.02
		$+12 \pm 2$	23 ± 3	13.06 ± 0.09
		$+26 \pm 10$	52 ± 11	12.92 ± 0.10
O VI	1032	-68 ± 13	~ 20	13.0 ± 0.3
		$+32 \pm 10$	~ 20	13.1 ± 0.02
O VI	1038	$+35 \pm 10$	~ 26	13.5 ± 0.02

A.2. *3C 273/0.09010*

Paper 1 reports that this system contains three Lyα absorption lines which are nearly completely disjoint in velocity while the O VI absorber is displaced by $\approx$ 30 km s^{-1} to higher velocity. The best fit to the redward of two closely-spaced Lyα components (see Figure 12) is quite acceptable but leaves open the possibility for the presence of a broad component that could align with the observed, symmetric O VI absorption.

In our reanalysis of this absorber we have fit the Lyα absorption with four components, constraining one of the components to align with the symmetrical O VI absorption line. Our best fit for this aligned component finds $b_{H\ I} = 49 \pm 3$ km s^{-1} and $b_{O\ VI} \approx 20$ km s^{-1} (see Table 9). The combination of b-values results in a thermal width of $\approx$ 46 km s^{-1} and log T (K) $\approx$ 5.1. Therefore, we judge that this absorption system likely, but not conclusively, contains a warm absorber. This new fit is shown in Figure 12.

A.3. *PG 1116+215/0.13850*

Despite a broad (b= 36 km s^{-1}), symmetric and aligned O VI absorption line well-measured with COS, Paper 1 finds only minimal evidence for a BLA setting a temperature of log T (K)=4.72, consistent with very low density gas

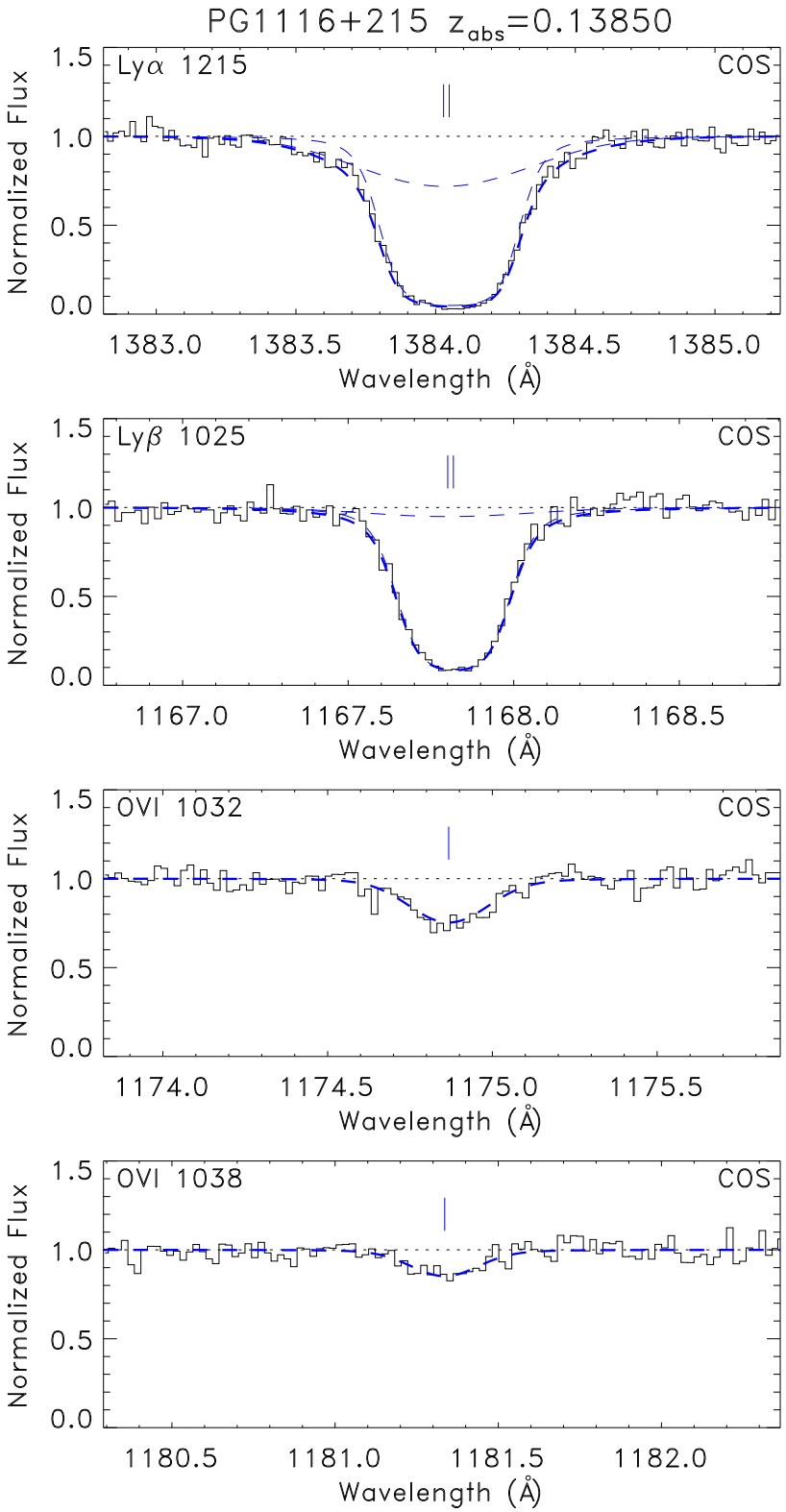

Figure 13. The Lyα, Lyβ and O VI doublet absorption lines for the PG 1116+215 $z_{\rm abs} = 0.13850$ absorber with our revised models (see Table 10) over-plotted in blue. The BLA component is displayed on the Lyβ profile for illustrative purposes only.

in photo-ionization equilibrium. The combination of the Lyα and O VI b-values obtained by Paper 1, suggests that the line widths are dominated by turbulence. This would be an unusual situation given the striking symmetry and lack of structure in the COS-observed O VI line.

An alternate extraction of the same data by Danforth et al. (2010) finds a slightly stronger blue wing to the Lyα line which is aligned with the O VI (see Figure 12). A best-fit $b(H\ I) = 86\pm$ 11 km s^{-1} BLA is found, which is aligned to within the velocity errors with the O VI 1031, 1038Å $b = 35\pm5$ km s^{-1} absorber (see Table 10). This combination

Table 10
Profile Fit Results: PG 1116+215 $z_{\rm abs} = 0.13850$

Species	λ_0 (Å)	v (km s^{-1})	b (km s^{-1})	log N (cm^{-2})
Lyα	1216	$+3 \pm 5$	86 ± 11	13.6 ± 0.1
		$+8 \pm 1$	31 ± 2	14.8 ± 0.1
Lyβ	1026	$+10 \pm 1$	28 ± 1	15.3 ± 0.1
O VI	1032	$+6 \pm 2$	37 ± 3	13.8 ± 0.1
O VI	1038	$+3 \pm 5$	32 ± 5	13.8 ± 0.1
N V	1238	0 ± 2	14 ± 3	12.9 ± 0.1
Si IV	1394	-7 ± 2	≤ 5	12.9 ± 0.1
C IV	1548	-9 ± 3	17 ± 4	13.3 ± 0.1
	1550	-1 ± 6	26 ± 5	13.4 ± 0.2
Si III	1206	-2 ± 1	11 ± 1	12.8 ± 0.1
C II	1334	-2 ± 1	8 ± 1	14.0 ± 0.1
	1036	$+2 \pm 1$	14 ± 2	13.8 ± 0.1
Si II	1260	-7 ± 2	15 ± 2	12.5 ± 0.1
	1193	-7 ± 1	13 ± 2	12.8 ± 0.1

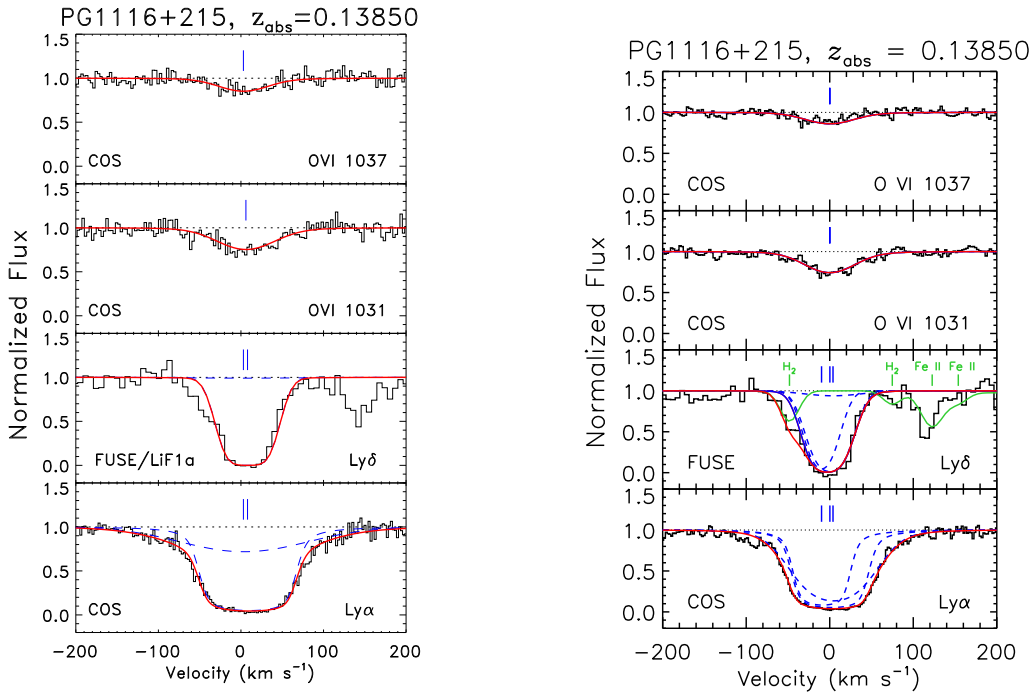

Figure 14. The Lyα absorption lines as extracted and fitted by this analysis (at left) and by Paper 1 (at right). The Paper 1 extraction includes an attempt to remove fixed pattern noise (see Paper 1 for details), which this analysis does not employ. In both cases a blue-wing is present which we fit as a BLA component using the extraction at left (see Table 10 for detailed solutions).

of observed b-values yields $b_T = 81 \pm 14$ km s^{-1}, log T (K)= 5.6 (+0.1/-0.2) and $b_{NT} \approx 30$ km s^{-1}. A narrower Lyα component is well-matched ($b = 31 \pm 2$ km s^{-1}) to the widths of the low ion metal lines (see Figure 13 and Table 10). However, a curve-of-growth (COG) analysis using 3 Lyman-series lines finds an order of magnitude more column density than as shown for Lyα in Table 7 and a 10 km s^{-1} lower b-value for the cool component. Also the N V 1238 Å and C IV 1548, 1550 Å absorptions have b-values intermediate between the C II and O VI absorptions. Clearly the photo-ionized absorber in this system is more complex than a single homogenous cloud. Using the COG values for the cool absorber does not change the best-fit to the warm absorber component.

For clarity in Figure 14 we show the Lyα absorption profiles for this absorber as extracted and fitted by Paper 1 (at left) compared to the extraction and analysis reported herein (at right). While a blue-wing is present in both cases, it is present more clearly in the extraction shown at left. In the spirit of the reanalysis presented here, we adopt the line-fit shown at left in Figure 14 in which a BLA is found coincident in velocity with the broad O VI (solution presented in Table 10). We conclude that the PG 1116+215/0.13850 absorption complex very likely contains a warm absorber.

A.4. *PHL 1811/0.17651*

The best fit to the 1038 Å O VI absorption is broad (b = 20 km s^{-1}) and symmetric; the 1032 Å line is obscured by Galactic Lyα. The C III 977 Å line shows two components, the red-ward component quite narrow ($b \approx 8$ km s^{-1}) and the blue-ward one unmatched either in Lyα or O VI. The two-component fit to the Lyα line in Paper 1 does not yield either a broad or an aligned component. Therefore, no absorber temperature was derived and no BLA obviously detected. However, the O VI velocity centroid is within the velocity spread of the Lyα absorption, suggesting that a BLA at the O VI velocity could be present.

However, in investigating this system further we find that for C III the broader, blue-ward component (see Figure A4 in Paper 1) is identified as Lyβ at $z = 0.12051$. Additionally, Lyγ in this system is confused by the presence of an Fe II HVC so that little useful detail can be derived from it. Refitting Lyα unconstrained by Lyγ can produce a two component fit with one component aligned with the broad O VI. However, the width of this line cannot be much broader than the fit in Paper 1. Therefore, our reanalysis of this system concludes that a warm absorber is not present, consistent with the conclusions of Paper 1.

A.5. *H 1821+643/0.17036*

In this case the O VI absorption is fitted by Paper 1 as two components, one of which is extremely broad ($\approx$ 80 km s^{-1}). However, the continuum is poorly defined in this region due to the presence to the blue of Galactic Si III and an intervening Lyman series line at a different redshift. The resulting O VI absorption is quite shallow (see Figure A6 in Paper 1) and, while a symmetrical O VI component could be present, the overall profile is not obviously Gaussian. The velocity centroid of the O VI is well within the velocity spread of the Lyα absorption line complex, which is fit by three overlapping components. The best-fit solution in Paper 1 does not yield an alignment between the very broad O VI component and any of the three Lyα components. A second, weaker O VI line coincident in velocity with a BLA component yields log T (K)= 5.10, but the O VI line fitting is uncertain due to an uncertain continuum.

In refitting this absorber we started by removing the higher-order Lyζ line at z =0.29686 using a model for the line strength and width obtained using curve-of-growth fitted values. Then, instead of allowing the fit to proceed without constraint as in Paper 1, the two O VI components were constrained to align with the two higher redshift components in Lyα. In this case a poorer fit to the data was obtained compared to that of Paper 1 but two aligned components resulted (see Figure 15). For the Lyα/O VI component at Δv $\approx$ -100 km s^{-1} the fitted H I and O VI lines have nearly equal b-values of $\approx$ 50 km s^{-1} implying that the line widths are dominated by NT motions and the bulk temperature of the gas is quite low, consistent with photo-ionization equilibrium. In our minimally constrained model, the component at $\Delta v \approx +30$ has $b_{OVI} = 47 \pm 8$ km s^{-1} and $b_{H\ I} = 34 \pm 2$ km s^{-1}, an unphysical result. Adding a fourth component specifically at the broad O VI velocity is allowed by the data but results in a $b_{H\ I} \approx 50$ km s^{-1}, yielding an absorber at log T (K) < 5.0, with substantial NT motions. Thus, attempts to constrain two Lyα and O VI absorbers to match in velocity result in a poorer fit than in Paper 1 and no second warm absorber. Therefore, we adopt the solution of Paper 1 for this absorber as its best description.

A.6. *Ton 236/0.19457*

The very broad (b =70 km s^{-1}) O VI measured with COS is somewhat symmetrical (see Figure A8 in Paper 1), but could have excess absorption redward of line center. Paper 1 had already fit a BLA with b =82 km s^{-1} which left most of the total b-value being due to NT motions but with a significant thermal component and a best-fit log T (K)=5.07. Thus, a warm absorber was judged to be present by Paper 1.

However, while neither the O VI nor the Lyα profiles demand it (i.e., the fits obtained in Paper 1 are fully acceptable), we have refit both lines with two components. The second component in O VI is $\sim$70 km s^{-1} redward of the stronger component shown in Paper 1, Figure A8. Constraining Lyα to match the two O VI components results in two BLAs with b= 45 and 90 km s^{-1}. These fits are shown in Figure 16 with parameters listed in Table 11. This alternative fit confirms that at least one warm absorber is present and that two broad components can fit these data. However, even attempting to constrain the lower redshift Lyα absorber does not yield a velocity alignment with the O VI and further requires $b_{O\ VI} \approx b_{H\ I}$. Thus, this component is significantly misaligned and the O VI and Lyα b-values cannot be used to constrain physical conditions. The higher redshift component has the Lyα and O VI lines aligned to within the rather wide errors. Adopting $b_{O\ VI} \approx 40$ km s^{-1} for the higher redshift absorber yields a thermal $b_T \approx 83$ (+16/-24) km s^{-1} and log T (K)= 5.8 (+0.2/-0.3). This is hotter than the warm absorber derived in Paper 1. Although this two-component fit is not demanded by the data, the O VI and Lyα profiles are suggestive of two absorbers, so we adopt the solution in Table 11 for the best description for this absorber. A single warm absorber is confirmed but at a higher temperature than derived by Paper 1.

A.7. *HE 0153-4520/0.40052*

Both the O VI and the H I are broad and have a complex profile in this absorber. Because the Lyα components are comparably broad to the O VI components aligned with them, Paper 1 judged most of the b-value to be NT and derived temperatures consistent with photo-ionization in a very low density gas.

A reanalysis of this system finds good two-component fits to O VI, Lyα and Lyβ, which are not inconsistent with the detailed fits in Paper 1. We conclude that, while a BLA is present, the b-values are consistent with photo-ionized gas in this system. Thus, we adopt the component fit of Paper 1 and conclude that no warm absorber is present.

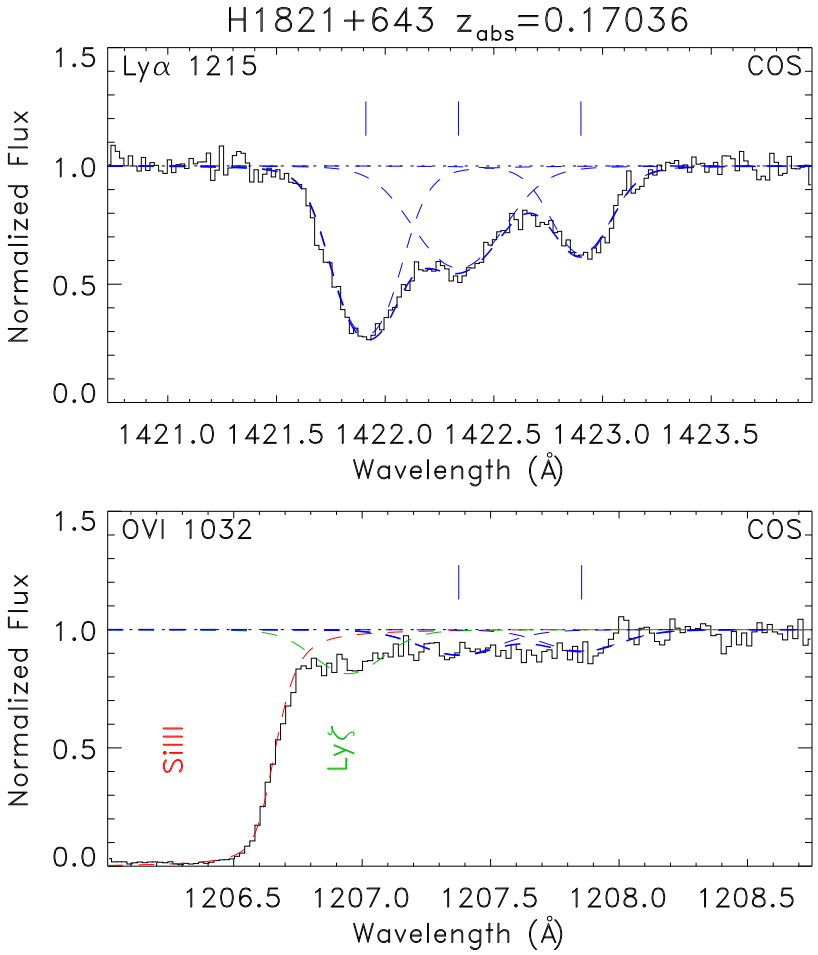

Figure 15. The Lyα and O VI doublet absorption lines for the H 1821+643 $z_{\rm abs} = 0.17036$ absorber with our revised models over-plotted in blue. Careful fits to the Galactic Si III and intervening Lyζ ($z_{\rm abs} = 0..29675$) are shown in red and green, respectively. In this case the new models are not so dissimilar from the Paper 1 models and no new warm absorber is claimed.

Table 11
Profile Fit Results: Ton 236 $z_{\rm abs} = 0.19457$

Species	λ_0 (Å)	v (km s^{-1})	b (km s^{-1})	log N (cm^{-2})
Lyα	1216	-7 ± 3	45 ± 3	13.9 ± 0.1
		$+25 \pm 10$	90 ± 9	13.7 ± 0.1
O VI	1032	-34 ± 6	37 ± 8	13.9 ± 0.1
		$+35 \pm 10$	40 ± 17	13.6 ± 0.2

A.8. *PKS 0405-123/0.09657*

Due to potentially different wavelength calibrations for the O VI line in the *FUSE* band and the Lyα line in the COS band, Paper 1 questioned whether the broad, symmetric O VI absorption at this redshift was associated with a narrow or a broad Lyα absorption, which differ only by 11 km s^{-1}. In the end Paper 1 concluded that the broad O VI was better aligned with the narrow Lyα requiring log T (K) = 4.30 (+0.21/-01.02), but noted that the warm absorber association appeared equally likely.

In this absorber the Lyβ line is detected clearly in the *FUSE* spectrum adjacent to the O VI absorber at a velocity 17 km s^{-1} lower than the O VI absorption based on our analysis. The detected Lyβ must be associated almost exclusively with the narrow Lyα component, which is 4–5 times stronger than the BLA. This analysis provides a wavelength offset for these two spectra which places the O VI absorption much closer in velocity to the BLA (Δ v = 6 km s^{-1}) than the narrow H I component. We conclude that the O VI is associated with a BLA in a warm absorber and retain the values suggested in Paper 1, including log T(K)=5.48±0.05. However, because the PIE/CIE determination rests solely on a wavelength solution which is uncertain at the level to which these two absorption systems differ, we conclude that this absorber's temperature can not be determined within a reasonable doubt. On this basis we have excluded this system from the analysis herein and ascribe it neither as a warm nor a cool absorber.

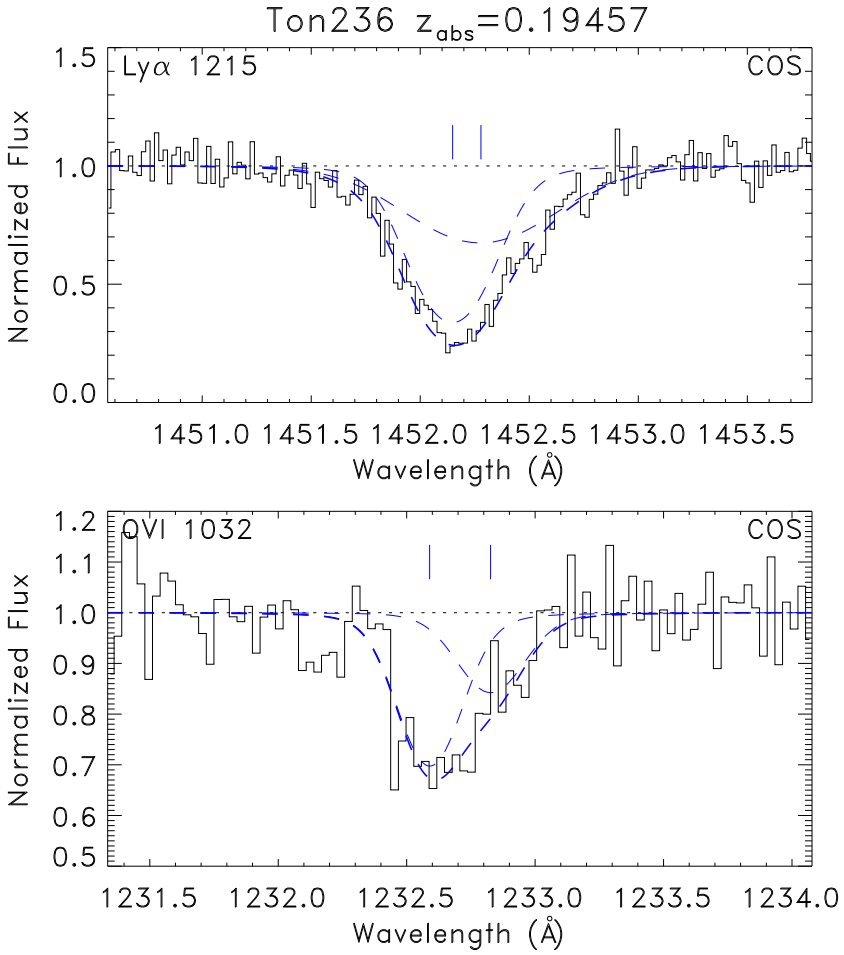

Figure 16. The Lyα and O VI 1032Å absorption lines for the Ton 236 $z_{\rm abs}$ = 0.19547 absorber with our revised models (see Table 11) over-plotted in blue. The redder O VI component is aligned with the broader Lyα component to within the errors in the velocity calibration.

Table 12
Profile Fit Results: PKS 0405−123 $z_{\rm abs}$ = 0.29770

Species	λ_0 (Å)	v (km s^{-1})	b (km s^{-1})	log N (cm^{-2})
Lyα	1216	-51 ± 30	100 ± 10	13.15 ± 0.10
		-45 ± 3	30 ± 3	13.78 ± 0.05
		$+29 \pm 10$	31 ± 8	13.3 ± 0.2
O VI	1032	-50 ± 4	56 ± 4	13.55 ± 0.10

A.9. *PKS 0405-123/0.29770*

In this case, the O VI absorption is very broad and symmetrical. In order to fit Lyα with the minimum number of components (2), the width of the Lyα is only slightly broader than its associated O VI. Paper 1 judged this O VI absorber to have a width dominated by NT motions and a derived temperature of log T (K) =4.62 consistent with photo-ionization in a low density gas.

The symmetrical O VI absorption suggests that the dominant broadening mechanism in this absorber is thermal. In this case a third component was added at the velocity of the broad O VI absorber to the two found in Paper 1. The resulting three Lyα components are shown in Figure 17 with their particulars recorded in Table 12. While the b-value of the very broad component is not tightly constrained, a significant column density BLA with b= 86 (+14/-17) km s^{-1} is suggested which results in log T (K) = 5.7(+0.1/-0.2), considerably hotter than the model adopted in Paper 1. We adopt this new three component fit which results in a new warm absorber in the sample.

A.10. *3C 263/0.11389*

This absorber has an O VI aligned with a rather narrow (b= 20 km s^{-1}) H I line leading Paper 1 to conclude that this absorber is in photo-ionization equilibrium. In addition, there are two BLAs with no associated O VI absorptions. Therefore, these absorbers are judged to be misaligned and are not interpreted in Paper 1.

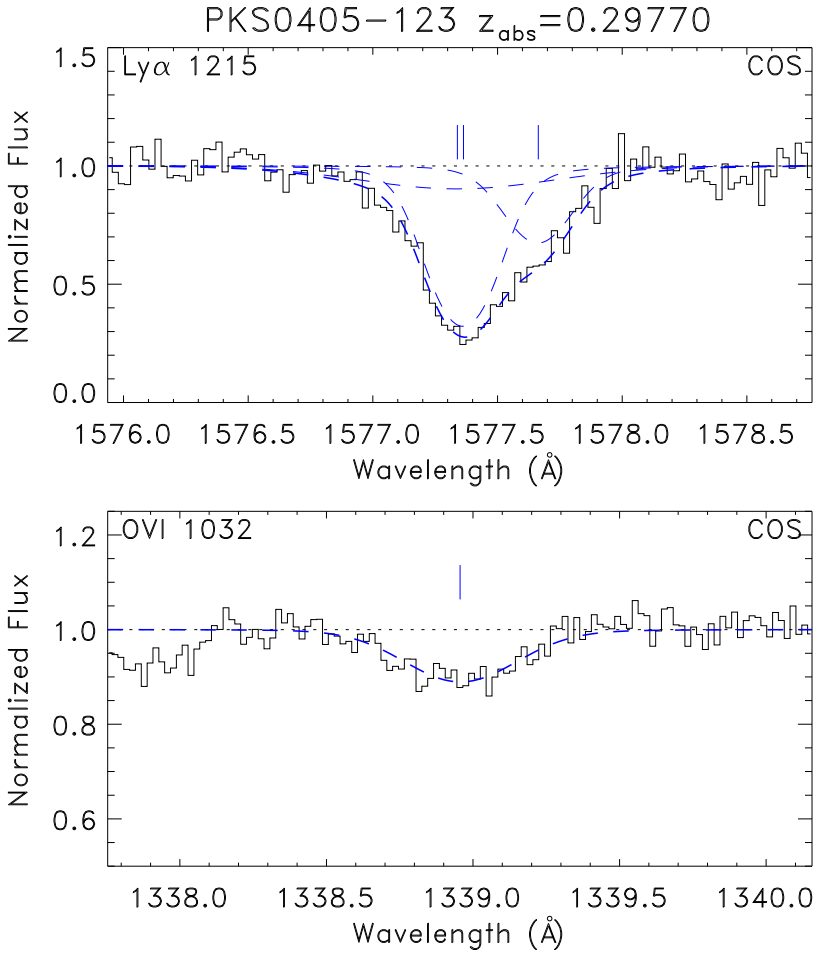

Figure 17. The Lyα and O VI 1032 Å absorption lines for the PKS 0405−123 $z_{\rm abs} = 0.29770$ absorber with our revised models (see Table 12) over-plotted in blue. The broad Lyα component is aligned with the O VI profile.

Our analysis reproduces the detailed three component fits in Paper 1, including the exact b-values of each H I component. In addition, we use the *FUSE* Lyβ absorption to make a two-line (Lyα/Lyβ) COG analysis which finds b= 48 km s^{-1} for the lowest velocity component, consistent with the b=47±1 derived from the Lyα line alone. This consistency suggests, but does not demand, that the lowest velocity H I component at Δv = -219 km s^{-1} is a metal-deficient BLA and warm absorber. The Δv = -44 km s^{-1} component is confirmed by our reanalysis to have a large b-value but the absence of detectable Lyβ for this component leaves us unable to draw any firm conclusion as to its physical details. Additionally, the Δv = -44 km s^{-1} portion of the Lyα absorption complex (see Figure A13 in Paper 1) appears to have structure in the absorption making it an unlikely BLA. We conclude that the detailed fit to this absorber obtained by Paper 1 is the best description of this absorber but also that an H I-only warm absorber is **possibly** present with log T (K) ≈ 5.14.

B. BASIC GALAXY DATA FOR GROUP MEMBERS ASSOCIATED WITH WARM, COOL AND MISALIGNED ABSORBERS

In this Appendix we tabulate the group members for all warm, cool and misaligned absorbers (in that order) with $N_{grp} \geq 8$ members (see Tables 5,6 & 7 in the main text). The absorber 3C 263/0.11389 with $N_{grp} = 7$ members has been added because it may contain a warm absorber (see Appendix A and Figure 7). The galaxy redshift data comes from a variety of sources including a combined redshift catalog of nearby galaxy redshifts (Catalog Stocke et al. 2006); the Sloan Digital Sky Survey [SDSS]; and our own MOS galaxy redshift surveys in Australia [AAT] or at WIYN or CTIO [HYDRA] (Keeney et al. 2014). A complete listing of all galaxies surveyed in these latter redshift surveys will be presented at a later time (Keeney et al. 2014). See Section 3 in the main text for a description of these various sources which are listed in column (4) of the following tables.

These tables include by column: (1) galaxy name or "..." if unnamed; (2) and (3) galaxy RA and DEC in J2000.0 equinox coordinates; (4) the source for the redshift as described above; (5) the heliocentric redshift ($\pm$ 30 km s^{-1}); (6) the galaxy g-band luminosity in L* units; (7) the impact parameter from the sightline to the galaxy in kpc; (8)the impact parameter from the sightline to the galaxy in units of the galaxy's virial radius (see Figure 1 in Stocke et al. 2013); and (9) the velocity difference between the galaxy and the absorber.

Table 13
Galaxy Group Members Near 3C 273 ($z_{\rm abs} = 0.00336$)

Name	Position (J2000)	Source	$z_{\rm gal}$	$L_{\rm gal}$ (L^*)	ρ (kpc)	$\rho/R_{\rm vir}$	Δv (km s^{-1})
McLin77	12:29:50.50, +02:02:08.8	Catalog	0.00519	0.009	46	0.81	547
TGN388Z111	12:29:50.57, +02:01:54.2	Catalog	0.00540	0.012	46	0.79	610
TGN387Z059	12:28:15.95, +01:49:43.7	Catalog	0.00300	0.021	77	1.20	−108
A1225+0152	12:27:46.50, +01:36:03.0	Catalog	0.00433	0.021	141	2.19	290
12285+0157	12:31:03.80, +01:40:34.0	Catalog	0.00369	0.043	155	2.12	97
12277+0254	12:30:14.20, +02:37:32.0	Catalog	0.00545	0.057	160	2.08	626
12265+0300	12:29:02.80, +02:43:19.0	Catalog	0.00525	0.061	168	2.14	565
A1225+0258	12:28:15.90, +02:42:02.0	Catalog	0.00777	0.021	171	2.66	1317
NGC 4420	12:26:58.00, +02:29:39.0	Catalog	0.00565	0.489	174	1.21	683
A1224+0146	12:27:15.60, +01:29:24.0	Catalog	0.00425	0.028	183	2.71	267
TGN387Z165	12:25:42.12, +02:09:24.8	Catalog	0.00500	0.021	216	3.36	490
A1225+0311	12:28:03.40, +02:54:37.0	Catalog	0.00496	0.073	225	2.77	478
TGN389Z231	12:32:46.45, +01:34:07.2	Catalog	0.00510	0.014	260	4.33	520
IC 3474	12:32:37.00, +02:39:51.0	Catalog	0.00576	0.073	268	3.30	717
A1230+0254	12:32:51.90, +02:37:46.0	Catalog	0.00592	0.021	277	4.31	764
TGN389Z221	12:33:20.76, +01:31:21.1	Catalog	0.00600	0.045	297	4.04	789
...	12:32:50.55, +02:47:50.3	SDSS	0.00359	0.009	300	5.31	69
TGN388Z200	12:34:27.59, +02:11:11.3	Catalog	0.00550	0.012	337	5.79	639
...	12:34:22.02, +02:19:31.4	SDSS	0.00587	0.078	337	4.08	750
NGC 4536	12:34:26.90, +02:11:18.0	Catalog	0.00603	2.410	337	1.39	798
NGC 4533	12:34:21.00, +02:19:34.0	Catalog	0.00585	0.097	337	3.86	743
NGC 4527	12:34:08.80, +02:39:13.0	Catalog	0.00579	1.562	350	1.66	726
TGN386Z061	12:23:30.01, +02:00:28.7	Catalog	0.00600	0.014	352	5.87	789
TGN386Z065	12:23:23.33, +01:48:53.5	Catalog	0.00600	0.014	364	6.07	789
A1232+0250	12:34:34.10, +02:34:11.0	Catalog	0.00616	0.028	366	5.43	838
...	12:34:34.99, +02:34:07.8	SDSS	0.00615	0.012	367	6.30	835
NGC 4457	12:28:59.20, +03:34:16.0	Catalog	0.00294	1.165	382	1.99	−126
A1227+0353	12:29:39.20, +03:36:43.0	Catalog	0.00446	0.066	393	4.92	329
12234+0342	12:25:58.96, +03:25:38.3	Catalog	0.00476	0.073	397	4.88	417
...	12:25:58.36, +03:25:49.0	SDSS	0.00472	0.083	398	4.73	406
A1230+0338	12:32:55.60, +03:21:34.0	Catalog	0.00245	0.073	406	4.99	−272
...	12:32:54.95, +03:21:46.3	SDSS	0.00253	0.002	407	8.76	−249
12213+0321	12:23:54.20, +03:05:07.0	Catalog	0.00620	0.052	417	5.50	850
12221+0335	12:24:40.10, +03:18:10.0	Catalog	0.00309	0.080	420	5.06	−80
12204+0302	12:22:56.40, +02:44:49.0	Catalog	0.00617	0.057	425	5.51	840
12194+0237	12:21:57.50, +02:20:40.0	Catalog	0.00611	0.047	455	6.14	822
TGN321Z038	12:32:25.84, +00:24:09.4	Catalog	0.00470	0.002	464	9.99	400
TGN321Z031	12:32:33.54, +00:24:17.1	Catalog	0.00420	0.005	467	9.17	251
NGC 4517A	12:32:28.20, +00:23:23.0	Catalog	0.00510	0.513	468	3.22	521
TGN321Z040	12:32:27.68, +00:22:07.7	Catalog	0.00490	0.012	472	8.11	460
NGC 4544	12:35:36.60, +03:02:04.3	Catalog	0.00385	0.128	477	5.09	146
12314+0349	12:33:55.40, +03:32:52.0	Catalog	0.00380	0.057	482	6.25	130
...	12:26:13.90, +03:50:13.7	SDSS	0.00270	0.002	483	10.40	−197
TGN320Z113	12:29:03.86, +00:06:13.7	Catalog	0.00380	0.031	490	7.15	131
NGC 4496A	12:31:39.20, +03:56:23.0	Catalog	0.00577	1.174	500	2.61	720
...	12:24:41.31, +03:43:17.4	SDSS	0.00620	0.012	503	8.64	849
A1222+0400	12:24:41.70, +03:43:35.0	Catalog	0.00621	0.047	504	6.80	851
NGC 4412	12:26:35.80, +03:57:57.0	Catalog	0.00765	0.369	506	3.87	1282
12309+0404	12:33:29.50, +03:47:40.0	Catalog	0.00304	0.038	517	7.27	−97
TGN322Z243	12:33:58.59, +00:23:12.3	Catalog	0.00520	0.005	518	10.17	550
A1231+0400	12:34:16.90, +03:44:04.0	Catalog	0.00809	0.002	533	11.47	1412
NGC 4517	12:32:45.40, +00:06:54.0	Catalog	0.00374	1.968	538	2.37	112
NGC 4480	12:30:26.50, +04:14:53.0	Catalog	0.00816	0.321	558	4.47	1433
TGN385Z025	12:20:11.20, +01:57:29.6	Catalog	0.00680	0.017	561	9.12	1028
12221+0416	12:24:39.30, +03:59:43.0	Catalog	0.00575	0.057	563	7.30	715

Table 13 — *Continued*

Name	Position (J2000)	Source	$z_{\rm gal}$	$L_{\rm gal}$ (L^*)	ρ (kpc)	$\rho/R_{\rm vir}$	Δv (km s^{-1})
A1224+0432	12:27:16.40, +04:15:42.0	Catalog	0.00546	0.012	567	9.74	629
NGC 4581	12:38:05.15, +01:28:40.3	Catalog	0.00606	0.321	582	4.67	808
A1220+0400	12:22:41.30, +03:43:34.0	Catalog	0.00621	0.047	582	7.85	851
TGN390Z245	12:38:05.30, +01:28:44.2	Catalog	0.00580	0.095	582	6.70	729
TGN385Z034	12:19:53.06, +01:46:23.5	Catalog	0.00660	0.028	583	8.64	968
···	12:20:33.95, +02:58:04.0	SDSS	0.00796	0.002	583	12.55	1375
12174+0204	12:19:52.00, +01:46:22.0	Catalog	0.00675	0.061	584	7.44	1014
A1218+0314	12:20:33.00, +02:58:10.0	Catalog	0.00795	0.009	584	10.34	1372
A1217+0203	12:19:51.60, +01:46:23.0	Catalog	0.00630	0.035	585	8.32	878
···	12:26:24.54, +04:19:00.8	SDSS	0.00775	0.002	594	12.79	1313
NGC 4587	12:38:35.50, +02:39:24.0	Catalog	0.00301	0.128	614	6.55	−106
···	12:36:34.93, +03:38:31.3	SDSS	0.00595	0.005	616	12.09	773
TGN389Z074	12:38:21.72, +01:12:06.9	Catalog	0.00420	0.007	619	11.45	251
12217+0430	12:24:14.40, +04:13:33.0	Catalog	0.00392	0.061	626	7.97	167
A1222+0441	12:25:08.60, +04:24:59.0	Catalog	0.00409	0.012	644	11.06	218
A1218+0403	12:21:19.50, +03:46:40.0	Catalog	0.00812	0.007	653	12.08	1423
NGC 4289	12:21:02.40, +03:43:20.0	Catalog	0.00873	0.073	658	8.10	1605
A1230+0451	12:32:57.60, +04:34:40.0	Catalog	0.00411	0.073	679	8.35	225
···	12:32:58.82, +04:34:45.0	SDSS	0.00405	0.007	680	12.58	207
12373+0156	12:39:50.10, +01:40:26.0	Catalog	0.00409	0.047	680	9.17	219
TGN389Z019	12:39:50.38, +01:40:21.5	Catalog	0.00430	0.052	680	8.96	281
TGN322Z009	12:39:02.47, +00:50:58.5	Catalog	0.00540	0.014	693	11.55	610
A1218+0421	12:21:19.50, +04:04:40.0	Catalog	0.00660	0.028	705	10.45	968
12342+0423	12:36:49.10, +04:06:17.0	Catalog	0.00205	0.033	707	10.20	−390
A1223+0505	12:25:33.20, +04:48:54.0	Catalog	0.00812	0.002	729	15.69	1421
NGC 4599	12:40:27.09, +01:11:48.8	Catalog	0.00612	0.243	744	6.54	826
···	12:21:39.57, +04:23:33.7	SDSS	0.00381	0.005	751	14.74	135
NGC 4600	12:40:22.99, +03:07:03.6	Catalog	0.00263	0.243	756	6.65	−220
NGC 4303	12:21:54.90, +04:28:25.0	Catalog	0.00523	5.673	757	2.34	559
NGC 4303A	12:22:27.30, +04:33:58.0	Catalog	0.00429	0.080	757	9.12	279
···	12:22:25.80, +04:34:04.8	SDSS	0.00428	0.005	758	14.88	274
···	12:22:27.24, +04:34:33.0	SDSS	0.00448	0.009	759	13.44	335
NGC 4378	12:25:18.07, +04:55:30.0	Catalog	0.00854	0.851	761	4.42	1547
12166+0408	12:19:09.90, +03:51:19.0	Catalog	0.00509	0.116	771	8.47	516
12177+0429	12:20:17.10, +04:12:05.0	Catalog	0.00578	0.061	773	9.84	723
···	12:41:11.58, +01:24:37.0	SDSS	0.00565	0.050	775	10.31	683
12387+0140	12:41:11.70, +01:24:37.0	Catalog	0.00579	0.139	776	8.13	727
TGN390Z138	12:41:39.13, +01:50:16.6	Catalog	0.00490	0.021	789	12.28	460
TGN322Z003	12:40:35.23, +00:46:12.7	Catalog	0.00550	0.007	789	14.59	639
···	12:27:26.97, +05:11:16.5	SDSS	0.00406	0.012	795	13.66	210
NGC 4292	12:21:16.40, +04:35:47.0	Catalog	0.00753	0.168	806	8.00	1247
NGC 4586	12:38:28.00, +04:19:08.0	Catalog	0.00266	0.517	818	5.62	−209
···	12:38:33.65, +04:18:28.6	SDSS	0.00224	0.066	820	10.28	−336
TGN390Z124	12:42:21.28, +02:03:59.3	Catalog	0.00460	0.040	831	11.58	371
12190+0503	12:21:34.07, +04:46:46.4	Catalog	0.00740	0.080	833	10.04	1207
12214+0527	12:24:03.20, +05:10:47.0	Catalog	0.00683	0.057	847	10.99	1037
12196+0514	12:22:11.00, +04:57:10.0	Catalog	0.00638	0.043	848	11.63	902
···	12:35:24.43, +05:02:53.8	SDSS	0.00606	0.009	850	15.05	808
NGC 4234	12:17:07.89, +03:40:56.3	Catalog	0.00676	0.255	855	7.40	1015
···	12:17:09.15, +03:40:59.2	SDSS	0.00672	0.165	855	8.49	1004
12225+0537	12:25:05.40, +05:19:46.0	Catalog	0.00662	0.052	861	11.35	975
···	12:25:35.33, +05:22:51.7	SDSS	0.00774	0.007	865	16.00	1310
···	12:32:36.19, +05:23:17.1	SDSS	0.00281	0.005	866	17.00	−164
···	12:40:25.92, +04:03:00.5	SDSS	0.00243	0.005	869	17.06	−279
···	12:42:59.75, +02:06:03.1	SDSS	0.00286	0.002	872	18.77	−149
NGC 4636	12:42:49.80, +02:41:17.0	Catalog	0.00365	2.897	876	3.38	86
···	12:19:27.76, +04:34:42.5	SDSS	0.00571	0.014	877	14.62	702
TGN250Z171	12:36:07.69, –00:59:18.7	Catalog	0.00320	0.007	882	16.31	−48
12194+0523	12:22:01.29, +05:06:00.2	Catalog	0.00637	0.080	885	10.66	900
NGC 4324	12:23:05.70, +05:14:59.0	Catalog	0.00556	0.657	887	5.61	658
TGN390Z102	12:43:19.56, +01:58:55.0	Catalog	0.00440	0.180	892	8.68	311
NGC 4643	12:43:20.20, +01:58:41.0	Catalog	0.00440	1.621	893	4.19	311
···	12:18:17.92, +04:24:07.9	SDSS	0.00666	0.005	899	17.65	987
···	12:42:17.85, +03:28:07.4	SDSS	0.00244	0.014	901	15.02	−276
A1216+0456	12:19:05.60, +04:39:33.0	Catalog	0.00783	0.019	907	14.41	1336
NGC 4592	12:39:19.10, –00:31:55.0	Catalog	0.00360	0.768	912	5.46	71
···	12:19:21.12, +04:46:24.5	SDSS	0.00689	0.005	917	18.00	1054
TGN322Z068	12:40:08.85, –00:21:04.7	Catalog	0.00530	0.038	919	12.92	580
···	12:41:57.06, +03:49:09.4	SDSS	0.00294	0.009	920	16.29	−126
12254+0600	12:27:55.80, +05:43:19.0	Catalog	0.00751	0.073	925	11.38	1241
12325+0542	12:35:02.80, +05:25:34.0	Catalog	0.00287	0.038	926	13.02	−146
···	12:32:25.50, +05:39:19.7	SDSS	0.00371	0.005	929	18.24	103
···	12:20:40.14, +05:06:18.2	SDSS	0.00563	0.009	932	16.50	679
···	12:41:45.19, +04:00:23.6	SDSS	0.00265	0.012	933	16.03	−212
12152+0446	12:17:47.80, +04:28:38.0	Catalog	0.00701	0.038	935	13.15	1092

Table 13 — *Continued*

Name	Position (J2000)	Source	$z_{\rm gal}$	$L_{\rm gal}$ (L^*)	ρ (kpc)	$\rho/R_{\rm vir}$	Δv (km s^{-1})
NGC 4255	12:18:56.10, +04:47:12.0	Catalog	0.00652	0.293	938	7.75	945
···	12:43:53.53, +02:37:59.6	SDSS	0.00462	0.007	939	17.36	377
···	12:18:11.61, +04:38:40.3	SDSS	0.00702	0.009	945	16.73	1094
···	12:44:14.96, +02:27:43.2	SDSS	0.00287	0.002	956	20.58	−146
···	12:43:21.06, +03:25:13.0	SDSS	0.00317	0.007	957	17.70	−57
NGC 4376	12:25:18.10, +05:44:30.0	Catalog	0.00379	0.203	957	8.93	129
NGC 4300	12:21:41.48, +05:23:05.1	Catalog	0.00771	0.203	958	8.94	1298
12404+0357	12:42:56.20, +03:40:36.0	Catalog	0.00315	0.066	958	12.01	−64
A1240+0341	12:43:22.20, +03:25:05.0	Catalog	0.00318	0.019	958	15.22	−53
···	12:21:15.35, +05:20:30.7	SDSS	0.00785	0.005	962	18.89	1343
12383+0448	12:40:50.20, +04:31:38.0	Catalog	0.00239	0.038	963	13.54	−288
···	12:40:50.33, +04:31:33.0	SDSS	0.00249	0.035	963	13.70	−261
···	12:23:18.44, +05:36:25.8	SDSS	0.00602	0.009	964	17.06	794
12169+0519	12:19:27.80, +05:02:51.0	Catalog	0.00614	0.061	965	12.29	832
12233+0605	12:25:52.80, +05:48:30.0	Catalog	0.00513	0.061	965	12.29	528
···	12:30:41.99, +05:52:43.6	SDSS	0.00771	0.005	966	18.97	1300
NGC 4630	12:42:31.40, +03:57:37.0	Catalog	0.00247	0.423	968	7.08	−265
NGC 4423	12:27:09.20, +05:52:47.0	Catalog	0.00369	0.128	969	10.34	99
···	12:44:07.96, +03:00:22.1	SDSS	0.00449	0.014	973	16.22	338
···	12:29:45.22, +05:55:12.8	SDSS	0.00274	0.012	973	16.72	−185
TGN391Z146	12:44:33.40, +01:44:12.8	Catalog	0.00320	0.021	973	15.14	−48
···	12:18:20.56, +04:51:13.6	SDSS	0.00691	0.007	975	18.03	1061
TGN323Z228	12:42:27.78, +00:02:51.7	Catalog	0.00500	0.017	978	15.90	490
···	12:19:49.15, +05:11:06.1	SDSS	0.00651	0.019	979	15.55	941
g1239340-005113	12:39:33.95, –00:51:13.2	Catalog	0.00558	0.021	982	15.28	662
···	12:37:07.02, +05:25:17.9	SDSS	0.00390	0.017	984	16.00	161
12346+0542	12:37:06.00, +05:25:17.0	Catalog	0.00375	0.038	984	13.84	115
TGN391Z147	12:44:34.40, +01:16:30.3	Catalog	0.00380	0.019	990	15.73	131
NGC 4580	12:37:48.30, +05:22:09.0	Catalog	0.00345	0.522	996	6.80	26
NGC 4632	12:42:32.03, –00:04:57.1	Catalog	0.00574	0.820	999	5.90	711
NGC 4268	12:19:47.20, +05:17:02.0	Catalog	0.00687	0.217	1000	9.12	1049

Table 14
Galaxy Group Members Near Mrk 290 ($z_{\rm abs} = 0.01027$)

Name	Position (J2000)	Source	$z_{\rm gal}$	$L_{\rm gal}$ (L^*)	ρ (kpc)	$\rho/R_{\rm vir}$	Δv (km s^{-1})
···	15:35:14.26, +57:30:53.2	SDSS	0.01033	0.073	302	3.72	17
···	15:38:02.75, +57:30:18.3	SDSS	0.01180	0.021	375	5.89	454
NGC 5987	15:39:57.38, +58:04:46.3	Catalog	0.01004	1.700	434	2.00	−69
NGC 5965A	15:34:13.80, +57:17:06.0	Catalog	0.01104	0.169	499	4.92	229
···	15:30:40.83, +57:53:01.1	SDSS	0.00969	0.001	526	12.30	−173
A1540+5741	15:41:09.60, +57:31:51.0	Catalog	0.01210	0.023	608	9.35	543
···	15:37:42.04, +57:05:06.5	SDSS	0.01158	0.027	650	9.73	390
···	15:33:57.97, +56:50:50.4	SDSS	0.01081	0.059	827	10.63	160
···	15:35:58.84, +56:41:08.3	SDSS	0.01068	0.012	927	15.85	121
···	15:43:31.90, +57:14:34.0	SDSS	0.01322	0.015	929	15.45	876
NGC 5965	15:34:02.30, +56:41:06.0	Catalog	0.01138	1.550	946	4.50	330
···	15:34:02.29, +56:41:08.5	SDSS	0.01127	1.120	946	5.01	295
···	15:40:54.32, +56:51:39.0	SDSS	0.01141	0.034	947	13.59	338
···	15:33:25.64, +56:41:56.5	SDSS	0.01117	0.013	950	16.02	266
···	15:38:44.84, +56:42:50.4	SDSS	0.01060	0.001	952	22.27	97
15436+5732	15:44:53.50, +57:21:42.0	Catalog	0.01320	0.090	1007	11.78	869
···	15:33:24.55, +56:36:31.5	SDSS	0.01178	0.053	1017	13.31	449
···	15:45:18.25, +57:24:34.9	SDSS	0.01323	0.081	1031	12.34	877
···	15:44:34.42, +57:12:43.7	SDSS	0.01187	0.042	1033	14.16	475
···	15:35:36.90, +56:27:42.1	SDSS	0.01121	0.377	1098	8.35	280
NGC 5971	15:35:36.00, +56:27:38.0	Catalog	0.01174	0.390	1099	8.28	437
···	15:35:27.41, +56:01:58.0	SDSS	0.01124	0.027	1425	21.32	288
···	15:30:51.80, +55:53:17.1	SDSS	0.01089	0.035	1620	23.04	183
···	15:31:04.87, +55:44:16.9	SDSS	0.01116	0.087	1722	20.23	265

Table 15
Galaxy Group Members Near PHL 1811 ($z_{\rm abs} = 0.07773$)

Name	Position (J2000)	Source	$z_{\rm gal}$	$L_{\rm gal}$ (L^*)	ρ (kpc)	$\rho/R_{\rm vir}$	Δv (km s^{-1})
PROCHASKA_22_1734	21:54:59.90, –09:22:24.0	Catalog	0.08098	0.723	35	0.21	904
PROCHASKA_22_2091	21:54:50.80, –09:22:33.0	Catalog	0.07880	0.324	235	1.88	298
PROCHASKA_22_2033	21:54:52.20, –09:24:37.0	Catalog	0.08080	0.089	283	3.31	854
PROCHASKA_22_2226	21:54:47.50, –09:22:54.0	Catalog	0.07765	0.944	310	1.75	−22
PROCHASKA_22_2103	21:54:50.90, –09:20:03.0	Catalog	0.07942	0.318	312	2.52	470
PROCHASKA_22_2225	21:54:47.30, –09:23:05.0	Catalog	0.07791	0.103	317	3.59	50
PROCHASKA_22_1202	21:55:14.10, –09:24:34.0	Catalog	0.08157	0.179	336	3.27	1068
PROCHASKA_22_1109	21:55:16.40, –09:24:07.0	Catalog	0.07376	0.838	360	2.11	−1104
PROCHASKA_22_1987	21:54:52.60, –09:26:28.0	Catalog	0.07963	0.307	410	3.34	529
PROCHASKA_22_2411	21:54:43.10, –09:19:48.0	Catalog	0.07838	0.058	465	6.02	181
PROCHASKA_22_1217	21:55:13.70, –09:18:05.0	Catalog	0.07458	0.861	467	2.69	−876
PROCHASKA_22_1070	21:55:17.30, –09:17:51.0	Catalog	0.07339	3.623	532	1.91	−1207
···	21:55:06.03, –09:16:27.0	SDSS	0.07866	0.797	538	3.20	257
PROCHASKA_22_1134	21:55:15.80, –09:27:21.0	Catalog	0.07769	0.253	539	4.71	−11
PROCHASKA_22_2234	21:54:47.90, –09:17:18.0	Catalog	0.08199	0.509	542	3.72	1185
PROCHASKA_22_1795	21:54:58.00, –09:28:30.0	Catalog	0.07691	0.090	546	6.39	−228
PROCHASKA_22_864	21:55:23.60, –09:19:06.0	Catalog	0.07369	0.052	566	7.50	−1124
PROCHASKA_22_2238	21:54:47.00, –09:28:01.0	Catalog	0.07359	0.398	591	4.42	−1152
PROCHASKA_22_2031	21:54:53.10, –09:15:58.0	Catalog	0.07811	1.084	600	3.20	106
PROCHASKA_22_1851	21:54:56.30, –09:29:17.0	Catalog	0.08070	0.171	621	6.12	826
PROCHASKA_22_2727	21:54:33.20, –09:23:31.0	Catalog	0.08006	0.146	627	6.48	648
PROCHASKA_22_1119	21:55:16.10, –09:29:09.0	Catalog	0.07749	0.155	678	6.87	−67
PROCHASKA_22_1106	21:55:16.30, –09:29:22.0	Catalog	0.07971	0.238	697	6.16	551
···	21:54:34.68, –09:27:16.6	AAT	0.07595	0.068	729	9.09	−495
PROCHASKA_22_2480	21:54:41.60, –09:15:46.0	Catalog	0.07545	0.216	733	6.75	−634
PROCHASKA_22_1691	21:55:01.80, –09:14:03.0	Catalog	0.07896	0.164	742	7.37	342
PROCHASKA_22_879	21:55:22.30, –09:29:07.0	Catalog	0.07636	0.554	750	5.04	−381
PROCHASKA_22_400	21:55:34.00, –09:19:35.0	Catalog	0.08104	0.105	754	8.48	921
PROCHASKA_22_2801	21:54:31.10, –09:18:23.0	Catalog	0.07732	0.064	755	9.50	−114
PROCHASKA_22_1659	21:55:02.50, –09:13:54.0	Catalog	0.07955	0.340	755	5.96	506
PROCHASKA_22_2239	21:54:46.40, –09:30:11.0	Catalog	0.07963	1.135	765	4.02	529
PROCHASKA_22_2284	21:54:46.90, –09:14:31.0	Catalog	0.07862	0.120	770	8.35	248
···	21:54:45.83, –09:30:12.7	AAT	0.07958	0.190	773	7.37	515
PROCHASKA_22_297	21:55:36.20, –09:20:17.0	Catalog	0.07805	0.461	782	5.59	89
PROCHASKA_22_2576	21:54:39.10, –09:15:32.0	Catalog	0.07950	0.119	783	8.57	492
PROCHASKA_22_2689	21:54:34.60, –09:16:32.0	Catalog	0.07854	1.567	786	3.74	225
PROCHASKA_22_2136	21:54:49.00, –09:30:47.0	Catalog	0.07779	0.262	792	6.80	17
PROCHASKA_22_2896	21:54:28.40, –09:18:49.0	Catalog	0.07764	0.108	792	8.80	−25
PROCHASKA_22_1668	21:55:00.60, –09:31:28.0	Catalog	0.08306	2.183	804	3.41	1483
PROCHASKA_22_2612	21:54:37.20, –09:15:34.0	Catalog	0.07813	4.084	807	2.78	111
g2155080-091324	21:55:07.96, –09:13:23.9	Catalog	0.07450	2.143	812	3.47	−898
PROCHASKA_22_870	21:55:22.70, –09:30:00.0	Catalog	0.07864	0.130	818	8.72	253
PROCHASKA_22_1871	21:54:56.90, –09:13:13.0	Catalog	0.07834	0.349	822	6.44	170
PROCHASKA_22_2921	21:54:27.00, –09:26:15.0	Catalog	0.08080	0.088	829	9.74	854
PROCHASKA_22_1401	21:55:08.10, –09:31:54.0	Catalog	0.08156	0.131	855	9.06	1065
PROCHASKA_22_769	21:55:25.00, –09:30:19.0	Catalog	0.07835	0.153	870	8.86	172
PROCHASKA_22_1295	21:55:10.80, –09:32:07.0	Catalog	0.07850	0.226	885	8.02	214
PROCHASKA_22_544	21:55:29.90, –09:29:38.0	Catalog	0.07758	1.378	893	4.41	−42
PROCHASKA_22_2620	21:54:37.70, –09:14:03.0	Catalog	0.07867	0.050	906	12.05	261
···	21:54:52.92, –09:32:43.0	AAT	0.08201	0.369	934	7.15	1191
···	21:54:55.71, –09:32:59.5	AAT	0.08388	0.398	948	7.09	1711
···	21:54:20.06, –09:18:02.7	AAT	0.08104	0.063	986	12.50	921
···	21:54:50.43, –09:33:18.5	AAT	0.08051	0.197	997	9.37	773
···	21:55:11.32, –09:33:46.4	AAT	0.08024	0.352	1031	8.02	698
···	21:54:39.86, –09:32:43.3	AAT	0.07923	0.366	1031	7.95	417
···	21:54:18.95, –09:17:03.0	AAT	0.07826	0.177	1046	10.17	147
PROCHASKA_22_3117	21:54:20.90, –09:29:20.0	Catalog	0.07860	0.405	1081	8.03	242
···	21:54:20.02, –09:29:26.0	AAT	0.08065	0.077	1102	13.34	812
···	21:55:14.56, –09:34:33.4	AAT	0.07868	0.376	1116	8.49	264
···	21:55:48.71, –09:17:37.5	SDSS	0.07898	0.371	1117	8.55	348
···	21:55:50.89, –09:26:27.2	AAT	0.08096	0.202	1139	10.63	899
···	21:55:04.74, –09:35:19.8	AAT	0.08012	2.723	1149	4.51	665
···	21:54:16.31, –09:29:01.6	AAT	0.07901	0.211	1150	10.63	356
···	21:55:42.38, –09:30:48.0	AAT	0.07848	0.310	1164	9.48	209
···	21:55:43.25, –09:30:41.5	AAT	0.07842	0.334	1173	9.34	192
···	21:54:50.83, –09:35:25.0	AAT	0.07859	0.216	1178	10.84	239
···	21:54:13.89, –09:15:49.9	AAT	0.08093	0.195	1195	11.31	890
···	21:55:40.09, –09:32:50.7	AAT	0.07754	0.087	1253	14.72	−53
···	21:55:50.78, –09:15:10.2	AAT	0.07735	0.255	1255	10.86	−106
···	21:54:07.71, –09:17:07.7	AAT	0.07938	0.062	1267	16.14	459
···	21:55:09.46, –09:36:45.2	AAT	0.07425	0.072	1285	15.81	−968
···	21:55:31.71, –09:34:53.6	AAT	0.08208	0.131	1290	13.66	1210
···	21:54:46.09, –09:08:21.1	AAT	0.07720	0.340	1292	10.19	−147
···	21:54:10.22, –09:15:11.3	AAT	0.08052	0.075	1293	15.69	776

Table 15 — *Continued*

Name	Position (J2000)	Source	$z_{\rm gal}$	$L_{\rm gal}$ (L^*)	ρ (kpc)	$\rho/R_{\rm vir}$	Δv (km s^{-1})
···	21:54:21.17, –09:33:07.7	AAT	0.07719	0.058	1298	16.80	−150
···	21:55:09.13, –09:36:55.8	AAT	0.08048	0.211	1300	12.02	765
···	21:54:17.84, –09:32:37.8	AAT	0.07929	0.244	1318	11.59	434
···	21:54:04.06, –09:27:17.0	AAT	0.07616	0.349	1330	10.42	−437
···	21:54:55.92, –09:37:30.2	AAT	0.07937	0.298	1345	11.11	456
···	21:55:48.56, –09:32:37.0	AAT	0.08027	0.135	1372	14.47	707
···	21:54:46.57, –09:37:31.3	AAT	0.07796	0.077	1381	16.72	64
···	21:56:04.86, –09:21:20.3	SDSS	0.07805	0.525	1390	9.48	89
···	21:54:27.72, –09:35:47.9	AAT	0.08075	0.436	1400	10.17	840
···	21:55:59.72, –09:29:04.4	AAT	0.08252	0.075	1405	17.05	1332
···	21:55:49.71, –09:33:12.1	AAT	0.07804	0.130	1425	15.20	86
···	21:55:11.66, –09:38:16.9	AAT	0.07769	0.313	1426	11.51	−11
···	21:55:41.45, –09:35:08.3	HYDRA	0.07963	0.324	1429	11.46	529
···	21:54:59.90, –09:38:38.3	AAT	0.07863	0.697	1441	8.97	250
···	21:55:26.03, –09:37:31.3	AAT	0.07926	0.055	1445	18.83	426
···	21:54:35.43, –09:37:22.7	AAT	0.08112	0.136	1446	15.25	943
···	21:55:03.46, –09:39:17.7	AAT	0.08134	0.123	1499	16.17	1004
···	21:54:35.95, –09:06:41.8	AAT	0.07479	0.137	1502	15.73	−818
···	21:53:52.61, –09:21:11.5	AAT	0.07863	0.302	1512	12.40	250
···	21:54:19.54, –09:08:15.4	AAT	0.07693	0.070	1556	19.23	−223
···	21:54:05.09, –09:11:40.4	SDSS	0.07907	1.041	1560	8.46	373
···	21:54:08.93, –09:34:23.5	AAT	0.07922	0.280	1567	13.15	414
···	21:54:09.08, –09:10:09.9	SDSS	0.08109	0.420	1580	11.63	935
···	21:55:50.88, –09:35:28.2	AAT	0.07922	0.147	1585	16.29	414
···	21:55:22.66, –09:05:18.5	SDSS	0.07589	0.647	1586	10.10	−511
···	21:55:50.87, –09:36:17.9	AAT	0.07982	1.045	1639	8.88	581
···	21:56:00.82, –09:33:41.5	AAT	0.07913	0.288	1640	13.67	389
···	21:54:34.96, –09:39:42.2	AAT	0.07377	1.035	1641	8.96	−1102
···	21:54:32.19, –09:05:10.0	AAT	0.08522	0.094	1659	19.22	2084
···	21:54:47.69, –09:40:59.7	AAT	0.08299	0.559	1677	11.18	1463
···	21:53:52.58, –09:13:59.6	AAT	0.07460	0.218	1684	15.36	−871
···	21:54:03.47, –09:35:06.0	AAT	0.08117	0.235	1698	15.13	957
···	21:56:02.76, –09:34:18.6	AAT	0.07968	0.065	1707	21.49	542
···	21:54:37.22, –09:40:51.5	AAT	0.08110	0.197	1722	16.18	937
···	21:55:40.31, –09:40:03.6	AAT	0.08155	0.044	1782	24.26	1063
···	21:53:49.75, –09:11:05.2	AAT	0.07361	0.060	1865	23.86	−1146
···	21:54:07.47, –09:05:51.9	AAT	0.07431	0.080	1885	22.71	−951
···	21:55:53.24, –09:40:20.9	AAT	0.08044	0.188	1954	18.75	754
···	21:55:42.92, –09:41:58.9	AAT	0.07654	1.045	1959	10.62	−331
···	21:53:58.38, –09:06:37.3	SDSS	0.07937	0.496	1968	13.65	457
···	21:56:03.02, –09:38:53.6	AAT	0.07526	0.171	1988	19.61	−687
···	21:56:07.28, –09:38:14.5	AAT	0.07874	0.139	2012	21.07	281
···	21:56:02.00, –09:39:40.2	AAT	0.07868	0.175	2025	19.83	264
···	21:55:54.48, –09:41:15.7	AAT	0.08201	0.093	2035	23.58	1191
···	21:53:55.27, –09:05:51.2	SDSS	0.07926	0.911	2064	11.71	426
···	21:56:35.39, –09:17:42.2	SDSS	0.08131	2.143	2097	8.97	995
···	21:56:13.01, –09:38:40.3	AAT	0.08100	0.465	2129	15.11	910
···	21:53:55.57, –09:04:37.7	AAT	0.07871	0.238	2139	18.89	273
···	21:56:03.60, –09:41:24.3	AAT	0.08110	0.240	2165	19.12	937
···	21:56:14.37, –09:41:04.4	AAT	0.07800	0.135	2299	24.24	75
···	21:56:15.05, –09:40:55.3	AAT	0.07681	0.179	2300	22.37	−256
···	21:56:47.63, –09:21:46.9	SDSS	0.07820	0.369	2324	17.79	131

Table 16
Galaxy Group Members Near PHL 1811 ($z_{\rm abs} = 0.13280$)

Name	Position (J2000)	Source	$z_{\rm gal}$	$L_{\rm gal}$ (L^*)	ρ (kpc)	$\rho/R_{\rm vir}$	Δv (km s^{-1})
···	21:55:06.29, –09:23:20.1	AAT	0.13743	0.230	214	1.92	1225
PROCHASKA_22_1474	21:55:06.50, –09:23:25.0	Catalog	0.13262	2.950	227	0.87	−48
PROCHASKA_22_1802	21:54:58.40, –09:18:56.0	Catalog	0.13541	0.616	507	3.28	691
···	21:55:09.52, –09:19:24.4	AAT	0.13207	0.230	512	4.61	−193
PROCHASKA_22_2425	21:54:42.30, –09:21:54.0	Catalog	0.13248	0.557	679	4.53	−85
PROCHASKA_22_2426	21:54:42.50, –09:21:12.0	Catalog	0.13220	0.583	690	4.53	−159
PROCHASKA_22_1848	21:54:56.40, –09:28:28.0	Catalog	0.13463	0.450	882	6.35	484
···	21:55:29.92, –09:22:35.3	AAT	0.13980	0.276	999	8.44	1853
···	21:54:47.16, –09:28:28.3	AAT	0.13543	0.557	1001	6.67	696
PROCHASKA_22_2222	21:54:47.10, –09:28:28.0	Catalog	0.13557	0.843	1001	5.81	733
PROCHASKA_22_2081	21:54:50.90, –09:29:17.0	Catalog	0.13635	0.271	1048	8.94	940
PROCHASKA_22_533	21:55:30.70, –09:23:58.0	Catalog	0.13590	2.301	1050	4.39	820
PROCHASKA_22_1950	21:54:53.70, –09:30:04.0	Catalog	0.13503	2.218	1125	4.73	590
PROCHASKA_22_2459	21:54:40.80, –09:29:07.0	Catalog	0.13573	0.513	1201	8.25	775

Table 16 — *Continued*

Name	Position (J2000)	Source	$z_{\rm gal}$	$L_{\rm gal}$ (L^*)	ρ (kpc)	$\rho/R_{\rm vir}$	Δv (km s^{-1})
PROCHASKA_22_213	21:55:38.90, –09:18:32.0	Catalog	0.13540	0.192	1425	13.58	688
···	21:55:42.58, –09:21:48.3	AAT	0.13328	0.455	1446	10.33	127
PROCHASKA_22_192	21:55:39.80, –09:14:52.0	Catalog	0.13431	0.446	1722	12.39	400
PROCHASKA_22_229	21:55:37.40, –09:31:37.0	Catalog	0.13502	0.797	1820	10.82	588
···	21:55:56.17, –09:20:39.7	SDSS	0.13417	2.580	1937	7.78	363
···	21:55:59.91, –09:21:49.7	SDSS	0.13438	0.985	2054	11.39	417
···	21:55:59.85, –09:25:09.5	AAT	0.13403	0.351	2087	16.24	326
···	21:55:50.03, –09:32:13.0	AAT	0.13573	0.820	2204	13.01	775
···	21:56:00.84, –09:16:25.0	AAT	0.13548	0.159	2253	22.69	709
···	21:55:58.19, –09:14:30.3	SDSS	0.13500	1.340	2288	11.39	583
···	21:56:09.01, –09:25:39.6	AAT	0.13456	1.264	2417	12.31	466
···	21:56:08.83, –09:28:17.2	AAT	0.13637	0.827	2509	14.67	945
···	21:56:08.90, –09:28:32.0	AAT	0.13675	0.255	2524	21.83	1045
···	21:56:14.67, –09:25:21.7	AAT	0.13723	0.342	2605	20.55	1172
···	21:56:02.50, –09:33:18.1	AAT	0.13310	1.479	2646	12.78	79
···	21:56:17.16, –09:23:46.7	AAT	0.13427	0.836	2665	15.58	389

Table 17
Galaxy Group Members Near PG 0953+414 ($z_{\rm abs} = 0.00212$)

Name	Position (J2000)	Source	$z_{\rm gal}$	$L_{\rm gal}$ (L^*)	ρ (kpc)	$\rho/R_{\rm vir}$	Δv (km s^{-1})
NGC 3104	10:03:57.80, +40:45:28.0	Catalog	0.00201	0.025	227	3.44	−31
10043+3913	10:07:22.90, +38:58:08.0	Catalog	0.00196	0.008	483	8.85	−48
10133+4125	10:16:15.60, +41:09:57.0	Catalog	0.00177	0.009	579	10.39	−104
NGC 3184	10:18:17.20, +41:25:26.0	Catalog	0.00197	0.817	639	3.77	−43
···	10:17:32.98, +43:08:41.4	SDSS	0.00378	0.002	678	14.97	496
···	10:25:50.79, +43:55:58.2	SDSS	0.00219	0.001	947	22.77	20
NGC 3198	10:19:54.80, +45:32:58.0	Catalog	0.00221	0.432	951	6.91	26
···	10:07:18.96, +47:00:23.4	SDSS	0.00211	0.018	960	15.39	−4
10042+4716	10:07:18.00, +47:00:22.0	Catalog	0.00190	0.027	960	14.36	−64
···	10:39:00.38, +41:40:08.8	SDSS	0.00226	0.002	1254	27.69	41
NGC 3319	10:39:09.40, +41:41:10.0	Catalog	0.00247	0.196	1259	11.91	105
···	10:39:12.85, +41:30:20.2	SDSS	0.00222	0.002	1261	27.84	30
···	10:35:12.07, +46:14:12.3	SDSS	0.00168	0.001	1352	32.51	−131

Table 18
Galaxy Group Members Near HE 0226–4110 ($z_{\rm abs} = 0.01750$)

Name	Position (J2000)	Source	$z_{\rm gal}$	$L_{\rm gal}$ (L^*)	ρ (kpc)	$\rho/R_{\rm vir}$	Δv (km s^{-1})
···	02:27:46.33, –40:51:17.1	HYDRA	0.01490	0.005	173	3.39	−766
···	02:27:44.79, –41:05:23.6	HYDRA	0.01524	0.012	214	3.63	−666
···	02:29:20.48, –41:02:30.2	HYDRA	0.01947	0.005	287	5.62	580
···	02:27:41.67, –41:09:48.3	HYDRA	0.01511	0.005	302	5.92	−704
···	02:26:38.02, –40:39:17.6	AAT	0.01792	0.004	551	11.12	124
N 954	02:28:52.20, –41:24:09.0	Catalog	0.01783	2.793	596	2.32	98
A0223-4039	02:25:14.62, –40:25:47.9	Catalog	0.01790	2.281	996	4.16	118
A0222-4136	02:24:36.00, –41:23:06.0	Catalog	0.01759	0.499	1044	7.24	25
A0222-4142	02:24:38.10, –41:28:33.0	Catalog	0.01679	0.318	1103	8.90	−210
g0228282-420423	02:28:28.20, –42:04:23.1	Catalog	0.01562	0.167	1441	14.31	−554
A0219-4142	02:21:26.90, –41:29:05.0	Catalog	0.01648	0.228	1782	16.03	−299
N 893	02:19:58.40, –41:24:12.0	Catalog	0.01684	2.547	2086	8.38	−193
A0219-4213A	02:21:11.75, –42:00:05.9	Catalog	0.01630	0.891	2169	12.40	−353
g0219535-413948	02:19:53.52, –41:39:48.1	Catalog	0.02059	0.220	2216	20.21	912
A0226-4259	02:28:20.23, –42:45:49.5	Catalog	0.01806	0.755	2328	14.06	166
IC 1812	02:29:31.77, –42:48:40.6	Catalog	0.01724	5.128	2407	7.68	−76
N 889	02:19:06.80, –41:44:55.0	Catalog	0.01754	1.745	2432	11.14	11
TGS920Z268	02:19:20.82, –42:03:04.2	Catalog	0.02120	0.123	2568	27.71	1090
A0227-4312	02:29:23.00, –42:59:04.0	Catalog	0.01719	1.312	2626	13.19	−92
A0228-4314	02:30:27.88, –43:01:36.6	Catalog	0.01849	4.721	2719	8.94	291
A0226-4317	02:28:47.10, –43:04:27.0	Catalog	0.01683	1.577	2731	12.89	−197

Table 19
Galaxy Group Members Near PG 1259+593 ($z_{\rm abs} = 0.04625$)

Name	Position (J2000)	Source	$z_{\rm gal}$	$L_{\rm gal}$ (L^*)	ρ (kpc)	$\rho/R_{\rm vir}$	Δv (km s^{-1})
···	13:01:14.75, +59:03:43.3	HYDRA	0.04608	0.068	89	1.11	−49
···	13:01:01.04, +59:00:06.8	SDSS	0.04624	0.504	138	0.96	−3
···	13:01:00.55, +58:58:04.4	SDSS	0.04621	0.752	238	1.44	−13
···	13:00:33.95, +58:58:56.9	SDSS	0.04601	2.378	325	1.34	−69
···	13:00:25.54, +59:02:18.6	SDSS	0.04658	0.188	334	3.20	94
···	13:00:50.54, +58:56:28.8	HYDRA	0.04627	0.033	347	5.00	6
···	13:01:40.19, +59:07:29.4	HYDRA	0.04700	0.067	351	4.38	215
···	13:00:22.13, +59:01:26.8	SDSS	0.04645	0.630	360	2.31	56
···	13:00:16.36, +59:03:18.1	HYDRA	0.04604	0.048	404	5.42	−60
···	13:00:15.08, +59:00:21.6	HYDRA	0.04716	0.046	419	5.65	261
···	13:02:12.65, +59:00:36.0	SDSS	0.04633	0.192	429	4.09	24
···	13:00:13.21, +58:58:54.9	SDSS	0.04639	0.292	456	3.80	41
···	13:00:20.61, +58:55:19.8	HYDRA	0.04634	0.034	524	7.52	26
···	12:59:26.08, +59:01:06.5	SDSS	0.04668	2.060	755	3.27	124
···	13:00:23.33, +59:15:48.6	SDSS	0.04415	0.423	827	6.05	−602
···	12:59:15.15, +58:59:11.6	SDSS	0.04672	0.197	846	8.01	134
···	13:03:13.51, +58:59:57.2	SDSS	0.04340	0.207	858	7.93	−817
···	13:00:21.64, +59:18:21.6	HYDRA	0.04340	0.108	960	10.75	−817
···	12:59:14.16, +58:50:59.5	SDSS	0.04620	0.238	1037	9.16	−15
···	13:03:05.09, +59:14:35.4	HYDRA	0.04337	0.103	1043	11.81	−825
···	13:00:12.07, +59:19:41.1	HYDRA	0.04448	0.157	1053	10.60	−507
···	12:58:51.62, +59:15:58.3	SDSS	0.04405	0.494	1249	8.72	−630
···	12:57:51.99, +59:14:43.9	SDSS	0.04381	0.332	1571	12.51	−700

Table 20
Galaxy Group Members Near PG 1116+215 ($z_{\rm abs} = 0.05897$)

Name	Position (J2000)	Source	$z_{\rm gal}$	$L_{\rm gal}$ (L^*)	ρ (kpc)	$\rho/R_{\rm vir}$	Δv (km s^{-1})
PROCHASKA_12_2071	11:19:05.50, +21:17:33.0	Catalog	0.06002	0.129	131	1.40	297
PROCHASKA_12_2154	11:19:03.10, +21:16:23.0	Catalog	0.05939	0.047	220	2.97	119
PROCHASKA_12_2048	11:19:05.40, +21:15:38.0	Catalog	0.05873	0.824	258	1.51	−68
PROCHASKA_12_1571	11:19:19.80, +21:22:28.0	Catalog	0.06128	0.189	281	2.68	654
PROCHASKA_12_808	11:19:38.40, +21:21:42.0	Catalog	0.06063	0.246	504	4.43	470
PROCHASKA_12_1312	11:19:24.30, +21:10:30.0	Catalog	0.05899	1.458	655	3.19	6
A1115+2129	11:18:33.70, +21:13:00.0	Catalog	0.05963	1.431	708	3.44	186
PROCHASKA_12_674	11:19:42.00, +21:26:10.0	Catalog	0.06138	0.125	713	7.64	682
PROCHASKA_12_2	11:18:29.20, +21:14:00.0	Catalog	0.06038	1.258	730	3.72	399
A1117+2143	11:19:43.60, +21:26:52.0	Catalog	0.06055	2.487	764	3.09	447
···	11:19:42.40, +21:27:16.4	HYDRA	0.06109	0.062	770	9.81	600
···	11:20:00.74, +21:26:45.9	HYDRA	0.06029	0.087	979	11.50	374
···	11:18:38.88, +21:06:37.1	HYDRA	0.06048	0.084	995	11.77	427
···	11:19:56.66, +21:08:45.4	HYDRA	0.05953	0.065	1057	13.31	159
···	11:20:12.27, +21:25:04.0	HYDRA	0.06016	0.166	1093	10.85	337
A1117+2148B	11:19:59.00, +21:31:53.0	Catalog	0.05976	0.625	1183	7.59	223

Table 21
Galaxy Group Members Near PG 0953+414 ($z_{\rm abs} = 0.06808$)

Name	Position (J2000)	Source	$z_{\rm gal}$	$L_{\rm gal}$ (L^*)	ρ (kpc)	$\rho/R_{\rm vir}$	Δv (km s^{-1})
···	09:56:12.27, +41:14:39.9	HYDRA	0.07018	0.137	595	6.23	589
···	09:56:11.37, +41:14:50.4	SDSS	0.06917	0.877	607	3.50	306
···	09:56:03.77, +41:20:03.3	HYDRA	0.06970	0.084	807	9.59	455
···	09:56:47.27, +41:03:27.8	HYDRA	0.07128	0.151	939	9.56	898
···	09:56:36.33, +41:03:04.0	SDSS	0.06875	0.615	996	6.45	189
···	09:56:19.93, +41:03:13.7	SDSS	0.06869	1.009	1068	5.88	170
···	09:56:27.65, +41:01:53.6	HYDRA	0.06899	0.241	1121	9.90	255
···	09:57:55.36, +41:06:25.9	HYDRA	0.06854	0.321	1166	9.35	129
···	09:56:40.78, +41:00:32.4	HYDRA	0.06794	0.087	1178	13.84	−39
···	09:55:34.18, +41:11:48.9	SDSS	0.06878	0.973	1189	6.59	196
···	09:56:24.30, +40:57:20.5	HYDRA	0.06983	0.079	1477	17.80	491
···	09:57:35.08, +40:57:51.9	HYDRA	0.06841	0.121	1514	16.41	93
···	09:55:12.88, +41:08:51.7	SDSS	0.06946	1.858	1558	6.98	388
···	09:56:57.93, +40:55:31.7	SDSS	0.07136	1.849	1562	6.99	922

Table 22
Galaxy Group Members Near PKS 2155–304 ($z_{\rm abs} = 0.05422$)

Name	Position (J2000)	Source	$z_{\rm gal}$	$L_{\rm gal}$ (L^*)	ρ (kpc)	$\rho/R_{\rm vir}$	Δv (km s^{-1})
A2155-3033B	21:58:41.60, –30:19:19.0	Catalog	0.05702	2.045	395	1.71	795
TGS329Z002	21:58:40.87, –30:19:28.8	Catalog	0.05660	2.959	408	1.57	677
TGS330Z126	21:58:23.84, –30:19:32.4	Catalog	0.05390	3.671	544	1.95	−91
TGS330Z102	21:58:57.17, –30:02:45.9	Catalog	0.05710	2.495	689	2.79	819
TGS331Z156	21:59:49.75, –30:16:19.2	Catalog	0.05630	3.264	812	3.02	592
TGS329Z018	21:57:52.80, –30:19:32.6	Catalog	0.05680	0.657	899	5.69	734
TGS330Z061	22:00:02.15, –30:02:03.4	Catalog	0.05460	0.511	1209	8.31	108
TGS330Z063	22:00:01.89, –30:38:05.1	Catalog	0.05580	1.878	1832	8.20	449

Table 23
Galaxy Group Members Near PKS 2155–304 ($z_{\rm abs} = 0.05722$)

Name	Position (J2000)	Source	$z_{\rm gal}$	$L_{\rm gal}$ (L^*)	ρ (kpc)	$\rho/R_{\rm vir}$	Δv (km s^{-1})
A2155-3033B	21:58:41.60, –30:19:19.0	Catalog	0.05702	2.045	415	1.80	−58
TGS329Z002	21:58:40.87, –30:19:28.8	Catalog	0.05660	2.959	429	1.65	−176
TGS330Z126	21:58:23.84, –30:19:32.4	Catalog	0.05390	3.672	572	2.05	−941
TGS330Z102	21:58:57.17, –30:02:45.9	Catalog	0.05710	2.494	724	2.93	−34
TGS331Z156	21:59:49.75, –30:16:19.2	Catalog	0.05630	3.263	854	3.18	−261
TGS329Z018	21:57:52.80, –30:19:32.6	Catalog	0.05680	0.657	946	5.98	−119
TGS330Z061	22:00:02.15, –30:02:03.4	Catalog	0.05460	0.511	1272	8.74	−743
TGS330Z063	22:00:01.89, –30:38:05.1	Catalog	0.05580	1.879	1926	8.62	−403

Table 24
Galaxy Group Members Near 3C 273 ($z_{\rm abs} = 0.09010$)

Name	Position (J2000)	Source	$z_{\rm gal}$	$L_{\rm gal}$ (L^*)	ρ (kpc)	$\rho/R_{\rm vir}$	Δv (km s^{-1})
TGN387Z035	12:28:51.87, +02:06:03.2	Catalog	0.08970	1.867	478	2.14	−110
McLin10	12:28:30.32, +02:10:43.8	Catalog	0.08760	0.112	1201	13.29	−687
A1225+0227	12:28:28.50, +02:11:08.0	Catalog	0.08798	0.912	1261	7.16	−584
TGN387Z067	12:28:07.65, +02:02:52.0	Catalog	0.09030	1.642	1497	6.95	55
TGN387Z068	12:28:06.93, +01:59:59.6	Catalog	0.08970	4.632	1548	5.09	−110
TGN387Z042	12:28:34.52, +01:48:15.7	Catalog	0.09210	2.311	1715	7.17	550
TGN387Z088	12:27:46.03, +01:56:15.6	Catalog	0.09180	1.265	2160	11.00	468
A1225+0212	12:27:45.00, +01:56:15.0	Catalog	0.09251	0.759	2161	13.05	662
TGN387Z081	12:27:53.42, +01:51:24.9	Catalog	0.09270	1.917	2205	9.78	715
TGN387Z102	12:27:19.49, +02:00:41.4	Catalog	0.08870	2.554	2728	10.96	−385
TGN387Z108	12:27:16.78, +02:00:33.7	Catalog	0.09200	1.069	2797	15.06	523
TGN387Z099	12:27:25.01, +01:50:59.0	Catalog	0.09250	1.059	2857	15.48	660
TGN387Z110	12:27:08.54, +01:59:41.3	Catalog	0.08780	3.438	3015	10.97	−633

Table 25
Galaxy Group Members Near 3C 263 ($z_{\rm abs} = 0.11389$)

Name	Position (J2000)	Source	$z_{\rm gal}$	$L_{\rm gal}$ (L^*)	ρ (kpc)	$\rho/R_{\rm vir}$	Δv (km s^{-1})
···	11:40:38.59, +65:51:21.8	HYDRA	0.11369	0.375	691	5.29	−54
···	11:39:41.36, +65:53:33.3	HYDRA	0.11581	1.713	743	3.43	517
···	11:39:48.94, +65:55:33.2	HYDRA	0.11560	0.455	970	6.93	460
···	11:39:44.02, +65:55:34.5	SDSS	0.11507	1.191	982	5.08	318
···	11:38:35.42, +65:53:05.2	HYDRA	0.11313	0.247	1232	10.83	−205
···	11:38:55.34, +65:58:00.6	HYDRA	0.11489	0.557	1495	9.97	269
···	11:39:57.80, +66:01:19.9	HYDRA	0.11485	0.277	1686	14.25	258